Molecular Design Strategies toward Improvement of Charge Injection and Ionic Conduction in Organic Mixed Ionic–Electronic Conductors for Organic Electrochemical Transistors

Nadzeya A. Kukhta,[∇] Adam Marks,[∇] and Christine K. Luscombe*
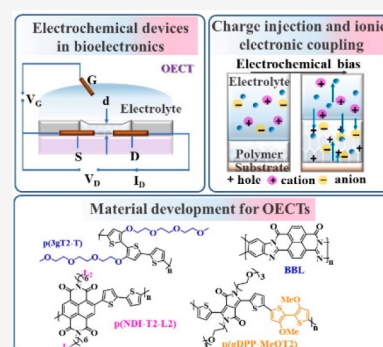
Cite This: https://doi.org/10.1021/acs.chemrev.1c00266

Read Online

ACCESS | Metrics & More | Article Recommendations

ABSTRACT: Expanding the toolbox of the biology and electronics mutual conjunction is a primary aim of bioelectronics. The organic electrochemical transistor (OECT) has undeniably become a predominant device for mixed conduction materials, offering impressive transconduction properties alongside a relatively simple device architecture. In this review, we focus on the discussion of recent material developments in the area of mixed conductors for bioelectronic applications by means of thorough structure–property investigation and analysis of current challenges. Fundamental operation principles of the OECT are revisited, and characterization methods are highlighted. Current bioelectronic applications of organic mixed ionic–electronic conductors (OMIECs) are underlined. Challenges in the performance and operational stability of OECT channel materials as well as potential strategies for mitigating them, are discussed. This is further expanded to sketch a synopsis of the history of mixed conduction materials for both p- and n-type channel operation, detailing the synthetic challenges and milestones which have been overcome to frequently produce higher performing OECT devices. The cumulative work of multiple research groups is summarized, and synthetic design strategies are extracted to present a series of design principles that can be utilized to drive figure-of-merit performance values even further for future OMIEC materials.

CONTENTS

Figure 1. Applications of bioelectronics. Panel 1: Schematic of the nanomaterials utilized for the production of electrically conductive cardiac tissue engineering scaffolds. Adapted with permission from ref 22. Copyright 2019 Elsevier. Panel 2: Schematic of electromagnetically controlled drug release. Reproduced with permission from ref 23. Copyright 2019 Wiley. Panel 3: Schematic illustration of the memristors as interneuron synapses. The insets show the schematics of the two-terminal device geometry and the layered structure of the memristor. Adapted with permission from ref 24. Copyright 2010 American Society of Chemistry. Panel 4: Schematic of the removal of PSS from the PPG by H_2SO_4 treatment. Adapted with permission from ref 25. Copyright 2017 Royal Society of Chemistry.

1. INTRODUCTION

In addition to electrons, biological systems employ an assortment of ions and noncharged molecules to enable communication, broadcasting, signaling, and health status management. Therefore, it is important to develop an interface that can translate electronic signals into the biological ones in order to achieve accurate electronic regulation. Thus, current and rising technologies for biointerfacing should employ ionic and molecular signaling for the improvement of efficiency and integration. In particular, bioelectronics, merging manufactured electronics and biology, has emerged as a promising platform for translating electronic signals into ionic ones[1−3] and vice versa, converting ionic signals into electronic signals (e.g., biosensors and ionic skins).[4−8] In recent years, applications in tissue engineering, drug delivery, electrophoresis, and physiology have also been developed.[9] These applications not only address regulation of the physiological cell-, organ-, and tissue-related processes from a chemistry perspective and provide exquisite topological and time-dependent resolution but also tackle selective sensing, recording, and monitoring of different signals and physiological states.[2] Electrophysiology, involving the use of electrodes for monitoring and vitalizing living tissues, is used for drug development and toxicity studies, as well as in tissue engineering and developmental biology.[10,11] Furthermore, because of providing technological routes toward cost-, power-, and size-efficient devices, organic bioelectronics is rapidly climbing the ladder of biosensing advancements.[2,12−14] Over the recent years, organic materials have also set foot into the arena of neuromorphic devices and memristors.[15,16] Building machines capable of mimicking the ability of the brain to multitask efficiently is one of the main goals of neuromorphic computing. These machines can transform high-performance computing, finding applications in performing local, low-energy computing for sensors and robots. Most of the research in neuromorphic devices has been centered on the emulation of various synaptic plasticity functions, including homeoplasticity.[16,17] Nowadays, bioelectronic devices can be chiefly utilized in copious healthcare-related applications, such as implants, sensors, and neural interfacing electrodes, to name but a few.[18−21] These principal applications of organic bioelectronic devices are presented in (Figure 1).

While developing new materials and device configurations for bioelectronics, it is worth remembering that the interaction of a bioelectronic tool with a living host can occur in several different ways upon implantation. First, the material can be inadvertently toxic, and the insertion can lead to adverse effects on the surrounding tissue causing inflammation, response of the immune system, or even cell/organ death. Second, the
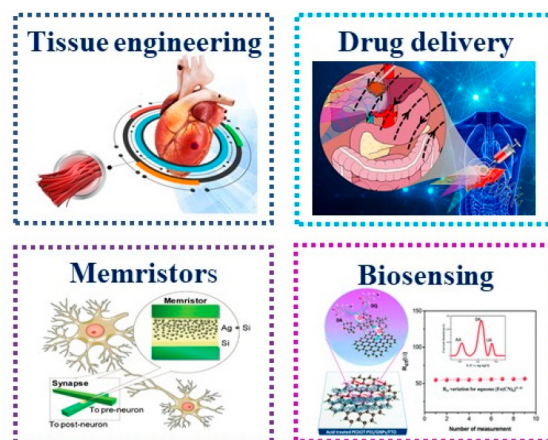
material might not interact with the living host, in other words, be bioinert. Third, the bioelectronic device can form a close relationship with the tissue of the host if the material is active biologically and innocuous. Finally, a biomaterial can be bioresorbable and dissolve in the host tissue, allowing only temporary device operation.[20,26] Additionally, organic semiconductors (OSC), widely utilized in bioelectronics, possess the merit of mechanical flexibility, as well as having easily modifiable surface structure. Being soft solids, organic semiconducting polymers possess low values of Young's modulus, 20 kPa to 3 GPa, which is comparable to the parameters of the living tissue (∼10 kPa) in contrast to the values of inorganic semiconductors (∼100 GPa).[26−28] Notably, inflammation reduction can be achieved through strain alleviation at the tissue/implant interface as a result of organic semiconductor softness.[29] As such, utilizing soft biopolymers also allows for potential biocompatibility and engineered multifunctionality.[30] Compliant materials can be better suited for biological systems because the interface between biological tissue and electronic devices can be improved while avoiding detrimental effects.[31]

These attractive features can be offered by conjugated polymers with their mechanical properties well-matched to the softness of biological systems. These properties, in turn, allow for the development of close bioelectronic relationships both at the macro- and nanoscale, allowing for proliferation and adhesion of cells, as well as polymer integration into the membrane of a cell.[2,32] Furthermore, the ability of conjugated polymers to conduct both electronic charge and ions (upon doping) has opened their way into many novel electrochemical applications, including bioelectronics and neuromorphic computing.[33] The propensity of a material toward conducting electrons and ions simultaneously is usually referred to as mixed conductance, while organic compounds transporting both types of charge carriers are called organic mixed ionic and

electronic conductors (OMIECs). Conjugated polymers present an ideal platform for mixed conductance: while electronic charge transport is supported along their backbone, the ionic transport can be allowed through the bulk. Not only do OMIEC polymers possess an intrinsic ability to oxidize and reduce reversibly, but also their soft interface has been proven to benefit polymer/protein interactions, for instance, promoting enzyme catalytic activity.[34] Additionally, OMIECs give rise to a number of innovative electronic devices, with the organic electrochemical transistor (OECT) taking the lead. The latter, in turn, can efficiently convert biologic signals of ionic nature into electronic signals, achieving significant amplification owing to the interplay of the electrolyte ions in the volume of the OMIEC material. Efficient mixed carrier conduction leads to electrochemical reactions within the bulk of a conjugated polymer due to compensation, for additional electronic charges, in the form of ions migrating from an electrolyte.[35] The ability of OMIECs to absorb and transport charges of ionic and electronic nature underpins the field of bioelectronics. Many of the bioelectronic devices, OECTs being one of them, rely on ion injection by means of an electrochemical bias application. This leads to a change in oxidation state of the conjugated polymer and motion of positive and negative ions inward the channel material, resulting in charge compensation of the latter.[35−37] Although this process provides the foundation for numerous technologies, investigations into ion injection and specific transport mechanisms in OMIECs is still in its infancy. Furthermore, it is important to understand that the motion of both electrons and ions is not independent but coupled. Hence, exploration of the ion conduction in OMIECs is closely connected to the electronic conduction and, in turn, to the structures of both conjugated polymers and ion charge carriers.[38]

In this review, we not only discuss the fundamental aspects of the charge injection and ionic/electronic coupling in organic mixed conductors but also provide a synopsis of the devices they find applications in. We provide an overview of the latest material developments in the field of OMIECs, particularly focusing on their application within OECTs. By classifying and discussing each type of OMIEC in detail, we aim to study the structure−property relationships and answer several questions: (i) Can we provide the molecular design rules toward the efficient OMIEC materials? (ii) What are current limitations within the field? What are the ways to tackle them? (iii) Which new applications could arise from the successful design of OMIECs?

1.1. Electrochemical Devices in Bioelectronics

1.1.1. Overview of Electrochemical Devices.
The development of the benchmark electrochemical device, OECT, by Wrighton and co-workers in 1984,[39] was inspired by the widespread application of conjugated materials in organic field effect transistors (OFETs). Therefore, to explicate the working principle and distinctiveness of the OECT, it is important to revisit that of OFETs. A typical OFET contains three terminals, namely source, drain, and gate electrodes, with a solid layer of a dielectric material sandwiched between a channel semiconductor and the gate electrode (Figure 2).

Application of two potentials, at the gate and drain electrodes, respectively, with the condition of a grounded source electrode, results in two voltages: the gate−source voltage (V_{GS}) and the drain−source voltage (V_{DS}). This process underpins the operational principle of an OFET. When
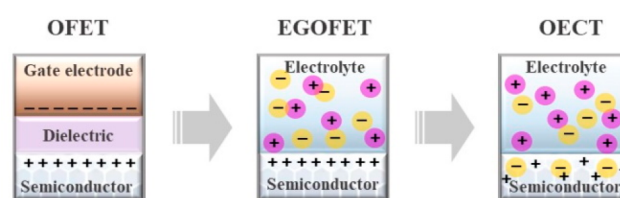

Figure 2. Evolution of organic electronics toward organic electrochemical transistors.

a negative or positive voltage is applied between the gate and the source electrodes, an electric field is induced in the semiconductor layer that attracts opposite charge carriers at the semiconductor/insulator interface between source and drain electrode, overlapping with the gate. Without the application of the gate−source voltage no charge accumulates at the interface between the semiconductor and the dielectric. As a result, the OFET is in its "OFF" state (this only applies to the ideal devices with zero threshold voltage). In turn, applying V_{GS} causes polarization of the dielectric, hence, accumulating charge carriers at the semiconductor−dielectric interface, and consequently turning the transistor "ON." Drain−source voltage compels the accumulated charge carriers to move from the source to the drain electrode, while the drain current (I_D) is monitored. As a result, the current and the charge density in an OFET can be tuned by the extent of the field applied.[40] Hence, a buildup of the electrostatic charge at the interface, induced by the gate, leads to the regulation of the channel conduction.[41,42] Replacing the solid gate dielectric material by a liquid electrolyte facilitates the movement of ions toward the organic semiconductor upon the application of an electrical current. This in turn leads to the formation of an electrical double layer along the electrolyte/semiconductor interface.[43] Such modified device architecture is named an electrolyte gated OFET (EGOFET), exhibiting a remarkably improved capacitance and operating at reduced gate voltages compared to OFET devices.[44]

1.1.2. Organic Electrochemical Transistors.
Provided that the organic semiconducting material is capable of ion infiltration, charge accumulation becomes characteristic of not only the channel/electrolyte interface, but also of the conjugated polymer bulk, due to the ability of ions to infiltrate and consequently affect electronic conductivity. The latter is the characteristic feature of an OECT.[42] Similarly to OFETs and EGOFETs, OECTs can operate both like a switch, by controlling the drain current and an amplifier by enhancing the power of an input signal on the way to the output.[45] In turn, similarly to OFETs, an OECT is a three-electrode transistor, containing a layer of liquid or solid electrolyte, through which the active semiconducting layer is gated (Figure 3).

The working principle of an OECT involves volumetric ion injection into the active layer of the organic semiconductor upon the application of a gate voltage across the electrolyte. This results in the oxidation state change of the mixed conductor, subsequently altering the conductivity of the active layer. Consequently, the resultant measurable difference in the drain current can be recorded.[46,47] Thus, an OECT combines both a direct sensing of ionic species and the inherent transistor amplification of the electrical signal.[45]

OECTs can operate in either depletion or accumulation mode. For the case of a depletion mode device, a highly conductive polymer, used as the active channel material, has an excess of free charge carriers. The most well-known example of
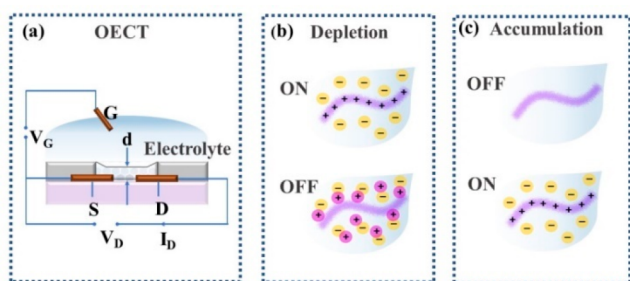
Figure 3. (a) Schematic of a typical OECT structure (S, source; D, drain; G, gate; d, channel thickness; V_G, gate voltage; V_D, drain voltage; I_D, drain current), (b) depletion, and (c) accumulation modes of OECT.

a depletion-mode OMIEC is (poly(3,4-ethylenedioxythio-phene) doped with poly(styrenesulfonate)) **PEDOT:PSS**. For instance, in the absence of a gate voltage, the transistor is in a switched "ON" state, as the mobile holes in the **PEDOT** unit are compensated by the sulfonate PSS groups. Upon application of a positive gate voltage, the injected cations replace the holes in the channel, thus switching the device OFF. On the other hand, in an accumulation mode device, semiconducting polymers are undoped when the device is OFF. When a gate voltage is applied, mobile ions, accumulated in the channel, increase the conductivity of the latter and turn the OECT ON.[42] The first examples of accumulation mode electrochemical transistors employed pristine conjugated polymers, such as polypyrrole,[48] poly(3-methyl-thiophene),[49] polyaniline,[50] and polycarbazole.[51] Accumulation mode OECTs featuring a turned OFF initial state consume less power than the depletion mode counterparts. As a result, OMIECs capable of operation in the accumulation mode, are particularly desirable for multiple bioelectronic applications.[52]

One of the most important and well documented figures of merit for an OECT is the transconductance (g_m). Transconductance refers to a ratio of the current response to the applied voltage. While in the case of OFETs the charges are localized only across the interface, resulting in the aerial dependence of the drain current (I_D) on the gate voltage (V_G), the volumetric ion injection in OECTs leads to the film thickness dependence of transconductance (eq 1, applicable for the saturation regime):

$$g_m = \frac{\partial I_D}{\partial V_G} = \mu C^* \cdot \frac{Wd}{L}(V_{TH} - V_G)$$

(1)

where g_m, transconductance; I_D, drain current; V_G, gate voltage; μ, electronic charge carrier mobility; C^*, volumetric capacitance; W, channel width; d, channel depth; L, channel length; V_{TH}, the threshold voltage.

Unlike in field effect transistors, where the electronic charge mobility μ defines the device performance, the μC^* parameter arose as a benchmark parameter for OECT materials, as it describes the innate properties of the channel conductors.[53] As a result, even materials with an inferior electronic charge mobility can possess a significant transconductance with sufficient volumetric capacitance. That, in turn, leads to the much more significant increase in transconductance in comparison to OFETs.[53,54]

OECTs have several particular features as a result of gating through an electrolyte: (i) geometry control of the gate voltage, and (ii) dependence of the response time on the

nature of the electrolyte and charge carrier concentration.[55] For instance, utilization of a polarizable gate electrode (Pt, Au) leads to the formation of two capacitors in the ionic circuit: one corresponding to the electrical double layer at the interface between the gate and the electrolyte, with the other being the volumetric capacitance of the channel. As a result of the subsequent arrangement of the capacitors the applied voltage decreases across the minute capacitor. To achieve efficient gating, the gate electrode should possess a significantly larger capacitance than that of the channel. Therefore, utilization of a nonpolarizable gate electrode (e.g., Ag/AgCl) can aid to minimize the voltage drop at the gate−electrolyte interface, thus warranting effective gating. Nevertheless, it should be noted that in certain sensing applications a small gate electrode is preferable, for instance, when a sensing reaction occurs at the gate with the channel acting as the transducer.[56] Additionally, mechanical softness and stretchability of OECTs render them more suitable for operation at the biointerface, when compared to OFETs.[57] Finally, insights into the performance of various organic semiconductors, utilized as OECT channel materials, can be borrowed from the fields of OFETs, OPV, and electrochromics, by employing (i) cyclic voltammetry (CV), (ii) grazing incidence wide-angle X-ray scattering (GIWAXS), (iii) transistor mobility, (iv) electrochemical impedance spectroscopy (EIS), and (v) spectroelectrochemistry.[20] These methods in direct relation to OECTs will be discussed later in this review.

1.1.3. Bioelectronic Applications of OMIECs. OMIECs and OECTs find wide application in a plenitude of biomedical applications including both research and health-care related uses. First, local current injection and neuron stimulation can be achieved, as reported by Williamson et al.[58] OECTs were also found to succeed in electromyogram detection upon the laser-assisted motor nerve bundle stimulation of a transgenic rat.[59] In electrophysiology, organic electrochemical transistors can be interfaced with electrically active tissues and organs to modulate cell activity, for example, a biocompatible **PE-DOT:PSS**-based microfabricated brain-placed OECT success-fully recorded epileptic seizures of a rat.[21] Cutaneous applications include recording an electrocardiogram when placed on human skin[60−62] and amplifying electrophysiological signals from the human brain, heart, and muscle.[61]

Drug screening can also be carried out using OECTs in conjunction with cell cultures. These applications generally involve the introduction of an ion motion barrier in the electrolyte, achieved by the cell monolayer deposition at the channel/gate boundary.[63] Thus, a spatial map of the electrophysiological activity[63] and monitoring of barrier tissue formation[64] can be acquired. Similarly, ion channels in supported lipid bilayers assembled on **PEDOT:PSS** channels were investigated.[65] Finally, upon the development of ion selectivity detection approaches, the detection of glucose and lactate, important electrolytes and metabolites, was achieved utilizing OECTs.[66]

The ongoing Coronavirus-19 pandemic has highlighted the need for rapid and simple testing in everyday conditions. As such, Arold, Grunberg, Inal, and co-workers have recently reported a nanobody-functionalized OECT with a modular architecture for the rapid quantification of single-molecule-to-nanomolar levels of specific antigens in biological fluids.[67] The sensors utilize a solution-processable glycolated polymer **p(g0T2-g6T2)** (see Figure 22) as the transistor channel material and bioconjugation of nanobody−SpyCatcher fusion

proteins on disposable gate electrodes. Impressively, results could be obtained within 10 min of exposure to a miniscule volume of an unprocessed sample, expressing outstanding specificity and single-molecule sensitivity in both human saliva and serum. Furthermore, the sensor can be reprogrammed for the detection of any protein antigen with the condition of the corresponding nanobody availability. The reported sensors were tested to detect not only green fluorescent protein but also SARS-CoV-2 and MERS-CoV spike proteins. Specifically, in case of COVID-19 screening, accurate reproducibility of the clinical results was observed.

While OECTs are benchmark devices finding applications in bioelectronics, a range of more complex iontronic systems, such as organic electronic ion pumps (OEIPs), ionic diodes and iontronic circuits, have also been developed.

1.1.3.1. Organic Electronic Ion Pumps. On demand delivery of biologically active species, especially targeting alkali ions and neurotransmitters, can be accomplished by exploiting the emerging organic electronic ion pump (OEIP) technology (Figure 4a).[68] The role of an OEIP is to transport ions or
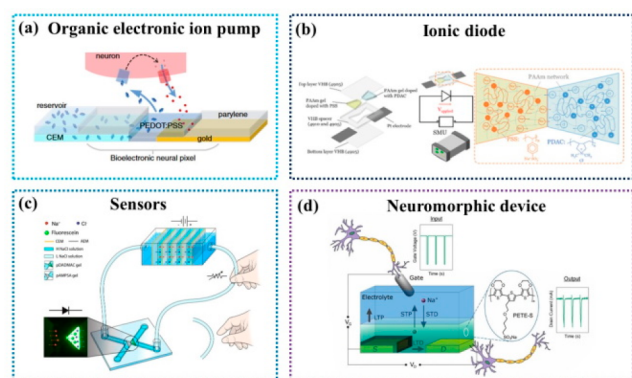

Figure 4. Bioelectronic applications of organic mixed conductors. (a) Bioelectronic neural pixel based on the OEIP utilizing **PEDOT:PSS**. Reproduced with permission from ref 74. Copyright 2016 the United States National Academy of Sciences. (b) Structure and fabrication of a hydrogel-based ionic diode. Reproduced with permission from ref 75. Copyright 2019 Elsevier. (c) Illustrative schematic of ionic circuit powered by reverse electrodialysis (RED). Voltage generated from RED is applied to microfluidic polyelectrolyte diode directly via tubes filled with electrolyte. Reproduced with permission from ref 76. Copyright 2017 Springer Nature. (d) Synaptic transistor based on the PETE-S polymer. Reproduced with permission from ref 77. Copyright 2019 Wiley.

biomolecules from an electrolyte reservoir to a target station (e.g., cells, tissue).[69] The ion conductive channel in an OEIP is sandwiched between two electrolyte reservoirs. For instance, the source reservoir contains the electrolyte with ready for transportation ions. In turn, the function of the second reservoir is to hold the biological object such as cell culture or tissue, targeted for the delivery of ions. The migration of ions occurs upon the application of an electric field between the electrodes. As a result, the source reservoir and the target outlet become divided and mobile charged species are electrophoretically "pumped" toward the oppositely charged electrode. The resulting ionic current is proportional to the applied electric field.[2] For instance, not only transport of protons, potassium, and sodium[56] was reported using the OEIP architecture but also biomolecules such as glutamate, acetylcholine, and γ-aminobutyric acid (GABA) has also been

delivered.[70−72] Unfortunately, large biomolecules, such as peptides and hormones, have not yet been successfully transported, presumably due to size-exclusion actions of the polyelectrolyte. Similarly to cation examples, the transport of anions (chloride and glutamic acid) has also been reported.[73]

1.1.3.2. Ionic Diodes. Ionic diodes, used for industrial electrolysis applications, are based on a junction between the polyions (polyanion and polycation) an example of a bipolar membrane. Ionic diodes can offer significantly more electronic control over ionic currents when compared to OEIPs. Bipolar membranes are prepared by using either anion- or cation-exchange membranes (AEM and CEM, respectively) as the electropohoretic transport channel. The selective transport of either positive or negative ions leads to proportional delivery rates and operating currents.[3] The current vs voltage characteristics of an ionic diode are apparently similar to that of a semiconductor p−n junction. Upon an application of bias, the dominant charge carriers in both layers of the bipolar membrane migrate toward the AEM/CEM junction in the middle, leading to a forward "on-current" between the electrolytes on either side of the bipolar membrane. The accumulation of ions at the junction can be observed, as the change of polarity at the junction prevents ions from crossing into the oppositely charged layers. Notably, when the concentration of ions in the junction becomes high enough, ion interchanging between AEM and CEM occurs.[78] When applying reverse bias, the dominant charge carriers will migrate in the opposite directions away from the junction. As a result, the junction becomes depleted of mobile ions, thus lowering the "off-current".[79,80] For example, a transparent stretchable ionic diode utilizing **PEDOT:PSS** was reported by Cai's group (Figure 4b).[75] Ionic diodes found application in electrical stimulation of neural interfaces as well. Additionally, miniaturized ionic polarization diodes, capable of neurotransmitter delivery and electrical stimulation of neural tissue, were developed by Simon, Tybrandt, and co-workers.[69]

1.1.3.3. Sensors. Because of high transconductance and voltage-efficient operations, OECTs can be incorporated in circuits.[55] As such, sensing applications are possible when combining OECTs with silicon-based integrated circuits (Figure 4c).[76] For instance, when compared to a single **PEDOT:PSS**-based OECT sensor, a circuit utilizing the same materials exhibited a 10-fold sensitivity increase.[82] Such enormous sensitivity enhancement can find use in metabolite detection. Thus, an iontronic circuit consisting of two **PEDOT:PSS**-based OECTs can be used for lactate sensing.[80] The intensity of electrocardiographic signals can be greatly improved, when a voltage amplifier, combining an OECT with a high transconductance value with a resistor, is exploited.[81]

1.1.3.4. Memory and Neuromorphic Devices. Currently, a great effort is dedicated to the development of the device networks binding computation and memory. Memristors, or transistors with a "memory" of their former electronic states, constitute the target of neuromorphic computing. The latter, in turn, are aimed toward the development of artificial technologies that imitate the capability of the neurological system, striving to increase computational efficiency.[47] The devices featuring either temporary or permanent changes in their electrical properties, leading to the short- or long-term memory simulation, underpin the operation of neuromorphic systems (Figure 4d).[55] Because of the intrinsic ion capability to affect the electrical state of the channel OECT material, OECT-based devices serve as a foundation for a number of

memory and neuromorphic devices.[55] Such important neuromorphic functions, as adaptation, paired-pulse depression, and dynamic filtering, were demonstrated by the first neuromorphic transistor based on a **PEDOT:PSS**.[82] Furthermore, power consumption was significantly lowered in polymer nanofiber based devices (energies reaching 1.23 fJ each synaptic spike).[83] Similarly, alternative architecture, utilizing a single gate and numerous channels, described the imitation of homeostatic plasticity functions of the brain.[84,85] Detailed information on the materials strategies for organic neuromorphic devices can be found elsewhere.[88]

1.2. Charge Injection and Ionic−Electronic Coupling in Organic Mixed Ionic and Electronic Semiconducting Materials for OECTs

To fully understand OECT performance, it is important to gain insight into electronic and ionic transport in OMIECs. As was mentioned previously, the properties of conjugated polymers make them an ideal platform for utilization in OECTs. Because of the permeability of conjugated polymers, ions in the electrolyte are able to infiltrate into the bulk of the transistor channel under the influence of an electric field (Figure 5a). First, the polymer film swells due to hydration by the electrolyte solution. Swelling leads to the penetration of water molecules and ions into the volume of the polymer film. When an electrochemical bias is applied, the previously infiltrated cations (in the case of a p-type OMIEC) are expelled from the film, which is followed by the injection of anions at higher voltages. As a result, the redox state of the organic semiconductor is altered and electrical conductivity of the channel is changed. Dedoping follows the process described above in reverse.[38] The reversible ion exchange and charge compensation process is at the core of the operational mechanism of OECTs, making them efficient transducers from ions to electrons capable of amplifying minor chemical signals.[86]

1.2.1. Electronic Conduction. At the materials level, charge injection and transport are tightly connected to the chemical structure and morphology of the polymer. Net ionic charge (the excess ionic charge) of the opposite sign is essential to ensure the occurrence of the electronic charge in an OMIEC. The doping process refers to the counterbalancing of the excess ionic charge with the electronic charge. This process leads to the increase in the electrical conductivity in the mixed conductor. An unequivocal electronic/excess ionic charge equilibrium concentration exists in the absence of an externally applied potential. This equilibrium depends on the energy of the OMIECs molecular orbitals. In the case of a sufficiently shallow highest occupied molecular orbital (HOMO), p-doping occurs if the condition of the hole stabilization of the OMIEC by an excess anion is met. Alternatively, when stabilized by a cation, negative electronic charge is energetically favorable in the case of a deep lowest unoccupied molecular orbital (LUMO), giving rise to n-doping. However, ionic−electronic charge coupling is destabilized and unfavorable in the case of a deep HOMO and a shallow LUMO, leading to the poor electrical conductivity of an undoped OMIEC. Notably, p-type OMIECs dominate the literature compared to their n-type counterparts. Therefore, development of n-type OMIECs is particularly important.[88]

Electronic conduction depends on both charge concentration and mobility. In turn, electronic transport in conjugated compounds is ensured by the overlap of π-orbitals regardless of
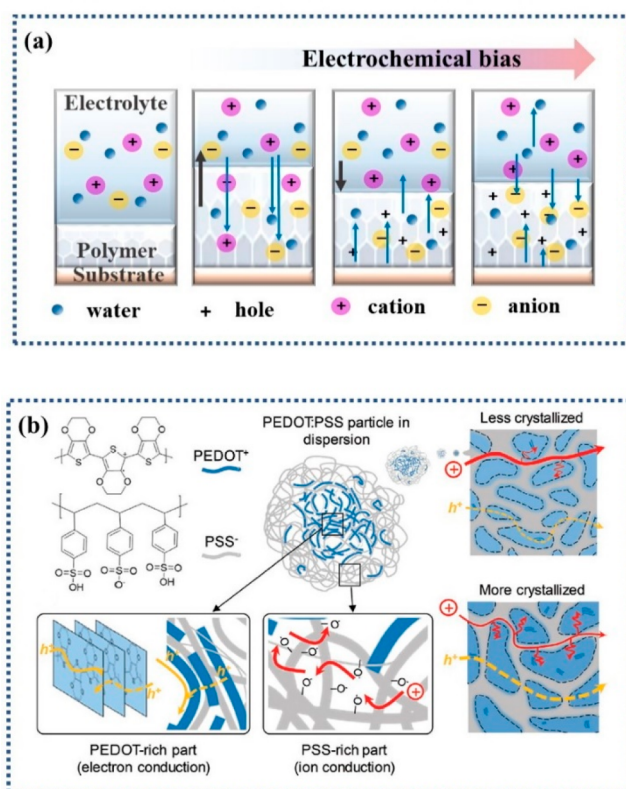

Figure 5. Polymer doping fundamentals on the example of a p-type polymer. (a) Mechanism of the polymer oxidation, including the stages of the swelling of the polymer film due to hydration and ion injection. Panel 1 shows the polymer on a conductive substrate. The polymer swells and hydrates drastically upon contact with the electrolyte. (panel 2) in the absence of bias. Hydration includes transport of water, positively and negatively charged ions, across the interface between the polymer and the electrolyte. Panel 3 shows that upon the initial hole injection into the bulk of the polymer film, cations are ejected and significant solvent volumes are expelled. Cation depletion leads to the anion injection into the film until the mass balance is restored. This is then followed by conventional charge compensation via anion injection (panel 4). The mechanism of reduction (dedoping) proceeds in a similar, though reversed, manner, whereby, the injection of cations and solvent follows the ejection of the anions. Black arrows refer to the change in the polymer film volume (swelling); the blue arrows correspond to the transport of charged species (injection/ejection) upon initial hydration (second panel) and subsequent bias (third and fourth panels). Adapted with the permission from ref 38. Copyright 2020 American Chemical Society. (b) Chemical structure of **PEDOT:PSS**, as well as a schematic depicting the particle microstructure of **PEDOT:PSS**. Schematic images of the **PEDOT** rich core region and PSS-rich region in the **PEDOT:PSS** particle. Schematic representing film microstructure of **PEDOT:PSS**. Electron transport takes place in (semi)crystalline regions of the polymer, featuring $\pi-\pi$ stacking, while ionic transport occurs in the amorphous regions subject to swelling upon hydration. Reproduced with permission from ref 87. Copyright 2020 Wiley.

the molecule size. The convergence of π-orbitals can occur intramolecularly (linearly and through space) and intermolecularly (through space). In the case of conjugated polymers, free electron migration along the whole polymer backbone allows for the linear intramolecular electronic transport, while π-stacking of the adjacent polymer chains leads to the intermolecular charge transfer and electron hopping between

the chains. In contrast to small, conjugated molecules, conjugated polymers, utilizing the same chromophore units, are capable of reaching higher charge mobility values owing to the higher concentration of the charge carriers.[47,89] Additionally, introduction of small molecule dopants to the polymer bulk can result in further enhancement of the number of charge carriers.[90]

In terms of molecular design, both efficient delocalization and minimized bandgap, essential for the improved electronic charge transport, can be achieved by constructing planarized backbones and utilizing rigid molecular units. Not only is polymer skeleton planarity beneficial for the extension of the linear charge conduction range, but it also enables interchain transport by means of $\pi-\pi$ stacking.[91] As a result, adequate charge transport can be achieved in the bulk of the polymer, which is potentially important for the target device applications. Regarding polymer morphology, $\pi-\pi$ stacking of the polymer chains results in the formation of crystalline regions, leading to higher electronic transport (Figure 5b).[92,93] Even though rigidification of the structure, leading to the charge hopping through the crystalline regions of the polymer, remains the main strategy for boosting the electronic conduction, high charge mobilities were reported also in the amorphous linear polymers with high molecular weight.[94]

1.2.2. Charge Injection and Ionic Conduction. The ability to transport ions sets OMIECs apart from other conjugated materials. As mentioned earlier, polymers tend to swell upon contact with the electrolyte. Softness and permeability of the polymers insures infiltration of ionic charge carriers of various size. As a result, a larger number of ions can be accommodated in the less dense, amorphous part of the polymer, leading to enhanced ionic conduction (Figure 5b). Ionic transport can be quantified as an ionic conductivity (σ_{ionic}), the ion conductivities total for each mobile ionic species; i, the summation of the products of the ion charge (z_i), number density (n_i), elementary charge (e), and mobility (μ_i):

$$\sigma_{ionic} = \sum_i n_i |z_i| e \mu_i \tag{2}$$

In turn, ionic mobilities and diffusivities (D) are interconvertible via the Einstein relation (eq 3), where k_B is Boltzmann's constant and T is temperature:

$$D = \frac{\mu k_B T}{e} \tag{3}$$

The contents of the electrolyte are exceptionally important for ionic conduction in the polymer bulk. First, the ionic pair (salt) of the electrolyte should be able to dissociate.[47] Otherwise, no response to the applied voltage will occur and no conduction will be observed. Hence, prompt dissociation of the counterion from the ion of choice must be ensured. For instance, lithium salts, often utilized in OECTs and batteries, tend to employ bulky counterions, such as bistriflimide (TSFI) and PF_6^-, to guarantee facilitated dissociation.[95] On par with dissociation, both the nature of the ion and that of the electrolyte/mixed conductor is of paramount importance to the rate of ion migration. As the activation energy, essential for ion hopping between the adjacent cavities of the matrix, increases with the size of the ion, larger ions have a tendency for slower movement and lower conductivity. This concept was successfully proven while investigating polar electrolytes.[96,97] Additionally, incorporating coordinating atoms, such as oxygen and nitrogen, into the dissolution medium was shown to

enhance the scope of dissociation by stabilizing the charge of the free atom.[98] For instance, poly(ethylene oxide) (PEO) is a generic example of a nonconjugated polymer ionic conductor. Owing to its high chain flexibility, leading to the coordination with a variety of cations (Na^+, Li^+, Mg^{2+}, K^+), PEO reaches high values of ionic conductivity.[102] However, its tendency to crystallize greatly inhibits conduction below the melting temperature.[99]

While ionic transport in nonconjugated polymers, such as PEO, was suggested to occur via the reptation-assisted ionic species random hopping along the polymer backbone.[100] As such, the mechanism of ion injection into the bulk of conjugated polymers is currently a hot topic. For instance, ions are subject to hopping in conjunction with the OMIEC skeleton segmental motion, analogous with the movement of nonconjugated conductors, in either dry or slightly hydrated films. The improvement of such transport, assisted by the segmental motion, can be achieved with the introduction of ion-coordinating species. Upon contact with a liquid electrolyte, ion transport proceeds more swiftly via solvated ion transport, displaying ion mobilities comparable to those of similar ions in water ($\mu_{ion} \approx 10^{-3}$ cm^2 V^{-1} s^{-1}).[101] In water-swollen OMIECs, rapid hopping of protons between water and hydronium species, following the Grotthuss mechanism, leads to enhanced proton conduction ($\mu_{h+} \approx 5 \times 10^{-3}$ cm^2 V^{-1} s^{-1}).[102] The most well-studied OMIEC, **PEDOT:PSS**, was found to transport not only smaller ions, with the ion mobility increasing in the range $H^+ > K^+ > Na^+$ but also a considerably bulkier choline cation.[101] As doping of the p-type conductive polymers leads to anionic transport, studying the effects of the commonly used anions is of use. Thus, property investigation of several doped thiophene-based polymers revealed that larger ions, such as TSFI and PF_6^-, are prone to more efficient doping when compared to the anions of smaller size (ClO_4^-, Cl^-). Not only have the larger anions shown a higher ion migration rate of into the polymer bulk but also a decreased level of hydration was observed.[103,104] Interestingly, the opposite trend was observed in polar materials, such as poly(2-(3,3′-bis(2-(2-(2-methoxyethoxy)-ethoxy)ethoxy)-[2,2′-bithiophen]-5-yl)thieno[3,2-b]thiophene) [**p(g2T-TT)**] (see Figure 21)[104] and perfluoroether electrolytes,[99] which are hydrophilic as opposed to the relatively hydrophobic poly(3-hexylthiophene-2,5-diyl) (**P3HT**).[103] The need for further anion specific investigations in OMIECs, considering the ionic species, the polymer and the solvent, remains.

1.2.3. Ionic−Electronic Coupling. It is worth noting that interactions of the ions with the conjugated polymer chains can lead to significant changes in the local structure, hence, affecting the electronic transport. Therefore, ionic transport in conjugated polymers cannot be addressed independently; instead, the coupling between ionic and electronic conduction needs to be studied. Owing to its volumetric nature, this coupling between the electronic and ionic charge species administers the whole range of electronic, physical, and chemical characteristics of the polymer. In turn, the dynamic control of this coupling oversees both charge accumulation and ion exchange, which can readily find application in various electrochemical devices, including OECTs.[86]

The concept of ionic−electronic coupling is closely related to the charge injection phenomenon. Electronic charge can be either injected or collected at the interface between an electrode and an OMIEC, it can be also transported via the π-conjugated backbone. The electrolyte-supplied dopant ion

helps to stabilize the electronic charge electrostatically. It is important to understand that most conjugated polymers generally do not undergo intrinsic electrochemical processes like well-defined molecules. Instead, charge is more often delocalized and distributed nonuniformly over a changing number of repeat units, with intermolecular ordering controlling this degree of delocalization. Therefore, charge injection cannot be considered as a faradaic process, while it does not fully preclude the latter. Neither can charge injection be labeled as an electrostatic phenomenon, as charge transfer occurs not between the dopant cations and the repeat units but between the contacting metal electrode and the OMIEC. Finally, OMIEC charging cannot be perceived as pseudocapacitive. For better understanding of the charge injection mechanism, Rivnay and co-workers suggest considering electronic state distribution, intermolecular interaction, disorder, and energy level related physical phenomena while describing the charge transport.[88]

The extent of electronic−ionic coupling in OMIECs can be modulated with an applied bias, while coupling through an electrolyte, which results in a potential-dependent capacitance, characterizes the efficiency of ionic−electronic coupling. Not only can this coupling cause the occupancy of electronic states to change, reversibly leaching the UV−vis transitions in electrochromic devices, but it is also responsible for the modulation of the OMIEC electrical conductivity in a variety of OECT and neuromorphic devices.[88] In application-relevant conditions, charge carrier mobility can depend on the carrier density in a nonmonotonic manner, with dopant concentrations and electronic charge carrier density ranging across several orders of magnitude. While at lower concentrations the dopant ions can act as Coulombic traps for electronic charge carriers,[105] increasing the dopant levels leads to a decrease of the charge hopping activation energy, hence boosting carrier mobility. However, at extreme doping levels, the increased disorder becomes the driving force for carrier localization, resulting in a plateau or even decrease in electronic charge carrier mobility.[106]

Compared to inorganic mixed conductors, with high ionic and electronic conductivities at elevated temperatures, that have been developed for applications in hydrogen separation membranes, organic mixed conductors possess much more complicated ionic−electronic coupling due to hydration and swelling. Therefore, understanding the interplay between ionic and electronic transport, ionic−electronic coupling, the dependence on processing, chemical structure, morphology, and electrolyte choice, as well as fundamental materials structure−property relationships, is of paramount importance.[107]

1.2.4. Morphology Effects. To investigate the ionic−electronic coupling, understanding of the changes in polymer morphology upon doping is crucial. While it is known that conjugated polymer films tend to expand and swell upon the electrolyte uptake, little is known about the morphological changes within the film. Examination of structure−property relationship of two polythiophene derivatives with ethylene glycol-based side chains, (poly(3-(methoxyethoxyethoxy)-thiophene) (**P3MEET**) and (poly(3-(methoxyethoxyethoxy-methyl)thiophene) (**P3MEEMT**) (see Figure 22), differing by an additional methylene spacer in the alkoxy substituent, by Dong et al., proved that doping with lithium bis-(trifluoromethanesulfonyl)imide (**LiTFSI**) leads to the disruption in the crystalline structure. Additionally, it was

observed that the dopant infiltrates both in the crystalline and amorphous domains even at low concentrations, although the preference was given to the amorphous areas. Indeed, studying the temperature dependence of ionic conductivity at various concentrations of **LiTFSI** confirmed that ionic transport is facilitated and dominated within amorphous regions of the film.[33]

Subsequent detailed experimental investigation of the annealed and unannealed films of **P3MEEMT**, possessing different degrees of crystallinity, by Flagg and co-workers, revealed very different hydration dynamics upon electrochemical doping.[38] As presented in Figure 6a, the annealed
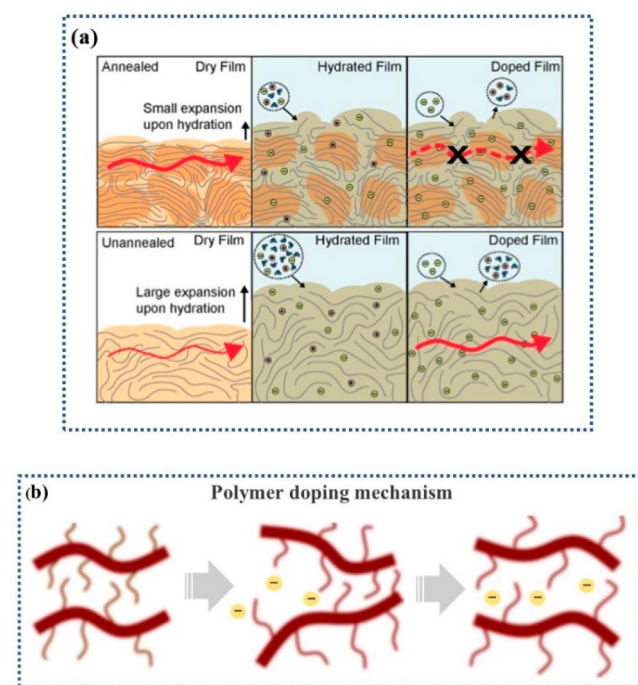
Figure 6. (a) Schematic underlaying the differences in doping and charge transport in the annealed and unannealed OMIEC films. Reproduced with permission from ref 38. Copyright 2019 American Chemical Society. (b) Schematic of the polymer doping mechanism, including the stages of unzipping and zipping of the polymer chains. Reproduced with the permission from ref 36. Copyright 2020 American Chemical Society.

film is more crystalline and shows higher mobility than the unannealed film prior to the electrolyte treatment. Upon treatment, both crystalline and amorphous regions swell in the annealed sample. In turn, the unannealed amorphous film facilitates more electrolyte solution infiltration and is prone to more efficient swelling. Interestingly, upon electrochemical doping, the overall mobility of the unannealed sample subdues that of the annealed one. Such decrease in the mobility of a crystalline polymer was attributed to the disconnection between the amorphous and crystalline regions, leading to film heterogeneity.[38] These results clearly point at the ionic−electronic coupling and the necessity of designing efficient OMIECs, retaining the trade-off between electronic and ionic conduction. Thus, while readily hydrated crystal lattices allow for faster anion injection, facilitating ion transport, the disruption in crystallinity due to hydration affects the electronic transport dramatically. The complex interaction between ionic and electronic transport, polymer structure,

steady-state, and time-dependent hydration upon electrochemical doping has an acute impact on the target OECT performance. By understanding these challenges, it may be possible to fine-tune the morphology of future OMIECs so that they benefit from improved polymer crystallinity.[38]

The design of conjugated OMIECs has borrowed inspiration from that of nonconjugated ion-transporting polymers, for instance, the widely applied ethylene glycol side chain strategy,[34−36,54,90] has been inspired by PEO. However, while the ion motion in PEO was assigned to polymer chain reptation,[100] the mechanism of ion uptake by the conjugated OMIECs remained unclear. Recently, Bischak and co-workers suggested that conjugated polymers can undergo reversible structural phase transitions during electrochemical oxidation and ion injection.[36] Using grazing incidence wide-angle X-ray scattering (GIWAXS) to study poly[2,5-bis(thiophenyl)-1,4-bis(2-(2-(2-methoxyethoxy)ethoxy)-ethoxy)benzene] (**PB2T-TEG**) (see Figure 21), a conjugated polymer with glycolated side chains, the authors showed that the polymer transitions between two structurally different crystalline states related to the electrochemical reactions in an aqueous electrolyte. While in the neutral form the morphology of the polymer in question is dictated by side chain crystallization, ion infiltration results in the disorder of glycolated side chains and $\pi-\pi$ stacking of the polymer backbone, which planarizes upon oxidation. The resulting phase separation is suggested to occur via the untwisting motion of the polymer, leading to the unzipping of the polymer chains (Figure 6b). Electrochemical oxidation of the unzipped regions of the polymer is proposed to be energetically beneficial, leading to a nucleation process and growth-associated kinetics of ion insertion. Upon oxidation and ion insertion, $\pi-\pi$ stacking dictates the morphology of the polymer, leading to the subsequent zipping of the polymer chains. A combination of GIWAXS and absorption experiments confirmed the observation of the ion−polaron pair, which requires sufficiently high ion and electron mobilities to diffuse in OMIECs. Of note, such reversible structure phase transitions upon electrochemical ion insertion were previously observed solely in inorganic materials.[108] Engineering structural phase transitions in conjugated polymers is proposed to be an efficient strategy for achieving desirable electrochemical properties and can find use in computing and energy storage applications.[36] As a general rule, understanding of the unzipping mechanism in semicrystalline OMIECs is exceptionally important for the design of future materials with controllable properties.

1.3. Characterization Methods of OMIEC Materials for OECTs

The complex interplay of molecular structure, electrolyte nature, and morphology are responsible for the properties of ionic and electronic transport, as well as ionic−electronic coupling in mixed conductors. To establish detailed structure−property relationships in these materials, materials scientists have developed and continue elaborating, a toolbox of characterization methods. To underpin the underlying processes in OMIECs, structural classification must be consolidated with both ionic and electronic transport processes, including ionic−electronic coupling. However, the dynamic nature of OMIECs makes steady-state measurements relating structure and properties inadequate. Alternative investigations of structure−property relationships need to be

conducted with a variety of conditions, for instance, tuning electrolyte concentrations and electrochemical potentials.[88]

Certain insights into OMIEC material properties can be acquired through numerous techniques commonly used in organic electronics (OFETs, OPVs, OLEDs, and electrochromic diodes). Thus, information extracted from cyclic voltammetry (CV), transistor mobility, electrochemical impedance spectroscopy, GIWAXS, and spectroelectrochemistry can prove valuable for understanding OMIECs inner properties.[20] For instance, CV uncovers the information about the oxidation and reduction potentials of the material, energy levels, and electrochemical stability.[109] In turn, in the context of OECTs, spectroelectrochemistry measurements allow for the evaluation of the polymer film doping efficiency by combinatorial accession of spectroscopic and electrochemical information. A generic spectroelectrochemical setup involves coating the conductive electrode with the material of interest and placing in the electrolyte solution along with counter and reference electrodes. To evaluate the electrochromic characteristics of the material, absorption is recorded at various voltages.[110] For example, in **PEDOT** doping, upon the application of increasingly positive potentials is accompanied by the occurrence of a polaronic absorption band around 900 nm along with the intensity drop of the shorter wavelength $\pi-\pi^*$ absorption band. This process is in turn followed by the disappearance of the polaronic absorption and consequent appearance of a bipolaron band (Figure 7a). Not only is this
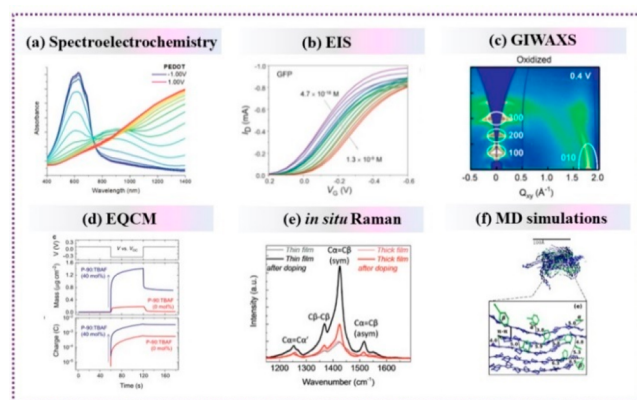

Figure 7. Schematic of the OMIEC and OECT characterization methods, discussed in this work. (a) Spectroelectrochemistry spectra of **PEDOT** on an ITO substrate with an applied gate voltage ranging from −1.0 V to +1.0 V, with increments of 0.1 V, recorded in an organic electrolyte. Reproduced with permission from ref 20. Copyright 2019 Wiley. (b) Electrochemical impedance spectroscopy (EIS) measurements conducted on **p(g0T2-g6T2)** polymer. Reproduced with permission from ref 115. Copyright 2020 Medxriv. (c) In operando GIWAXS pattern of dry oxidized **PB2T-TEG** polymer. Reproduced with permission from ref 36. Copyright 2020 American Chemical Society. (d) EQCM-D recording of neat **P-90** and **P-90:TBAF** systems, exposed to 0.1 M NaCl (aqueous) electrolyte at 0.45 V electrochemical-doping potential. Reproduced with permission from ref 116. Copyright 2020 Springer Nature. (e) In situ Raman **PEDOT:PSS** films spectra recorded prior to and following the electrochemical reduction (at 0.6 V vs Ag/AgCl for 10 min in 0.1 M NaCl). Reproduced with permission from ref 117. Copyright 2018 Royal Society of Chemistry. (f) Snapshot of the **PEDOT:TOS** structure along with a zoom of a representative crystallite, acquired by means of molecular dynamics (MD) simulations. Reproduced with permission from ref 118. Copyright 2017 American Chemical Society.

technique useful for studying charging and discharging in OMIECs, but it is also helpful for the identification of chemical degradation upon the formation of bipolaron states.[20,111,112] Electrochemical impedance spectroscopy (EIS) presents an invaluable opportunity to concurrently separate and characterize ionic and electronic transport, as well as quantify ionic−electronic coupling. In EIS, current−voltage small signal analysis is exploited to measure the frequency-dependent impedance of the OMIEC channel. As a result, ionic and electronic mobility, and conductivity, as well as ionic−electronic coupling, characterized by volumetric capacitance or electrochemical density of states, can be extracted. OMIECs generally present significantly more complex impedance spectra, hence, they require the exploitation of transmission line models for complete analysis. Nevertheless, EIS offers a reliable route toward characterization of the magnitude of ionic−electronic coupling, recorded as the frequency or voltage-dependent capacitance (Figure 7b).[88,113,114] Finally, evolution of the morphological microstructure upon water exposure can be related to the ionic−electronic coupling by combining OECT studies with ex situ GIWAXS. For example, combining GIWAXS, moving front ion transport and resonant soft X-ray scattering methods while investigating the properties of **PEDOT:PSS** unraveled the decrease in ionic transport, associated with the development of a beneficiary for the electronic transport percolated microstructure.[37,104] GIWAXS also proved useful in thorough texture investigation of dry polymer films of the dialkoxybithiophene-*co*-thienothiophene derivatives **p(g2T-TT)** with various side chains, confirming side chain control of the lamellar spacing and $\pi-\pi$ stacking (Figure 7c).[35]

In addition to unveiling the intrinsic properties of OMIECs, full comprehension of the electrolyte-swollen structure of the latter can be unraveled by in operando and in situ characterization.[119] For instance, combination of in operando GIWAXS and spectroscopic studies has confirmed preferential occupancy of the amorphous regions by the dopant ions and correspondent electronic charge transport in the crystalline domains in poly(3-hexylthiophene).[120] This result verified the predominantly amorphous structure of OMIECs, while the results obtained from X-ray are limited to the crystalline domains. Noteworthy, time-resolved structural evolution of an OMIEC during electrochemical doping and dedoping was recently reported using in operando GIWAXS. Unequal rates of structural changes were revealed by time-resolved operando GIWAXS when compared to the steady-state in situ measurements.[119] Invaluable information on the effects of swelling on the polymer structure can be obtained by electrochemical quartz crystal microbalance with dissipation monitoring (EQCM-D). The latter technique helps to evaluate the amount of electrolyte incorporated into the film upon doping, as excessive amount of water in the electrolyte is known to impede the electrochemical switching speed and impair the doping process reversibility. In situ changes in the polymer film mass can be recorded by employing EQCM-D, monitoring the OMIEC, which is coated onto a piezoelectric crystal, as the film experiences electrochemical contact with the electrolyte (Figure 7d). The change in dissipation of energy of the oscillating crystal, as well as changing frequency, reflects the mass gain of the polymer film during the doping process.[35] While examining the properties of **p(g2T-TT)**, upon doping by EQCM-D, GIWAXS, and in situ Raman spectroscopy, Inal et al. observed a decrease in hole mobility, resulting from the

excessive water uptake and permanent lamellar disruption upon doping. Consequently, further hydration of the **p(g2T-TT)**-based OECT yielded transconductance reduction, raising the concern of the pertinent level of hydration in efficient OECTs. These observations proved that swelling of the OMIEC channel, while necessary, should be addressed with caution in order to avoid adverse changes in the microstructure of the OMIEC film.[121] While EQCM-D provides insights on the effects of polymer swelling, it is also useful for studying the doping mechanism. Thus, EQCM-D examination of the thiophene-based polymer **P3MEEMT** showed that the polymer loses mass during the early stages of doping, suggesting significant expulsion of cations takes place prior to conventional doping via anion injection.[38] This result was elegantly verified by direct ion concentration measurement in polymer films employing glow discharge optical emission spectroscopy (GDOES): while prior to the application of a gate bias both cations and anions are present in the film, the concentration of cations was found to decease rapidly upon applying an oxidative potential the application of an oxidative gate potential. Consequent doping leads to the increase of the anion population in the film. Finally, upon the removal of bias the initial number of cations and anions is restored.[38]

In operando and in situ spectroscopic and microscopic techniques can also contribute to probing the amorphous domains. For instance, in situ Raman spectroscopy was exploited while evaluating the degree of ionic−electronic coupling, as well as measuring the nature of electronic charging in OMIECs (Figure 7e).[98,117] Additionally, the domain-specific electrochemical potential, resulting in the heterogeneity map, was obtained using electrochemical strain microscopy.[122] In situ atomic force microscopy (AFM) can also be applied to examine polymer surface morphologies upon doping and dedoping: in situ AFM measurements of **p(g2T-TT)** polymers with various ethylene glycol (EG)-based side chains showed that the OMIECs bearing highest EG content revealed an expansion of their surface after doping.[35]

Thorough understanding of structure−property relationships in OMIECs calls for a combinatorial theoretical and experimental approach. However, complex dynamic structure of OMIECs requires costly computational resources for modeling the dynamic properties. Molecular dynamics simulations, investigating the molecular scale structure, interactions, and their effect on ionic and electronic transport, as well as ionic−electronic coupling, have been reported (Figure 7f).[33,118] Furthermore, it is expected that multiscale modeling will be essential to bridge the gaps of structural and transport information that are experimentally inaccessible.[88] While the number of structure−property investigations in OMIECs is still limited, the overall picture, essential for the fabrication of more efficient OECTs, has begun to emerge. However, further investigation of polymer microstructure is crucial for the design of future OMIECs.

2. MATERIAL DEVELOPMENT FOR OECT APPLICATIONS

2.1. Materials Requirements

Having reviewed the operation principles, applications, and principal features of OECTs, it is important to discuss the synthetic design requirements and considerations of the active layer OMIEC materials. To achieve a trade-off in the OECT performance, new materials exhibiting maximum transconduc-

tance at voltages within the stable operating regime of the transistor/electrolyte system should be designed.[123] To accomplish this condition, the material of choice must support both electronic and ionic conductivity, displaying an adequate charge mobility, and show resistance toward external factors, such as temperature, electrical bias, moisture, and air. Furthermore, a fragile balance that allows for the following features must be fulfilled: (i) sufficient permeation of ions from the electrolyte throughout the bulk of the OMIEC film, while preventing dissolution, maintaining structural integrity, (ii) reversible transport of ions, (iii) transporting electronic charges while preventing ionic dopants, from the electrolyte, acting as trap sites, and (iv) extreme sensitivity to the surrounding media (e.g., electrolyte, analytes, and confounding species), which will be contingent on the desired OECT device application.[124] Last but not least, OMIEC materials must be biocompatible to qualify for practical bioelectronic applications. All of these conditions can be successfully accomplished by organic semiconductors, and in particular, by OMIEC conjugated polymers.

2.2. Materials Classification

There are several approaches to the classification of OMIECs. First, according to the ability to solvate mobile ionic species, OMIEC materials can be divided into two categories: those which intrinsically bear ionic charge and those which do not. For polymer-based OMIECs, this translates into the difference between polyelectrolytes and polymer electrolytes.[88] For instance, OMIECs bearing ionic charge, either exist as a self-balanced zwitterion or carry a stable ionic moiety, accompanied by a counterbalancing ion or a stabilized electronic charge.[125] Alternatively, some OMIECs are not inherently charged, however, they may contain polar moieties capable of ion solvation. Conversely, for noncharged OMIECs, ionic moieties can permeate into the bulk of the OMIEC upon interaction with an electrolyte.

Furthermore, OMIEC materials can be classified according to their chemical composition: homogeneous type, whereby ionic and electronic charge transport occurs within an individual material or in a blend of the materials; heterogeneous type, if the regions of merely ionic and electronic conductivity are segregated. Historically, the most reported and commercially available OMIEC, **PEDOT:PSS**, which represents a prototypical example of a two-component, heterogeneous OMIEC material.[126] Block copolymers, macromolecules with distinguished segments of ionic and electronic conduction, represent another example of the heterogeneous type.[127] While heterogeneous OMIECs are subject to the microphase separation between ion conducting and π-conjugated components, the materials of the homogeneous type do not suffer from this issue. Homogeneous OMIECs generally incorporate charged or polar groups, often through side chain engineering utilizing EG-based moieties, within a single material, producing a bulk mixed conduction phase by distributing ion solvating fragments along the polymer backbone. Such homogeneous systems are known to share a plethora of common features with traditional conjugated polymers, with the notable addition of enhanced ion miscibility, while also limiting detrimental swelling effects incurred from the hydration sphere surrounding ionic dopants.[88,121] Detailed accounts on the homogeneous and heterogeneous types can be found elsewhere.[47,88]

Finally, OMIECs can be categorized according to the nature of the dominant electronic charge carrier within the polymer backbone. As such, materials are generally referred to as p-type and n-type. Whereby, p-type semiconductors are generally constructed from electron rich (donating) fragments and transport holes and n-type materials utilize electrons as charge carriers and are comprised of electron deficient (withdrawing) moieties. In this review, we focus on the classification of OMIEC materials according to the electronic charge carrier (p/n-type). The detailed description of p/n-type materials along with the discussion of the fundamental features of doping is presented below.

2.3. Organic Semiconducting Polymers

2.3.1. Charge Carrier Classifications: *p*-Type or *n*-Type.
Organic semiconductors are the most common active layer mixed conduction materials and are generally comprised of conjugated polymers, the first of which, polyacetylene, was reported by Shirakawa in 1967.[128] Following the sp²-hybridized bonding regime, the resultant alternating single bond−double bond structure in the conjugated backbone results in one-dimensional delocalization of the π-electrons, forming a filled valence band (π-band) and empty conduction bands (π*-band).[129] The energy difference between these two bands is defined as the bandgap, which generally ranges from 1 → 4 eV for a semiconductor.[130] For conjugated polymers, the magnitude of the bandgap and the energy levels of the HOMO and LUMO are the most important characteristics for determining the optoelectronic properties, heavily influencing their respective device performance.

Conjugated polymers are bonded together through strong intramolecular interactions but exhibit weaker intermolecular electronic interactions due to poorer electronic wave function overlap between adjacent chains. This manifests in the ground state as a localization of the wave function to a single chromophore. These effects combine to facilitate conjugated polymers holding an excess of charge, arising from oxidation, reduction, charge injection (doping), or photoinduced charge transfer. This additional charge, formally a quasi-particle, is defined as a polaron which can either be positive (Figure 8) or negative (Figure 9) depending on the charge carrier, a hole or electron, respectively.[131]

Figure 8. (a) Structural changes of poly(*p*-phenylene) and the resultant HOMO and LUMO level occupancies for the neutral (ground state) and positively charged ((bi)polaron) excited states.[132] (b) Electron-rich thiophene-based p-type polymers **P3HT**[133] and **PBTTT**.[134]

Most π-conjugated polyaromatic materials contain electron-rich aromatic cores, with relatively high HOMO levels thus operating as p-type semiconductors.[135] Over the last 40 years, the thiophene moiety has gained an extraordinary popularity as one of the most widely exploited building blocks for polymer OFET devices, with the most famous thiophene-based material
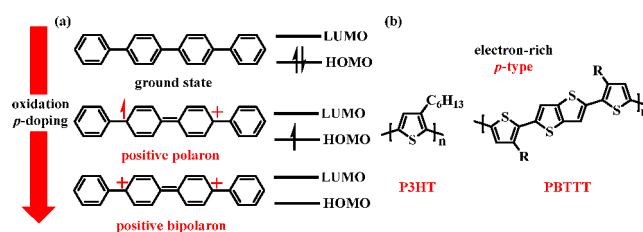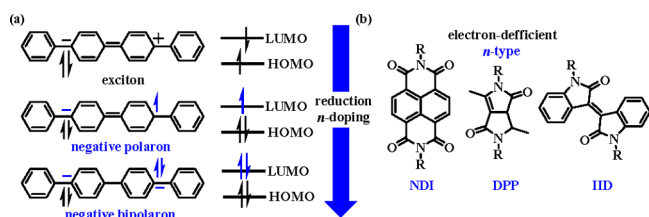
Figure 9. (a). Structural changes of poly(p-phenylene) and the resultant HOMO and LUMO level occupancies for the neutral (exciton) and negatively charged ((bi)polaron) excited states.[132] (b) Electron-deficient building blocks: naphthalenediimides (**NDI**),[137] diketopyrrolopyrrole (**DPP**),[138] and isoindigo (**IID**).[139]

to date being poly(3-hexylthiophene) (**P3HT**), an alkylated polythiophene which has been synthetically manufactured to adopt a regioregular structure.[133] The field of OSCs has been dominated by p-type materials, with multiple approaches to improve their stability and performance being extensively investigated. These strategies range from side chain engineering to studying the torsion of the backbone and introducing conjugated units into the polymer backbone.[136] Employing these rules, work within the McCulloch group raised the HOMO energy (~0.3 eV, cf. **P3HT**), by delocalized electrons along the extended aromatic polymer chain, creating a series of copolymers based on thieno[3,2-b]thiophene (**TT**) and thiophene rings namely **PBTTT**, enhancing the charge carrier mobility through the highly organized morphology imparted by interdigitation of the side chains.[134]

A common method to improve semiconductor performance in inorganic materials is to dope them via the addition of external atoms, often boron (p-type) or phosphorus (n-type), to modify the intrinsic conductivity.[140] Rather than simple atom substitutions in the crystalline lattice, organic materials are doped by either oxidation or reduction reactions (chemically or electrochemically). This phenomenon can be applied to organic semiconductors, however, the level of doping varies wildly, from ppm (around 1%) for inorganics and up to ~35% for organics.[129]

Similarly, to inorganics, OSCs can be doped in the solid state, but owing to their inherent processability can also be doped in solution, which is often a much simpler method and is a major advantage for organic materials. Generally, this involves a form of redox chemistry, either oxidation (p-type) or reduction (n-type). This is a facile process and can be achieved simply by treating a solution of the OSC with a complementary dopant solution, the doped OSC can subsequently be deposited using conventional solution processing techniques. This method is not without its flaws; in this case, the dopant will also be deposited along with the OSC, which could lead to disorder, lowering device performance and OSC conductivity, once the critical dopant concentration is surpassed.[129] The Sirringhaus group[141] has shown that this can be avoided through solid-state doping, using vacuum deposition to treat prefabricated OSC films, observing diffusion in the bulk similar to solution doping.

p-Type doping involves removing electrons from the HOMO; conversely, n-type doping adds electrons to the LUMO, and both scenarios increase the charge carrier density, altering the conductivity and optoelectronic properties.[129,142] Taking the p-type doping of **P3HT** with FeCl$_3$ as an example of chemical doping, oxidation of the OSC forms a positive radical, referred to as a polaron, which is stabilized by the

reduced dopant counterion. Formation of the positive polaron shifts the relative HOMO level and shrinks the optical bandgap, facilitating an observable change in the absorption spectrum, the absorption at 520 nm is suppressed as the new 790 nm polaron absorption forms. Upon increased levels of doping, further oxidation forms a dication, namely a bipolaron. Here the optical bandgap is reduced even more and a low energy NIR absorption dominates the resultant UV−vis spectrum (Figure 10).[143] The same effect can be achieved
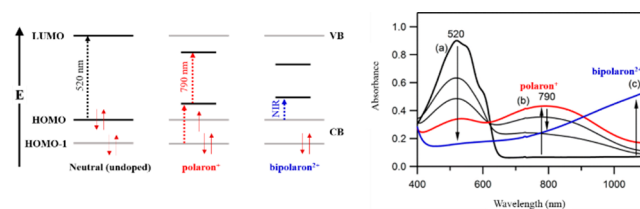

Figure 10. Schematic of the HOMO-1, HOMO, and LUMO levels of undoped, polaron$^+$ and bipolaron^{2+}, respectively. Allowed optical transitions are represented by dashed arrows and correlate to the absorption spectrum for **P3HT** doped with FeCl$_3$. Reproduced with permission from ref 143. Copyright 2015 American Chemical Society.

via electrochemical doping which involves placing the OSC between a metal electrode and an electrolyte. Extra charge carriers are injected from the metal electrode into the OSC, assuming the electron energy levels are appropriately aligned to facilitate charge transfer.

An alternative approach to doping will be discussed herein, whereby a material can be doped upon the interaction with an aqueous electrolyte containing mobile ionic species, the basic operating principle of an OECT.

2.3.2. Current Materials Design Challenges. Similarly to OFET devices, OECTs can operate in accumulation mode (where the active material is a semiconductor, e.g., a conjugated polymer and the device turns "on" upon voltage application)[144] or in depletion mode (where the conductive polymer serves as an active material and the device is "on" at no external bias).[145] One such example of the operation of an n-type accumulation mode OECT is illustrated below (Figure 11). Here application of a positive gate voltage leads to the

Figure 11. Operation principle of a n-type accumulation mode OECT (a) electron injection from the source upon applying a positive gate bias with cations migrating into the film, (b) transport through the n-type doped OSC from source to drain, (c) reversal of the gate bias leading to oxidation of the n-type doped OSC, electron collection at the source, and migration of the cations out of the active layer (i.e., switching).

reduction of the organic semiconductor as electrons are injected into the OSC channel and cations from the electrolyte migrate into the bulk OSC layer to compensate for the negative charges accumulating along the polymer backbone. This is equivalent to a volumetric n-doping of the OSC, which facilitates electron transport toward the drain electrode. Finally, the n-type doped OSC is oxidized back to its neutral

form upon reversing gate voltage, accompanied by cations migrating back into the electrolyte out of the OSC bulk.

Currently, the number of reported p-type (hole transporting) OECT materials greatly surpasses the number of published n-type (electron transport) materials. Furthermore, the performance of n-type OMIECs is overshadowed by their p-type counterparts by up to several orders of magnitude. Importantly, reduced power consumption, faster circuit speeds, and enhanced operational stability are expected from the development of complementary logic circuits, which is only possible with improved n-type materials, with performance metrics well-matched with current p-type materials.[42] Notably, the computed theoretical transport mechanisms adopted by both holes and electrons are identical and thus should not be considered as the limiting factor in the mediocre performance of n-type OMIECs.[146]

Indeed, the general poor OECT performance of n-type materials is derived from the electrochemical instability of most n-type OSCs which are commonly sensitive to air.[147] This is opposed to an inherent chemical instability, which means that synthetic manipulation can be invoked to improve the operational stability of these materials. However, the number of air-stable n-type materials is fleeting, and most electron transport devices are limited by electron traps, generated by moisture and oxygen, impeding the performance of n-type OTFTs.[148] While doped n-type materials are also prone to oxidation by a number of species including ozone and hydrogen peroxide, the most important reactions are those occurring with oxygen and water, as these potentials reside within the working electrochemical window of most common n-type OSCs.[149] Furthermore, the LUMO energy level was shown to dictate thermodynamic stability toward the electrochemical reactions, demonstrating that a shallow n-doped LUMO is subject to oxidation by both water and oxygen.[150] Importantly, when accounting for the overpotentials of these redox reactions, a LUMO level below ~ -4.0 eV is necessary to ensure stability in ambient conditions.[151] This is an essential syntenic design rule for any potential air-stable n-type OECT materials and one which should be carefully considered. These stability limitations and more specific synthetic design strategies for future n-type materials has been well summarized by Griggs et al.[152]

Encouragingly, these requirements have been met, for numerous examples,[91] generally by utilizing electron deficient units or through the inclusion of electron-withdrawing functionality. Common electron-deficient building blocks include naphthalenediimides (**NDI**),[137] diketopyrrolopyrrole (**DPP**),[138] and isoindigo (**IID**).[139] Alternatively, the electron density of aromatic building blocks can be further modulated by the introduction of heteroatoms or cyano groups to withdraw additional electron density.

Fortunately, manipulation of the LUMO level is not the only method toward n-type materials stability improvement, this can also be achieved by considering the $\pi-\pi$ stacking distances between polymer backbones. Reducing these can provide a kinetic obstacle to the diffusion of extrinsic molecules within the electron-transport layer, thereby limiting the number of oxygen molecules in close proximity to the OSC and improving operational stability.[153] An example of this is the relatively stable n-type material, poly-(benzimidazobenzophenanthroline) (**BBL**), which exhibits high performance in a number of applications, ascribing the

enhanced stability to the rigid ladder-type packing motif adopted in the solid state.[42,154]

Another generic explanation for n-type instability can be understood by comparison of LUMO and HOMO delocalization in n-type and p-type polymers, respectively. Typically, in higher performing p-type OSCs, the HOMO is generally delocalized across the entire polymer backbone, with a small excess presiding on the electron-rich moiety.[155,156] Conversely, for n-type materials, the LUMO is often highly localized on the electron deficient moiety, causing electrons to become restricted to the lowest energy portions of the backbone.[157] With these points of lower energy, mobility decreases due to low intermolecular electronic coupling arising from increased distances between electron wave functions.[152]

2.4. Synthetic Design Strategies

The following portion of the review will focus on OECT active layer materials, which are specifically designed to facilitate both ionic and electronic charge transport. As mentioned above, such materials can be both p- or n-type in nature. Recent studies have demonstrated the importance of considering the effects of electronic and ionic conduction in tandem. Savva et al. studied a series of polymers consisting of an identical p-type [2,2′-bithiophen]-5-yl)thieno[3,2-b]thiophene conjugated backbone with an increasing percentage of hydrophilic, ethylene glycol side chains.[35] Their electrochemical performance was evaluated and analyzed to conclude a direct relationship between OECT device performance and balancing the mixed conduction. While the incorporation of hydrophilic side chains is essential to facilitate ion transport and thus OECT operation, polymer swelling may have adverse effects on balancing mixed conduction. It was shown that heterogeneous water uptake disrupted electrical conductivity within the polymer film, slowing response times and yielding poorer transconductance values. As such, the structure–property relationship must be carefully considered for high performing mixed conduction polymers and subsequent OECT devices.[35] While there is no defined template for constructing high performance OMIEC materials, general design initiatives can be garnered from the expansive literature. Ultimately, decisions made at the molecular level will determine the resultant device performance, as such synthetic manipulation of OMIEC materials must consider the effect on polymer stability, mobility, and swelling, all of which can be tuned through synthetic design.

2.4.1. Donor−Acceptor Copolymers.
Currently, OMIEC literature is dominated by donor−acceptor (D-A) copolymers, which are comprised of alternating electron-donating and electron-accepting units. The overall optoelectronic properties of a D−A polymer are determined by the hybridization of the parent monomer HOMO−LUMO energy levels which form an intramolecular charge transfer complex (ICT). Such copolymers can be synthetically designed to optimize the optoelectronic properties by manipulating the parent monomers with the HOMO level residing solely on the donor fragment, while the LUMO level is generally more localized on the acceptor moiety, allowing the energy levels to be tuned relatively independently, a major advantage in terms of molecular design.

Following the rules of the perturbation theory, the HOMO of the donor unit interacts with the HOMO of the acceptor, splitting to yield two new bonding orbitals for the D−A copolymer. The LUMO levels also interact with each other,

splitting to form two new hybridized antibonding orbitals (Figure 12). Electrons redistribute into these hybridized
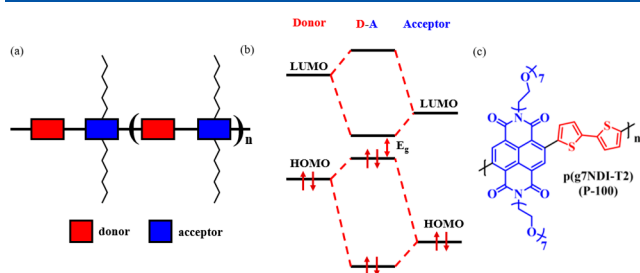

Figure 12. (a) Donor−acceptor alternating copolymer schematic, (b) molecular orbital hybridization of parent donor and acceptor monomers reducing the bandgap (E_g) of the D−A copolymer, and (c) an example of a D−A OMIEC polymer **p(g7NDI-T2)**, abbreviated as (**P-100**).[158]

orbitals, leading to an overall increase in HOMO energy and a decrease in LUMO level, narrowing the optical bandgap. As such, the HOMO wave function is mainly localized on the donor unit while the LUMO wave function is more localized across the acceptor unit.[130]

An example of this is **p(g7NDI-T2)**, abbreviated as (**P-100**)[158] a D−A copolymer composed of an electron-rich bithiophene (T2) unit that is coupled with the strong acceptor naphthalenediimide (NDI) moiety. The copolymer displays a narrow optical bandgap (1.33 eV) and a relatively deep LUMO (high electron affinity) of −4.17 eV, which allows for electrons to be injected into the copolymer, thus operating as an n-type material. While current literature is dominated by examples of donor−acceptor polymers, there are also multiple reports of both all donor polymers and more recently acceptor−acceptor n-type polymers.[159,160] The ability to manipulate the electronic properties of the resultant copolymers facilitates the fabrication of both hole and/or electron transport materials, which are essential for OECT active channel layers.

2.4.2. Bandgap Engineering. The search for true "*organic metals*" requires the bandgap (E_g) to be reduced as close as possible to zero, thereby increasing the thermal population of the conduction band and in turn increasing the intrinsic number of charge carriers. Subsequently, this will increase the intrinsic electrical conductivity, reducing the need for oxidative or reductive doping, while also stabilizing the corresponding doped states.[161] However, owing to the considerable development of OSC devices, π-conjugated polymers with tailored electronic properties are now essential and the search for the lowest possible bandgap is no longer the primary focus. Fortunately, the bandgap engineering toolbox has expanded alongside the popularity of OSC devices (Figure 13).[130,162]

Conjugated polymers exist in the ground state as a resonance between aromatic (confined π-electrons) and quinoid (delocalized π-electrons) forms. As aromaticity is lost during this conversion, the overall resonance energy of the quinoid form is lower. Therefore, stabilizing the quinoid form will lead to a reduction in bandgap energy of related conjugated polymers.[163] This resonance conversion can be described by the bond length alternation term (BLA) defined as the average of the difference in bond length between adjacent C−C bonds and describes the ratio of aromatic to quinoid population. The BLA can be manipulated by tuning the aromatic stabilization resonance energy of the conjugated
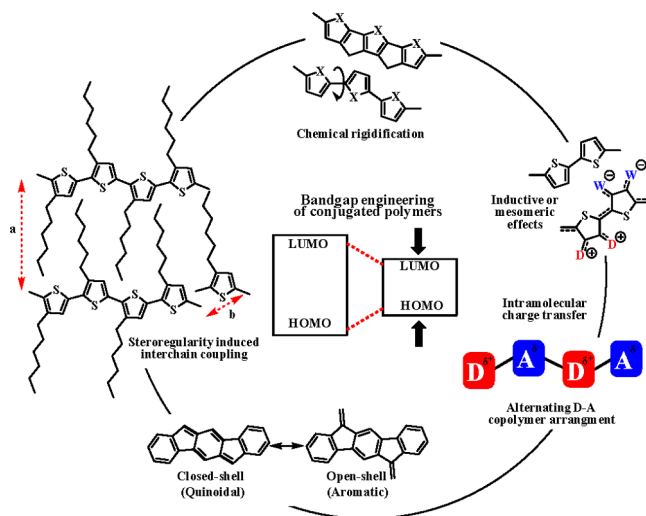

Figure 13. Cumulative illustration of common bandgap engineering strategies. Adapted with permission from ref 130. Copyright 2009 American Chemical Society.

backbone, decreasing aromaticity will facilitate π-electron delocalization favoring the quinoid form, decreasing BLA and HOMO−LUMO bandgap concurrently.

The introduction of chemical rigidity is also known to alter the bandgap energy with increased planarity in the conjugated polymer backbone, significantly lowering E_g. This is due to a combination of reduced rotational disorder and an overall decrease in BLA. Examples of conformational locking through the inclusion of carbon−carbon double bond linkages have been shown to produce rigid fully fused polymers with narrow bandgaps.[160]

Another bandgap manipulation strategy is to tune the HOMO and LUMO energy levels through the incorporation of electron-donating or electron-withdrawing substituents. Electron-donating units (alkyl, alkoxy, or alkylsulfonyl groups) raise the HOMO level, whereas electron-withdrawing groups (nitro, carboxyl, or cyano units) lower the LUMO. These effects can be combined to minimize the bandgap, where the aromatic core and functional groups can be seen as an alternating donor−acceptor system.[162] These inductive and mesomeric effects must be carefully considered during the design of any conjugated polymer requiring a judicious selection of side chain functionality.

Finally, the intermolecular properties in the solid state can also alter the bandgap due to induced interchain delocalization leading to a stereoregular structure. This highly ordered closely packed arrangement can also increase charge carrier mobility. One drawback of this phenomenon is the loss of solubility with increased π-stacking interactions.[130] These strategies for bandgap manipulation are summarized illustratively (Figure 13), and it is clear that while backbone manipulations and donor−acceptor combinations can contribute heavily to the bandgap, the choice of functional side chains must also be carefully considered. These considerations can also determine the behavior of the resultant materials, specifically the ability for a material to act as a p- or n-type material which heavily depends on both bandgap engineering and overarching HOMO/LUMO energy level manipulation.

2.4.3. Solubilizing Side Chains. While strong π-bonding interactions are essential for good charge transport, this renders many conjugated polymer and small molecule systems

poor solubility at appreciable concentrations. Good solution processability is, however, an essential property for successful device fabrication and is governed by multiple structural factors. These include the degree of polymerization, nature and length of solubilizing side chains, the polarity of attached functionalities, backbone rigidity, and intermolecular interactions.[130] The simplest and most utilized design strategy for increasing polymer solubility is through the introduction of aliphatic side chains covalently attached to the polymer backbone. The addition of linear alkyl chains is an undoubtable method for increasing solubility in common chlorinated solvents (e.g., chloroform and chlorobenzene), while branched alkyl chains induce even greater solubility.[164]

However, one cannot simply add aliphatic chains to a polymer without caution, as the inclusion of alkyl side chains is typically accompanied by the introduction of significant disorder within the polymer packing structure, which in turn can negatively impact device performance. An optimal material must strike a balance to render the material solution processable without hindering the charge transport properties. One such example is **PBTTT** (Figure 8), which forms a highly ordered semicrystalline interdigitated phase, in the solid state, when functionalized with linear alkyl chains, facilitating high charge carrier mobility.[134]

The strategy of introducing aliphatic solubilizing chains has also been used for **DPP** and **NDI** (Figure 9) copolymers, which aggregate so strongly that it is generally necessary to include branched alkyl chains to induce solubility in common organic solvents.[138,165,166] The strength of aggregation in these units is facilitated by the presence of polar carbonyl and imide moieties, respectively, which form a hydrogen bond network. Inducing solubility is not the only role that side chains play when designing a conjugated polymer, in fact the importance of side chain engineering cannot be understated. Furthermore, specifically for OMIECs the overall aliphatic content must be finely balanced with the ionic conduction content in order to facilitate efficient mixed conduction and not drown out ionic conductivity.[35]

Side chains can be also used to tune multiple photophysical properties, including bandgap, absorption, emission, molecular packing, and charge transport.[164] An essential component for high performance OMIEC material is considerable hole/electron mobility, as such when designing novel materials, a balance must be struck between polymer processability and morphological properties in order to maximize charge transport. As such a diverse toolbox of side chains has been reported over the last few decades as the field of conjugated polymers has continued to expand,[164,167] including side chains bearing ionic,[168] electron donating, electron accepting, hydrosilanes,[169] and hydrophilic oligo ethylene glycol (OEG) functionalities,[144,159,170] which will be detailed separately herein, as these OEG side chains are of key importance to the majority of high performing OMIEC materials.

2.4.4. Ethylene Glycol-based Side Chains.

In recent years, research in organic electronics has seen an uptake in the number of so-called "*mixed conduction*" (mixed ionic/electronic transport) polymers, with the majority of these containing polar OEG chains (Figure 14). These OEG side chains, which from here onward will also be referred to simply as *glycol* chains, have been demonstrated to facilitate ion transport in aqueous electrolytes, thus facilitating ion penetration into the bulk volume of the polymer during electrochemical doping.[158] This is facilitated by the lone pairs
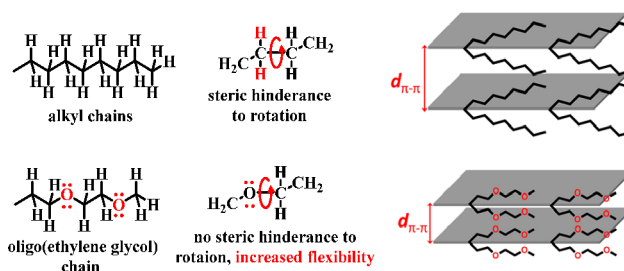

Figure 14. Schematic illustration of the increased flexibility and reduced $\pi-\pi$ stacking distance for OEG chains compared to their alkyl counterparts.[176]

on the oxygen atoms, which can hydrogen bond with polar protic solvents and also chelate to cations.[171] Conjugated polymers with glycol chains can transport electronic charge carriers along the molecular scaffold and ions between the chains, the inclusion of these polar side chains has been reported within multiple electronic architectures, including OPV,[172] OFET,[173] OTE,[174,175] and OECT[144,158,159] devices.

Compared with their typical alkyl counterparts, glycol side chains endow a smaller $\pi-\pi$ stacking distance, narrower optical band gap, enhanced surface energy, and higher dielectric constant (Figure 14). The shorter $\pi-\pi$ distance is a result of amplified flexibility compared to hindered alkyl chains, allowing for more efficient packing of polymer backbones.[176]

A poignant example of incorporating OEG side chains was presented by Giovannitti et al.,[170] where replacing alkyl chains with glycols afforded the high performing OECT material **p(g2T-TT)** exhibiting high volumetric capacitance, transconductance, and currents compared to the alkylated analogue **p(a2T-TT)**, which only functioned as an OFET material. The inclusion of glycol chains shifted the mode of operation into the bulk doping and transport regime, transitioning from OFET to OECT operation, facilitated by ion penetration and hydration (Figure 15). This design strategy has been exploited

Figure 15. Molecular structures and OECT cross-section schematic of ionic interactions of alkylated **p(a2T-TT)** and glycolated **p(g2T-TT)**. Cations (Na$^+$) are depicted in blue, anions (Cl$^-$) are in white, and holes are distributed along the polymer backbone in gray. Adapted with permission from ref 170. Copyright 2016 National Academy of Sciences of the U. S. A.

numerous times by the McCulloch group and others to improve device performance, biocompatibility, and produce mixed conduction systems.[20,34,144,158,159,168,170] It should be noted, however, that while the use of glycol chains has fueled the rapid abundance of OMIEC materials, glycolated polymers often require extensive monomer purification which is synthetically costly.

2.4.5. Hybrid Side Chains. Following the well documented use of solubilizing side chains (generally hydrophobic in nature) to improve both mobility and processability, in addition to the use of hydrophilic side chains, such as ethylene glycol chains, to facilitate ionic conduction, a newly emerging OMIEC design strategy is to include hybrid side chains, facilitating ionic conduction while also improving processability. Specifically, within aqueous electrolyte OECTs, these hybrid side chains have been hypothesized to prevent encroachment of ions at the polaron delocalization locations along the polymer backbone, thus preventing trapping of charges and potentially increasing charge carrier mobility. Indeed, this has been shown as a viable approach for both p- and n-type OMIECs, with hybrid alkyl-glycol side chains imparting enhanced substrate adhesion and operational stability,[54] improved volumetric capacitance,[177] ability to limit detrimental swelling, enable reversible redox-reactions, and improve $[\mu C^*]$ values,[178] respectively, across multiple publications.

2.4.6. Alternative Hydrophilic Side Chains. The majority of recent OMIEC literature has focused on the inclusion of ethylene glycol-based side chains, typically triethylene glycol, to facilitate ion transport, however, some notable alternatives have also been presented. These include the hybrid side chains, discussed above, as well as sulfonated, hydroxylated, carboxylic acid, and lysine-based side chains, respectively.[179−182] Nevertheless, the low cost and widespread commercial availability of ethylene glycol chains, which can be readily varied in terms of both chain length and functionalities, renders glycol-based side chains as the current gold standard for OMIEC design. Indeed, the highest performing OECT materials each feature glycol side chains as the ionic conduction component.[152,183] Despite this, the lack of side chain diversity within the current library of OMIEC materials is an undeniable hole in the literature, and future studies are expected to investigate alternatives, although it should be noted that such studies will be extremely synthetically costly.

2.4.7. OMIEC Design Conclusion. As the field of bioelectronics continues to blossom, the wide variety of OMIEC materials which have been reported demonstrates both the viability of the vast number of different backbones and side chain compositions, which can be employed as active layer OMIEC materials. The design principles outlined above can be used to drive the development of future OMIEC materials. However, it must be noted that even the slightest synthetic design alteration can lead to a pronounced effect on the resultant materials mobility, stability, and swelling to name but a few. The following sections of this review will focus on summarizing and highlighting the history of OMIEC materials. More specifically, OMIECs used as active channel layer materials in OECTs and are separated into hole transport (p-type) (section 2.5) and electron transport (n-type) (section 2.6) materials, respectively, with each section further divided into material category subsections. A combination of the documented history and current state of the art OMIEC materials, utilizing the design principles and considerations outlined above, can be used as a platform for future OMIEC material design for high OECT performance.

2.5. p-Type Mixed Conduction Materials

2.5.1. Initial OECT Channel Materials. Early OECT channel materials consisted of polypyrrole (**PPy**) and polyaniline (**PANI**) (Figure 16), with electropolymerized **PPy** coated
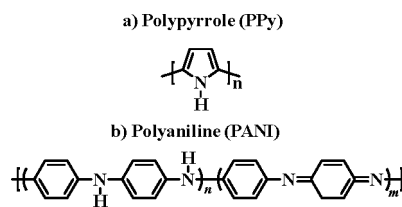

Figure 16. Early conducting polymer motifs (a) polypyrrole (**PPy**) and (b) polyaniline (**PANI**).

gold electrodes as the first reported example implemented into an OECT in 1984.[48] Since this landmark implementation, further examples of **PPy** are scarce, predominantly due to its instability toward oxidation, as the doped polymer has a tendency to cross-link, yielding inoperable devices.[20,48] These limitations were sought to be alleviated by polyaniline-based channel materials, which can be synthesized from cheaper starting materials, have similar conductivity, and increased polyelectrolyte stability compared to **PPy** derivatives.[184−186] Indeed, tremendously enhanced stability was reported for the devices maintaining up to 80% of their initial I_{SD} over the course of 10 h.[50] A higher transconductance of 0.4 mS and faster switching times represented a significant improvement in the OECT device performance compared to the previously developed **PPy** derivatives.

PANI-based OECTs have also been successfully implemented as chemical sensors.[50] Previous studies increasing the pH from 1 to 6 resulted in a remarkably lower source−drain current (I_{SD}), which was attributed to the chemical dedoping of the highly conductive form of **PANI**, emeraldine salt, to the poorly conductive base form of emeraldine, occurring at pH 5.5.[187] However, as noted by the authors, **PANI** materials require a low operating pH, limiting some bioelectronic applications which often occur at physiological pH levels. When returning to pH 1, the original source−drain current values could not be re-established, thus pointing to the irreversibility of the system. Furthermore, **PANI** films were reported to deteriorate swiftly, losing conducting irreversibly when maintained at higher than 0.7 V vs SCE potentials or when operated in elevated pH solutions (pH > 6). This lack of stability upon oxidation at moderate pH severely limits the operational window of resultant bioelectronic devices, and these limitations required more stable materials to be developed.[188]

2.5.2. PEDOT Derivatives. The third family of conducting polymers investigated for OECT devices are polythiophene and, in particular, poly(3,4-ethylenedioxythiophene) (**PEDOT**) derivatives. Research into these sulfur-containing heterocycles has dominated the published literature over the past two decades.[20,188] Unlike previous **PPy** and **PANI** derivatives, polythiophenes share good stability toward both chemical and electrochemical alteration, in addition to general resistance toward oxidation in air.[189,190] The most famous example of a polythiophene derivative is **PEDOT** (Figure 17), a conductive polymer synthesized by following the oxidative polymerization protocol of 3,4-ethylenedioxythiophene (**EDOT**). The impressive electrical conductivity (300 S cm^{-1}) of **PEDOT** was further improved upon coupling with another polymer, namely poly(styrenesulfonate) (**PSS**), yielding the commonly referred to gold standard OECT material: poly(3,4-ethylene dioxythiophene):poly-(styrenesulfonate) **PEDOT:PSS** (Figure 18). Indeed, depend-
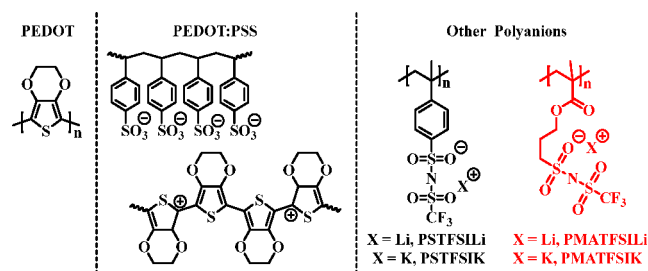
Figure 17. Representative chemical structures of **PEDOT**, **PEDOT:PSS** and alternative polyanions.[192]

Figure 18. Schematic illustration of the molecular design strategy enhancement of conductivity incorporating PEG with **PEDOT:PSS**. Reproduced with permission from ref 196. Copyright 2013 Royal Society of Chemistry.

ing on processing and treatment methods, the electrical conductivity of **PEDOT:PSS** has been shown to reach up to 3000 S cm^{-1}, an order of magnitude improvement upon **PEDOT** and an even more impressive increase from previous **PPy** and **PANI** derivatives.[126,191]

PEDOT:PSS quickly became the most common and studied conductive polymer within OECTs and subsequent biosensors incorporating these devices, owing to the unmatched performance and wide commercial availability. As such, recent publications of the aforementioned, less stable **PPy** and **PANI** derivatives are scarce at best. The goalposts had been shifted, and research transitioned away from the search for the most adequate OECT material toward the development of enriching the properties of **PEDOT:PSS**-based OECTs.[20,188]

The two main features of a high performing conducting material are the ability to maintain a secure charge injection capacity in addition to displaying sustained charge mobility. Previous studies have concluded that conductivity enhancements are related to the inherent polymer structure, as well as different counterions presence, and these properties have been manipulated by numerous groups to improve the stability, wettability, and overall electronic properties of **PEDOT:PSS** polymer blends.[193] For example, thermal treatment (annealing) represents a simple way toward enhancing the **PEDOT:PSS** films conductivity through film fabrication, which has been shown to improve conductivity by an order of magnitude (10^{-3}–10^{-2} S cm^{-1}).[194]

Despite the numerous desirable features displayed by **PEDOT:PSS**, the acidic nature of **PSS** constitutes one notable disadvantage, as it can corrode processing printheads and have undesired reactions with materials adjoining the bioelectronic device active layer.[195] To combat this, a novel series of

PEDOT derivatives was presented by Inal et al. utilizing less acidic (trifluoromethylsulfonyl)sulfonylimide (TFSI) polyelectrolytes, with the alternative anions displayed in (Figure 17).[192] By incorporating TFSI into both polystyrene and polymethacrylate backbones of differing lengths, **PEDOT:PSTFSILi100**, **PEDOT:PSTFSIK20**, **PEDOT:PSTFSIK250**, and **PEDOT:PMATFSILi80** were reported. The first three materials demonstrated very promising OECT performance, as the transconductance values (2.5–3.5 mS) and switching speeds were found to match the (at the time) state-of-the-art **PEDOT:PSS** devices. On the other hand, **PEDOT:PMATFSILi80** devices showed relatively lackluster performance, with transconductance values less than half that of **PEDOT:PSS** devices. The authors attributed this to the low hole conductivity and reduced swelling capability, which led to limited ion transport. These results showed how the polyanion phase could be used as a means to control the OECT performance. Interestingly, the swelling behavior of these **PEDOT:polyanion** systems was inherent to the polyanion composition, a design principle which could be exploited through synthetic polyanion dopant engineering.

Using an alternative approach, researchers have systematically studied the influence of different additives, namely ethylene glycol (**EG**) and polyethylene glycol (**PEG**), on the conductivity of **PEDOT:PSS** films (Figure 18).[196] Atomic force microscopy (AFM) phase images indicate that these additives alter the conformation of the polymer, forming a more linear extended coil structure. Typically, **PEDOT** and **PSS** are held together by Coulombic attractions imparting a more coiled structure owing to the repulsion from extended **PSS** chains.[193] This ionic interaction, between **PEDOT** and **PSS**, is screened by the addition of **EG** or **PEG**, forming hydrogen bonds with both **PSS**$^-$ and **PSSH**, consequently enhancing the phase separation between **PEDOT** and **PSS** and leading to an overall more linear conformation (Figure 18).[196] Subsequently, the electrical conductivity was shown to improve drastically, by more than 4 orders of magnitude from 0.3 to 805 S cm^{-1}.

Further investigations, using Raman spectroscopy, indicate that treatment with **EG** alters the preferred coiled resonant **PEDOT** chain structure (benzoid) to preferred linear or expanded-coil structure (quinoidal form) (Figure 19). Electron

Figure 19. Benzoid (preferred coiled structure) and quinoid form (preferred linear or expanded-coil structure) of **PEDOT**.

spin resonance (ESR) studies suggest that approximately half of the polarons in the **EG** doped **PEDOT:PSS** films pair to bipolarons, with the polaron corresponding to a positive charge on a single unit and a bipolaron indicative of two positive charges delocalized over multiple units.[197] This clearly suggests that the conformational change from the coiled structure the more linear form results in greater delocalization of the charge along the **PEDOT** backbone, demonstrated by the transition from polarons to bipolarons.

These findings were also supported by research into the influence of postdeposition treatments, e.g., UV or UV-ozone,

which have also been shown to enhance conductivity.[198,199] Here, again, the authors hypothesized that the enhanced conductivity was due to a structural change toward the more linear, quinoidal form. Postulating that the quinoidal form prevented losses from charge-trapping deficiencies and showed enhanced $\pi-\pi$ stacking.

While the development of **PEDOT:PSS** as a channel material undoubtably advanced the field of OECTs, there are still some drawbacks to this system, notably: (i) the complex structure, which limits utilization as a benchmark polymer device architecture, (ii) the inability to be completely reduced to the natural charge state, yielding lower on–off ratios compared to alternative channel materials, and (iii) the limited volumetric capacitance performance parameter, owing to the bulky nature of **PSS** minimizing the amount of active **PEDOT** in order to maintain an equal composition ratio.[159,200] Research spanning across the past decade has sought to tackle these limitations through synthetic advancement, producing an array of active layer OECT materials, spanning from glycolated conjugated polymers to polyelectrolyte materials.[20]

2.5.3. Benchmarking Organic Mixed Conductors.

Prior to continuing the discussion of mixed conduction OECT materials, an extremely noteworthy publication from three leading academics, Inal, Malliaras, and Rivnay, must be mentioned.[53] As organic mixed conductors began to garner significant attention guidelines for benchmarking OECT performance was published in an attempt to level the arena and provide a figure of merit for material comparison across the field. Materials for OECTs require both efficient electronic transport and adequate ion injection in order to maintain good capacitance. The authors showed that μC^* value, corresponding to the outcome of multiplying the volumetric capacitance (charge storage capacity) and electronic mobility, is the most appropriate materials/system figure of merit, supported by their comparison of 10 previously published OECT materials (Figure 20).[53] Where appropriate, this value will be presented
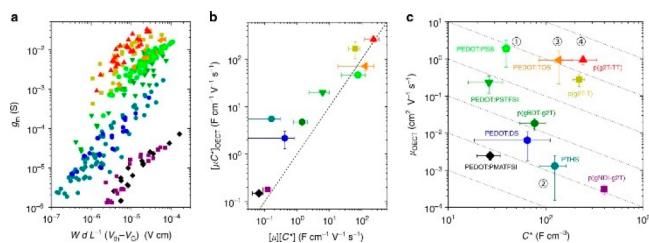

Figure 20. (a) OECT Transconductance (g_m) as a function of channel geometry and operating conditions. Each point represents one OECT measurement; each color/shape corresponds to one material. (b) The linear slope of $[\mu C^*]_{OECT}$ as a function of μ_{OECT} of the product and $[\mu][C^*]$. (c) $\mu_{OECT}-C^*$ overview of previously reported materials. Dotted lines correspond to constant $[\mu C^*]$ product. Reproduced with permission from ref 53. Copyright 2017 Springer Nature.

within the following discussion, however, notably prior to this article, the common figure of merit for these materials was the transconductance (g_m), as such, this value will also be used to compare performances.

While a comparative benchmark value, such as $[\mu C^*]$, is an invaluable tool to actively compare the OECT performance of different active-layer materials, this value is not the be-all-end-all when it comes to comparing OMIEC materials. Indeed, many bioelectronic applications, mentioned throughout, do

not rely on high OECT performance to function and instead are reliant on factors such as mobility, swelling, and stability to name but a few. Furthermore, publications released prior to the aforementioned benchmarking paper tended to not report a $[\mu C^*]$ value, which limits the comparison of some materials. Despite these noteworthy points, the following sections will utilize $[\mu C^*]$ as the main figure of merit for comparing the OECT performance of various OMIECs, discussing other metrics (stability, transconductance, synthetic novelty etc.) where appropriate.

2.5.4. Glycolated Polythiophene Derivatives.

The emergent and exciting class of glycolated semiconducting materials has dominated the field of OECT channel materials over recent years. These glycol chain decorated semiconducting polymers mirror previous conjugated polyelectrolyte materials in that the electronic charge transport occurs along the π-conjugated backbone while ion transport is facilitated by the hydrophilic glycol side chains. The addition of polar glycol side chains has been shown to alter morphology, microstructure, and optoelectronic properties of resultant semiconducting polymers.[173,201,202]

In 2016, the first reported glycolated semiconducting polymers for OECTs were published, reporting polymers containing either a glycolated benzodithiophene or bithiophene backbone unit.[159] These motifs were chosen to allow the oxygen atom of the ethylene glycol chain to be directly attached to the conjugated backbone, facilitating the electron donating nature of the oxygen and affording highly planar polymer backbones, mimicking the beneficial structural properties of **PEDOT:PSS**. These glycolated monomers were subjected to Stille homo- or copolymerization with either thiophene (**T**) or bithiophene (namely **2T** or **T2**) monomers to produce five unique polymers: **g2T-T**, **gBDT**, **gBDT-2T**, **gBDT-T**, and **gBDT-g2T** (Figure 21).

Consequent investigations into the OECT performance of these materials showed that polymers containing glycolated bithiophene moieties substantially outperformed those based
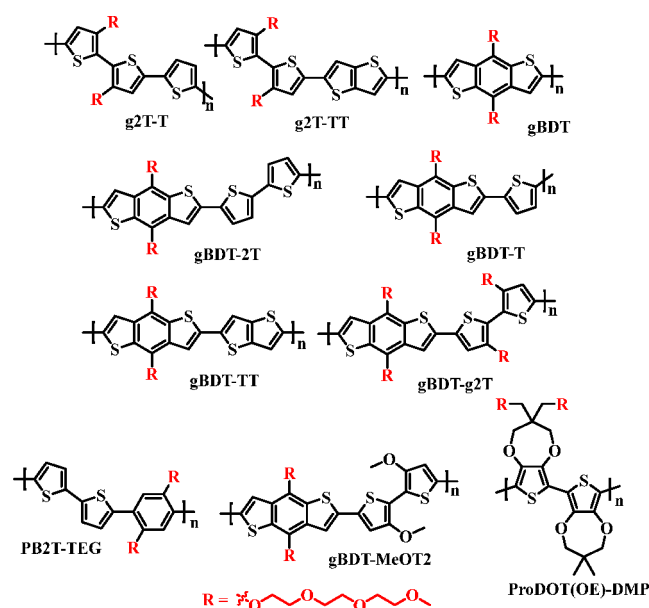

Figure 21. Chemical structures of multiple OECT channel material p-type glycolated semiconducting polymers, polythiophene derivatives bearing triethylene glycol side chains.

on glycolated benzodithiophene showing much improved peak transconductances. The reduced performance of **gBDT**, **gBDT-2T**, and **gBDT-T** was accredited to the negligible hole mobilities ($\sim 5 \times 10^{-3}$ cm^2 V^{-1} s^{-1}), owing to their comparatively large π-stacking distances of 3.7 Å. This was compounded by the poor electrochemical properties, with low-lying HOMO values ~ -4.85 eV and near nonexistent electrochromic activity, which is generally indicative of difficulties with electrochemical doping.[20] These findings were also supported from a molecular standpoint, with glycolated benzodithiophene polymers exhibiting a higher degree of twisting compared to the glycolated bithiophene polymers, which were planarized by the attractive sulfur–oxygen interactions. With dihedral angles close to 0°, around the central C–C bond, **gBDT-g2T** and **g2T-T** polymers showed 0.4 eV higher HOMOs in addition to spectroelectrochemical measurements, revealing a significant polaron absorption band.[159]

OECT devices incorporating **gBDT-g2T** and **g2T-T** as the active mixed-conduction channel materials achieved peak transconductance values of 0.47 and 7.9 mS, respectively. Both closer π-stacking distances and preferred edge-on microstructures were prescribed as the dominant factors increasing hole mobility and subsequent OECT performance, following eq 1, for **g2T-T** devices. Focusing on the top-performing material, altering the casting technique and manipulating device dimensions further increased the transconductance to 21 mS with a benchmarked [μC^*] value of 167 $\pm$ 65 F cm^{-1} V^{-1} s^{-1}, unprecedented at the time of publishing, for an accumulation mode OECT device.[52] At the same time, **g2T-T** devices were also found to outperform conventional **PEDOT**-based devices, which operate in depletion mode. Notably, given the theoretically proven scaling of transconductance with channel thickness, the $\sim$40% increase in transconductance is well-explained.[200]

Two years later, in 2018, a follow-up study was published demonstrating improved OECT performance and stability of glycolated benzodithiophene containing polymers.[112] Here, the aforementioned glycolated benzodithiophene monomer was copolymerized with thieno[3,2-*b*]thiophene (**TT**) and 3,3′-dimethoxy-2,2′-bithiophene (**MeOT2**), affording **gBDT-TT** and **gBDT-MeOT2**, respectively (Figure 21). The increased HOMO energies (-4.70 and -4.31 eV, respectively) compared to the **gBDT-2T** reference, led to lower OECT turn-on voltages. In addition, **gBDT-MeOT2** devices showed a 4-fold increase in transconductance (1.82 mS) and stable on-currents over 300 cycles.

Another study presented **g2T-TT** and the analogous alkylated derivative **a2T-TT** (Figure 15) as a case study for altering the operation mode of OECTs through side chain engineering.[170] The newer **g2T-TT** polymer can also be considered comparable to **g2T-T**, where the thiophene comonomer was replaced by a more rigid thieno[3,2-*b*]thiophene unit. This replacement led to negligible changes in the optoelectronic properties with near identical HOMO, LUMO, and bandgap values for both **g2T-TT** and **g2T-T**. However, 2D grazing incidence X-ray scattering confirmed that **g2T-TT** possesses shorter π–π stacking distances, hence, explaining the improved hole mobility of 0.95 cm^2 V^{-1} s^{-1} compared to 0.28 cm^2 V^{-1} s^{-1} for **g2T-T**. Indeed, this led to the highest reported transconductance to date for an OECT in accumulation mode,[52] with a g_m of 27 mS and a benchmarked [μC^*] value of 261 $\pm$ 29 F cm^{-1} V^{-1} s^{-1} while also maintaining

rapid switching times and on–off ratios.[170] The authors also demonstrated the ability to transition from pure interfacial field-effect transistor (FET) operation to bulk doping/transport by simply replacing the hydrophobic alkyl side chain with the hydrophilic ethylene glycol moiety. This hypothesis of ion penetration and hydration facilitation by the glycol side chains, without affecting electronic mobility, for **g2T-TT** compared to **a2T-TT**, has been validated as a synthetic approach to develop functioning OECT materials from OFET building blocks.[20,53]

An alternative OECT channel material was reported by Savagian et al., namely **ProDOT(OE)-DMP** (Figure 22),
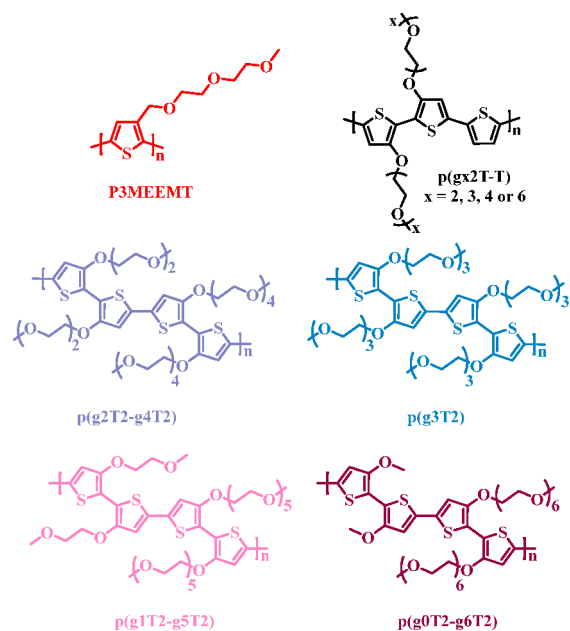

Figure 22. Chemical structures of modern examples of p-type OECT channel materials.

whereby **ProDOT** was copolymerized with a glycolated **ProDOT** derivative.[183] The **ProDOT** backbone was selected over the 3,4-ethylenedioxythiophene (**EDOT**) backbone owing to the synthetic ease of functionalizing the propylene bridge, incorporating solubilizing and glycolated side chains, respectively, while also preserving the high electron density of **EDOT**. Notably, from a synthetic standpoint, **ProDOT(OE)-DMP** was not only the first **ProDOT**-based OECT channel material but was also synthesized by direct(hetero)arylation polymerization (DHAP), another first for an OECT active channel material. This polymerization technique is favorable over the more commonly used Stille cross-coupling, which requires highly toxic stannylated monomers which can leave organotin residues despite purification regimes.[20,203] Furthermore, as DHAP foregoes the use of any highly toxic stannylated monomers, this polymerization technique is highly attractive for in vivo device applications, with studies showing DHAP materials generally contain less residual metals compared to other polymerization procedures.[204] The fabricated OECT devices, containing **ProDOT(OE)-DMP**, yielded impressive on–off ratios in the region of 10^5, on par with previously reported **g2T-TT** devices. Despite this, the maximum transconductance achieved was 0.62 mS, a notable decrease from **g2T-TT**, and can be accredited to the much reduced hole mobility of **ProDOT(OE)-DMP**. The **Pro-**

DOT's twisted neopentyl-linked seven membered rings limit hole mobility due to defects and disorder when cast as films. **ProDOT(OE)-DMP** presents the inaugural example of a glycolated OECT active channel material designed from the ground up based on the capacitive properties, high electrochromic contrast, and impressive electrochemical stability of the backbone, opposed to the typical synthetic modification of a traditional OFET or OPV material.

Employing a similar technique to the previously discussed **g2T-TT** material, the Luscombe group synthesized a glycolated **P3HT** derivative, namely poly(3-{[2-(2-methoxyethoxy)ethoxy]methyl}thiophene-2,5-diyl) (**P3MEEMT**) (Figure 22).[38] This material showed a $[\mu C^*]$ = 49.1 ± 5.0 F cm^{-1} V^{-1} s^{-1} in 100 mM KCl, which further increased when tested in 100 mM KPF$_6$, to $[\mu C^*]$ = 96.7 ± 10.2 F cm^{-1} V^{-1} s^{-1}, demonstrating the importance of the identity of the dopant used. Replacing the alkyl side chain for with a glycol-based moiety afforded $[\mu C^*]$ values similar to that reported for typical **PEDOT:PSS**[53] systems and a factor of 5 increase on **P3HT** ($[\mu C^*]$ = 10.4 ± 3.1 F cm^{-1} V^{-1} s^{-1}). A significant effect on the polymer hydration, leading to a packing-density effect, was observed while doping. This caused faster kinetics in **P3MEEMT** compared to the **P3HT** standard. A follow-up doping mechanism investigation highlighted the significance of the charge compensation mechanism which needs to be further studied to benefit future OMIEC design approaches.[200]

Motivated by a Li$^+$-ion conduction polymer battery paper[33] and utilizing the aforementioned **P3MEEMT** (Figure 23),
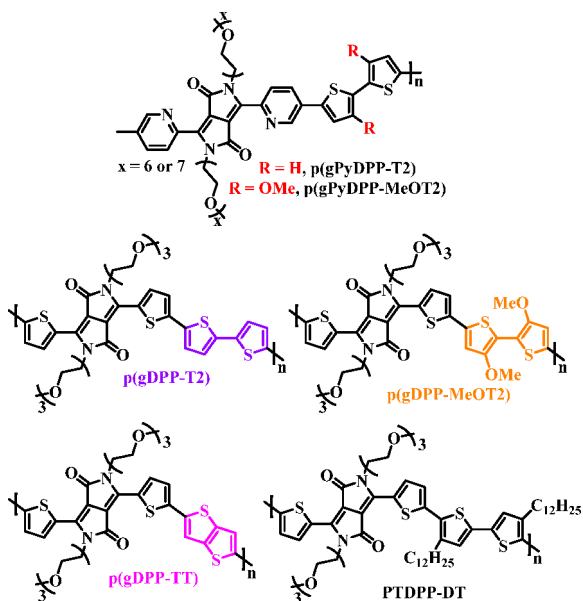

Figure 23. Structures of selected, OMIEC DPP derivatives utilized as OECT active channel materials.

Schomde et al. investigated the effect of the nature of diethylene glycol linkage on crystallinity, mixed conduction, and overall OECT device performance for a series of hybrid spacer polythiophene homopolymers. More specifically, three glycolated polythiophene derivatives were synthesized by controlled polymerization using Kumada catalyst transfer polymerization (KCTP). A methyl spacer (**P3MEEMT**), ethyl spacer (**P3MEEET**), or no spacer (**P3MEET**) were used to join the diethylene glycol side chains to the

polythiophene backbone.[177] Electrochemical impedance spectroscopy (EIS) was exploited to probe the ionic charge storage capability. This study revealed a linear uptick in C* upon increasing the length of the alkyl spacer between the thiophene backbone and diethylene glycol chain, with **P3MEEET** recording a volumetric capacitance of 242 ± 17 F cm^{-3}. This was attributed to the increased accessibility of the diethylene glycol side chain and thus an enhanced ion transport as well as the higher structural order of **P3MEEET**. Importantly, the nature of linkage between the polymer backbone and hydrophilic side chain plays a tremendously significant role in the complex ion uptake, swelling, and mixed conduction balance in OECTs and can be used as an effective synthetic design strategy to modulate these properties.

Up to this point, the majority of research efforts have been dedicated to optimizing the OECT device performance by engineering of the mixed conducting polymers' conjugated backbones, an alternative approach was adopted by Moser, who first explored the effects of varying the length of the ethylene glycol side chain.[200] Here, a series of glycolated polythiophenes (based on **g2T-T**) decorated with EG chains bearing 2−6 EG repeat units was reported (Figure 22). OECT data elucidated a strong correlation between the ethylene glycol side chain length and device performance, suggesting careful consideration of the length and overall glycol content must be considered. While minimizing the glycol side chain length appeared to enhance both the capacitance and charge transport properties of the polymers, the necessity of keeping the side chain sufficiently long to render solubility, processability, and crucially for OECT device operation, ionic transport, exists. Nonetheless, these are important structure−property design considerations for future channel materials.

Shortly following this work, Moser published a second series of glycolated polythiophenes, distributing the glycol side chain length between each **T2** monomer while retaining the overall glycol content across the series (Figure 22).[183] While side chain distribution did not affect optoelectronic properties across the series, this synthetic side chain engineering approach significantly altered the degree of water uptake upon device operation. Careful synthetic optimization led to OECT devices of **p(g2T2-g4T2)** and **p(g1T2-g5T2)**, demonstrating unequaled $[\mu C^*]$ values of 496 and 522 F V^{-1} cm^{-1} s^{-1} as well as high current retentions (87% and 98% over ≈700 electrochemical switching cycles, respectively), presenting a significant improvement in OECT channel materials. The report showed that each polymer within the series displayed differing degrees of passive swelling upon electrolyte exposure and drastically varied active swelling, increasing from 4% to 10% to 168% and peaking at 249% for **p(g0T2-g6T2)**, **p(g1T2-g5T2)**, **p(g2T2-g4T2)**, and **p(g3T2)**, respectively. The authors hypothesize that the differences in active swelling are related to the varied abilities of each individual glycolated bithiophene unit to take up and stabilize water molecules in their doped state. Notably, there appears to be nonlinear positive relationship between ethylene glycol side chain length and water uptake with a cutoff point occurring after reaching three ethylene glycol repeat units. This finding was corroborated by another report in which doubling the overall glycol content led to an approximately 600% increase in the polymers active swelling, while subsequent doubling of the overall glycol content caused a reduced upsurge in the active

swelling of approximately 50%.[35] These distributed glycol side chain materials are an excellent example of how the field of OECT materials has progressed during the past decade, combining synthetic strategies to optimize the conjugated backbone structure with diligent side chain engineering to produce two of the highest performing p-type OECT channel materials to date.[53]

2.5.5. Diketopyrrolopyrrole (DPP) Derivatives. The electron deficient DPP building block has a rich history within the field of organic transistors.[205] Utilizing side chain engineering to introduce glycol side chains, facilitating ionic conduction, presents a new class of OMIECs and another viable option for OECT channel materials (Figure 23).[111,206−208] The first example of DPP polymers implemented as an OECT channel material was presented by Giovannitti et al.[111] Here, two pyridine-flanked DPP polymers, namely **p(gPyDPP-T2)** and **p(gPyDPP-MeOT2)**, were designed to improve electrochemical stability against detrimental side products, such as H_2O_2, from the oxygen reduction reaction (ORR). The authors suggest that the bimethoxy decorated T2 unit stabilizes the hole polaron through localizing the wave function, increasing redox stability compared to the undecorated T2 containing polymer. Importantly, this study illuminates the potential negative side effects of redox-active conjugated polymers operating in a biologically relevant environment and emphasizes the effect of previously overlooked side reactions which must be considered for clinical applications.

More recently, a series of three thiophene flanked DPP polymers was presented by Moser et al.[23] Here the length of the ionic transport facilitating glycol side chains were reduced to three units compared to seven for the previously described pyridine flanked DPP materials. The polymer backbone was methodically adjusted to probe structure−property relationships of D−A channel materials, in contrast to the more common all donor materials, detailed throughout section 2.5.4. Implementing three thiophene-based monomers, **T2**, **MeOT2**, and **TT**, which have previously been discussed within the **gBDT** series of polymers, afforded three p-type thiophene flanked DPP materials (Figure 23). The operational stability of each material was determined using the standard figure of merit: recording the percentage retention of the initial current as a function of OECT switching cycles. Corroborating with the pyridine flanked DPP investigation, **p(gDPP-MeOT2)** showed the highest operational stability, retaining 99% of the initial current following 100 min of electrochemical cycling, while **p(gDPP-T2)** and **p(gDPP-TT)** retained only 53% and 9%, respectively. However, OECT performance did not concur with the trend in operational stability, with **p(gDPP-T2)** displaying the highest performance with a $[\mu C^*]$ of 342 ± 35 F cm^{-1} V^{-1} s^{-1}. Each material recorded a comparable C*, and thus the increased performance was ascribed to the higher degree of order for the **T2** derivative, resulting in improved hole mobility compared to both the TT and MeO derivatives. Additionally, computational simulations were employed to investigate the nature and extent of polaron delocalization across the series, further confirming the improved performance of **p(gDPP-T2)**, which showed even and extended polaron delocalization.

The electrochemical doping response of **PTDPP-DP** (Figure 23) was investigated in two different electrolytes, demonstrating the role of the anion in affording high performance OECT materials.[208] Utilizing tetrafluoroborate

(BF_4^-) anions, within the aqueous electrolyte, afforded an almost 4-fold increase in OECT performance with a $[\mu C^*]$ of 559 ± 65 F cm^{-1} V^{-1} s^{-1} compared to 149 ± 61 F cm^{-1} V^{-1} s^{-1} within a standard chloride anion containing electrolyte. The authors prescribed this to the larger crystallographic radius of the BF_4^- anions conferring an increased doping efficiency compared to the smaller chloride anions. Each DPP investigation has presented invaluable insight toward the design of high performing and operationally stable OMIECs for OECTs. Synthetic control of undesirable side reactions, the importance of matching energetics and the choice of dopant anion all play a crucial role in the resultant OECT performance and should be considered when designing future active channel OMIEC materials.

2.5.6. p-Type Summary. Following preliminary studies of **PPy** and **PANI**-based devices, the overwhelming majority of high performing OECT channel materials have been derived from **PEDOT** derivatives or from previously known OFET polymer structures. Considering all the reports detailed above, some common design principles can be garnered which have driven the synthetic direction of the field. An important property present within all high performing active materials is backbone planarity, affording tighter π-stacking, benefiting both hole and electron mobilities. This syntenic design strategy was evidenced when comparing **g2T-TT**, which showed a higher transconductance due to tighter π-stacking compared to **g2T-T**. Notably, previous reports with **PEDOT:PSS** and alkyl functionalized polymers demonstrate that well-ordered domains can lead to slower ionic transport, which in turn reduces electrochemical switching speeds.[37] Manipulation of the ionization potential, principally controlled by the HOMO energy level of the polymer, is also another important factor to consider. Fundamentally, for sufficient p-type operation, the IP needs to be small enough to facilitate doping of the polymer within water's electrochemical potential window (5.3−4.05 eV at pH 7).[149] Generally, polymers with raised HOMO energy levels (reduced IPs) are more stable to electrochemical cycling, however, an extremely shallow ionization potential could lead to depletion mode behavior, resulting in lower on/off ratios. The inclusion of 3-alkoxy and 3,4-dialkoxy moieties has been shown to effectively raise the HOMO energy level of substituted thiophenes, in addition to increasing electrochemical stability, as evidenced by both **gBDT-2T** and **gBDT-MeOT2**.[112] Distribution of hydrophilic ethylene glycol side chains has also been shown to dramatically alter OECT performance, specifically due to modulating the water uptake upon device operation.[183] Vigilant optimization of the water uptake and polymer swelling has afforded the state-of-the-art p-type channel materials and should also be carefully considered when designing future materials aiming to improve on these devices. Each of the aforementioned p-type materials has one or more unique material design aspect(s), and through the accumulation of these ideas and concepts, materials such as **p(g2T2-g4T2)**, **p(g1T2-g5T2)**, and **PTDPP-DP**, which demonstrate unprecedented $[\mu C^*]$ values, have been crafted. Furthermore, the DPP-based polymers, presented above (Figure 23), provide crucial insight into structure−property relationships beyond just performance metrics and elucidate stability, side reactions, and OECT architecture/fabrication as key factors for future OMIEC material design. Forthcoming research will aim to continue to utilize these design principles, and with the combined knowledge, documented throughout this review, will hope to produce channel materials with even

higher OECT performance. Perhaps, arguably more importantly, the bioelectronics community would benefit from the optimization of electron transporting (n-type) materials, which have historically lagged behind their p-type counterparts. The combined efforts of various research groups in the field of n-type OMIEC materials will be summarized in the following section.

2.6. n-Type Mixed Conduction Materials

2.6.1. Naphthalenediimide (NDI) Derivatives. In an analogous approach to the aforementioned modification of thiophene-based building blocks, to obtain p-type polymers such as **g2T-T**, Giovannitti investigated combining a glycolated bithiophene monomer with a glycolated naphthalenediimide (**NDI**) to afford **p(gNDI-gT2)** (Figure 24).[144]
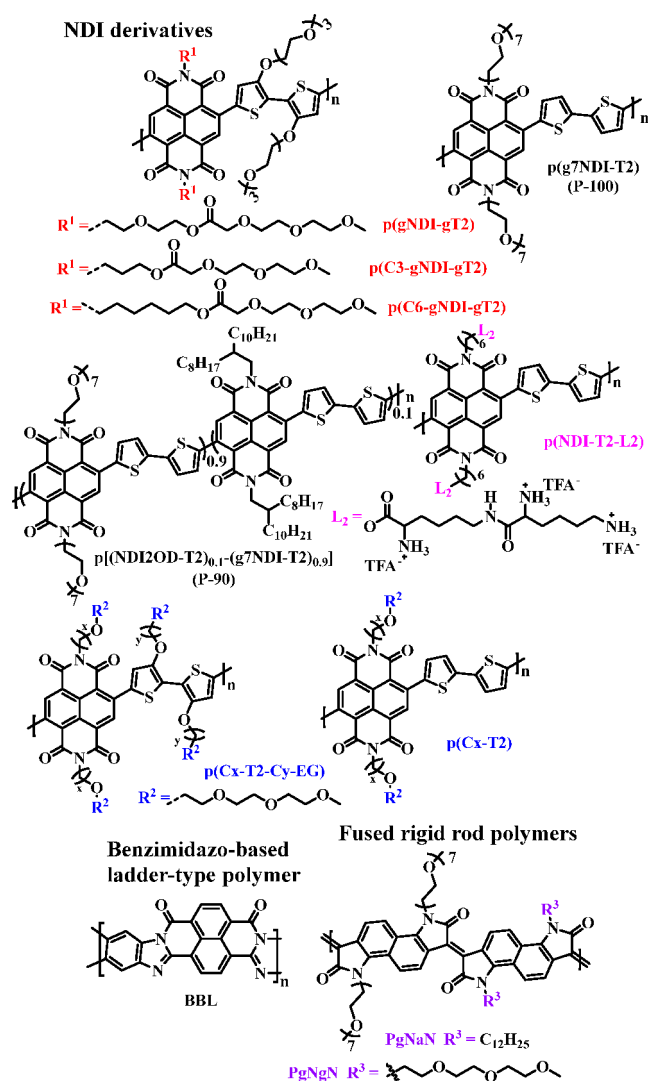

Figure 24. Structures of selected n-type, electron transport, OECT active channel materials.

Fabricated OECT devices showed ambipolar behavior with both p- and n-doping in aqueous solution, in addition to good operational stability after 2 h of operation. Notably, omission of the ethylene glycol side chains from the bithiophene unit restricted ambipolar charge transport properties due to the 0.7 eV lower lying HOMO energy level for the **p(gNDI-T2)** analogue. A subsequent study presented a series of modified

p(gNDI-T2) copolymers with slightly varied and elongated ethylene glycol side chains.[158] Here, the linear 7-unit glycol side chains tethered to the **NDI** core were progressively replaced by branching ($C_8H_{17},C_{10}H_{21}$) alkyl chains to produce a series of random copolymers, **P100**, **P90**, **P75**, **P50**, **P25**, **P10**, and **P0**, with the overall glycol content reducing from 100% to 90% to 75% to 50% to 25% to 10%, and finally to 0%, respectively (Figure 24). Each polymer with a total glycol side chain percentage <75% showed no operational n-type OECT behavior, owing to the restricted ability to volumetrically charge upon increasing alkyl content. This hypothesis was validated by the poor swelling ability and limited ion uptake, confirmed by cyclic voltammetry and dissipation measurements. Encouragingly, operational n-type OECT devices were fabricated with **P75**, **P90**, and **P100** active layers, all of which showed similar performance, culminating with a thickness normalized transconductance of 0.21 S cm^{-1} and peak transconductance of 1.1 μS for **P90**.[158] Nonetheless, these materials could not compete with the performance of **p(gNDI-gT2)**, where ambipolar n- and p-type operation lead to a high values of peak transconductance (21.7 and 13.4 μS, respectively) and on−off ratios (3.2 × 10^3 and 2.0 × 10^2, respectively). Furthermore, the use of random copolymers is not ideal, from a synthetic point of view, due to likely batch-to-batch variations.[178,209]

More recently, the effect of introducing an alkyl spacer between the **NDI** core and the ethylene glycol side chain has been investigated through the fabrication of **p(C3-gNDI-gT2)** and **p(C6-gNDI-gT2)** (Figure 24).[178] The introduction of hydrophobic propyl and hexyl spacers sought to minimize detrimental swelling in close proximity to the conjugated polymer backbone, balancing the mixed conduction properties necessary for operational OECT operation. The authors discovered that both alkyl spacer containing polymers outperform the parent ethylene glycol decorated polymer **p(gNDI-gT2)**, in thickness normalized transconductance, electron mobility, and [μC^*] performance parameters. Notably, the introduction of an alkyl spacer reduces the volumetric capacitance by more than two-thirds, this is, however, compensated by the more than 4-fold increase in electron mobility for **p(C3-gNDI-gT2)**. The presence of the alkyl spacers also leads to remarkable stability in n-type OECTs, with no decrease in the ON current after 2 h of operation. Ultimately, **p(C6-gNDI-gT2)** with a [μC^*] of 0.16 F V^{-1} cm^{-1} s^{-1} confirms the inclusion of an alkyl spacer acting as a protective sheaf against detrimental swelling close to the polymer backbone is an effective synthetic design strategy to improve n-type OECT performance.

This structure−property relationship was further explored by Ohayon et al., who reported a new family of donor−acceptor polymers, again based on the **gNDI-T2** backbone, delving into side chain modifications on both the acceptor and donor moiety (Figure 24).[210] The inclusion of an alkyl spacer, directly tethered to the polymer backbone, separating the core from the hydrophilic ethylene glycol side chains, was again proven to affect the film order, crystallinity, and consequently, the electron mobility. This study presented even more evidence which corroborated Giovannitti's work, demonstrating ambipolar charge transport, induced by the introduction of electron-donating groups (methoxy, EG side chains) to the **T2** core, which also considerably alter the polymer microstructure, limiting n-type performance.[144] After screening various different backbone structure compositions, the best OECT

performer was identified to be the unsubstituted **T2** polymer, subsequently, the authors focused on manipulating the side chains tethered to the **NDI** unit. Ultimately, it was found through GIWAXS studies that the polymer backbone order was optimized for the polymer with a six-carbon spacer, hitting a "sweet spot" between the distance of the hydrophilic glycol side chains away from the conjugated core. Indeed, **p(C6-T2)** was shown to outperform other reported n-type OECT materials,[156,172] with a $[\mu C^*]$ of 1.29 F V^{-1} cm^{-1} s^{-1}, approaching the previous state-of-the-art values of **BBL** devices, which have been documented as the highest performing electron transport material for n-type OECTs.[211] The impressive $[\mu C^*]$ values are a result of a dramatic increase in electron mobility, which was shown to rise linearly with increasing the length of the alkyl spacer, up to six carbon atoms, peaking at 4.74×10^{-3} cm^2 V^{-1} s^{-1}. **p(C6-T2)** devices also showed remarkable stability across a range of voltage cycles and 3 h operation under consistent pulsed gate voltages. The authors theorized that the high mobility of **p(C6-T2)** could be attributed to striking a balance between the lamellar ordering, as well as opposing backbone and $\pi-\pi$ stacking ordering trends. It is also noteworthy that the high mobility of **p(C6-T2)** may be in part due to the increased molecular weight, indeed **p(C6-T2)** displayed the highest molecular weight (M_n = 25.0 kDa) and number of repeat units (27) for the entire family of materials within this study.[210] While this was mentioned anecdotally when comparing the drop in OECT performance of **p(C8-T2)**, the direct link between molecular weight and OECT performance was not investigated further. Interestingly, a true and thorough study into the effects of increased molecular weights on OECT performance parameters is yet to be published. One could anticipate that the number of repeat units would have an impact on multiple performance factors owing to the bulk-governed OECT operation, as opposed to the interface-governed OFET performance. Thus, the natural progression for further insights into the structure−performance relationships for OMIECs would include a detailed molecular weight study.

Recently, a unique lysine derivative (**L2**) decorated **p(NDI-T2)** analogue, namely **p(NDI-T2-L2)**, was reported (Figure 24), the first biofunctionalized n-type polymer verification, specifically designed for lipid membrane interfacing.[182] Because of their orientation on the polymer film surface, the lysine chains facilitated zwitterionic lipid vesicles assembly into supported lipid bilayers.[212] While the OECT performance data was meagre, in comparison to state-of-the-art materials, with the best device recording a $[\mu C^*]$ of 0.31 F V^{-1} cm^{-1} s^{-1}. However, performance parameters were not the focus of this study, and **p(NDI-T2-L2)** demonstrates sufficient performance in microscale transistors for biosensing applications alongside impressive operational stability in biologically relevant electrolytes. This report is an important, application-based form of evidence for the validation of bioelectronic organic mixed ionic conduction materials for use in biological environments.

2.6.2. Benzimidazo-based (BBL) Ladder-type Polymer.
Perhaps the most well-known and extensively studied example of an n-type active layer material is poly-(benzimidazobenzophenanthroline) (**BBL**) (Figure 24).[211] Indeed, up until very recently, **BBL** was the pinnacle n-type performer, with an impressive $[\mu C^*]$ of ∼0.65−1.0 F V^{-1} cm^{-1} s^{-1}.[42] This value can be largely attributed to the record volumetric capacitance of 930 F cm^{-3}, which surpasses most of

the best NDI-based OECTs (∼400 F cm^{-3}) by more than 2-fold. This occurs due to **BBL**'s lack of solubilizing side chains which enable the material to store charge in closer proximity to the polymer backbone compared to **NDI** derivatives.[211] Furthermore, the covalently bonded structure prevents twisting, which minimizes disorder and trapping sites, to maximize charge transport along the rigid ladder-like backbone.[154,211]

After a long-term storage in ambient conditions, as well as upon 1 h operation in water, the devices also exhibited high stability. However, as is the case for the majority of reported materials, side chains are often required to impart solubility and enable the use of traditional solution-based polymerization techniques and processing methods. The absence of any side chains renders **BBL** only processable from strong organic acids. Historically, **BBL**-based devices also suffer from slow response times (∼1 s) on account of the limited number of ions diffused throughout the active layer.[42,211] This could be improved by introducing glycolated side chains to encourage ion uptake, however, this would undoubtably compromise the volumetric capacitance. Nevertheless, because of the side chains' synergetic effect of ion injection into the bulk and overall doping efficiency enhancement,[174] the diminished capacitance could be addressed by the improved response time and is one of the focal points for current ladder polymer research.[42,213] A differing approach to synthetic manipulation was employed by Surgailis et al., who evoked an alternative method of film fabrication (spin-casting vs spray-coated) to afford micrometer-scale BBL OECT devices.[214] These devices showed state of the art n-type performance ($[\mu C^*]$ of 1.99 F V^{-1} cm^{-1} s^{-1}) and response times of 5.2 ms, a remarkable improvement over the initial publication and validation of device fabrication methods as a major consideration for improving OECT device performance.

2.6.3. Fused Acceptor−Acceptor Rigid Rod Polymers.
Recent publication of **PgNaN** and **PgNgN** polymers further investigated the concept of a fused rigid rod type polymer backbone (Figure 24), comprised of a glycolated naphthalene cored bis-isatin unit coupled to an alkylated/glycolated naphthalene cored bis-oxindole monomer, respectively.[160] Similarly, to **BBL**, these materials were synthetically designed to reach an almost torsion-free π-conjugated backbone with an acceptor−acceptor configuration. This electron poor structure led to deep LUMO values of 4.28 and 4.35 eV, respectively, and coupled with the fused backbone afforded the highest performing n-type mobilities OECT of up to $6.50 \pm 1.01 \times 10^{-3}$ cm^2 V^{-1} s^{-1}. Indeed, the mobility value of **PgNaN** surpasses that of **BBL**, by an order of magnitude, also mildly surpassing the state-of-the-art **NDI**-based **p(C6-T2)** polymer.[210,211] In addition to the impressive electron mobility, both **PgNaN** and **PgNgN** are synthesized via an acid catalyzed metal-free aldol condensation polymerization, a process absent of any toxic metals or organotin monomers, common to most other polymerizations, a foremost benefit for potential bioelectronic applications in living organisms.[20]

Chemically, **PgNaN** and **PgNgN** differ only by the composition of the side chains residing on the bis-oxindole monomer, with **PgNaN** composed of a 50:50 ratio between alkyl and glycol side chains compared to the fully glycolated **PgNgN** derivative. This chemical manipulation is sufficient enough to significantly lower the μC^* compared to that of the mixed alkyl/glycol (**PgNaN**) derivative. This trend is reminiscent of the tendencies observed for the previously discussed **NDI** series with **P-90** and **P-100**.[158] The take-home

message from both of these systems appears to be that incorporation of some degree of alkyl side chains is essential for high OECT performance. This is likely due to the negative effects of polymer swelling upon OECT operation, which will be exacerbated for all of the glycol derivative, as glycol chains facilitate ion chelation and subsequent swelling, limiting electron transport, a concept corroborated from the recent **NDI**-based carbon spacer studies.[121,178,210] With a $[\mu C^*]$ of 0.66 F V^{-1} cm^{-1} s^{-1}, **PgNaN** compares very favorably with the fused ladder-type polymer **BBL** while having the distinct advantage of being easily processed from common organic solvents and synthesized from a nontoxic aldol condensation. Incorporating various synthetic design principles and material engineering optimizations outlined throughout this review should allow for the OECT performance of these fused electron-deficient glycolated rigid rod polymers to be further improved and truly surpass that of **BBL**.

2.6.4. n-Type Summary. Apart from **BBL** and the recently published **PgNaN** and **PgNgN**, the only n-type systems studied, within OECTs, have been based on **NDI** derivatives. While this limits the overall synthetic design principles that can be garnered for n-type materials, significant progress has been made to improve OECT performance.[152] Furthermore, sufficient side chain engineering studies have been conducted which elucidate important design criteria. As mentioned above, multiple studies have corroborated the importance of both side chain composition and distribution on the resultant polymer performance. Specifically, the inclusion of an alkyl spacer, directly tethered to the polymer backbone, separating the core from the hydrophilic ethylene glycol side chains, was proven to affect the film order, crystallinity, and thus, the electron mobility. This inclusion of a protective alkyl sheaf has resulted in state-of-the-art n-type materials ($p(C6-T2)$) with impressive electron mobilities of 4.74×10^{-3} cm^2 V^{-1} s^{-1} and operational stability over multiple cycles.[210] Electron mobilities have been further increased to $6.50 \times 10^{-3} cm^2 V^{-1} s^{-1}$ for **PgNaN** devices, where the fused polymer backbone leads to more efficient charge transport. These values are a marked improvement for the field of n-type OECTs, which have, historically, considerably lagged behind the hole mobilities presented by p-type materials. The overall upward trend of $[\mu C^*]$ figure-of-merit values is also extremely promising for the wider field of bioelectronics as many practical applications require balanced performance of n- and p-type materials.[20,215] Through incorporating both the side chain manipulation techniques and polymer backbone optimizations, future *n*-type materials can be expected to further improve in both performance and stability.

2.7. Conclusions and Outlook

Substantial research and development have been conducted by the bioelectronics community since the inception of the organic electrochemical transistor in 1984. Indeed, OECTs have become a staple device for mixed-conduction materials, offering impressive transconduction properties alongside a relatively simple device architecture which has been employed within multiple biological applications.[188] The operating mechanism, for OECTs, varies drastically from common dielectric and electrolyte-gated organic field effect transistors, with semiconductor doping occurring throughout the entire bulk and is not limited to the interface. Owing to this necessary condition for efficient OECT operation, OMIECs capable of simultaneous ionic and electronic charge conduction, have

emerged as the most successful and well-documented channel materials.

The aim of this review was to discuss the current situation in the field of OMIECs for OECT devices and answer the following questions: (i) Can we provide the molecular design rules toward more efficient OMIEC materials? (ii) What are current limitations within the field? (iii) What are the ways to tackle them? And finally (iv) which new applications could emerge from the successful design of emergent OMIECs?

In regard to the first and second questions, the widespread commercial availability of **PEDOT:PSS** alongside the materials high hole transporting mobility and impressive chemical stability has rendered this material as the gold standard go-to OECT channel material. However, the prevalence of **PEDOT:PSS** (and related derivatives) throughout the literature may be a consequence of convenience, as the highly complex structure severely limits the potential structure–property relationships required from a model system. As such, the past decade has seen a surge in the number of novel organic mixed ionic electronic materials, especially p-type materials owing to the inherent instability of n-type materials.[152] The majority of these are based on either conjugated polyelectrolytes or glycolated semiconducting polymers, both of which have been shown to repeatedly outperform **PEDOT:PSS**-based devices.[53] The much improved volumetric capacitances and ability to compare intricate molecular design principles has solidified these polymers as the pinnacle OECT mixed conduction material system from both a performance and synthetic design point of view. The expansion of the field has also allowed for the development of n-type channel materials, and while their performances have historically lagged behind their p-type counterparts, great strides have recently been made to close this gap.

Currently, the highest transconductance values, on/off ratios and $[\mu C^*]$ figure-of-merit values are reported for channel materials bearing various oligoether (glycol) side chains. In a similar vein to **PEDOT:PSS**, glycol chains of varying lengths have widespread commercial availability, making them synthetically attractive. Alkyl–aryl–ether linkage leads to electron donation and IP reduction when grafting glycolated side chains directly to the polymer scaffold, hence, stabilizing the oxidized states. In the case of sulfur-containing backbones, noncovalent S–O interactions particularly favor polymer planarity. Recent studies have investigated the optimal length and overall density of glycol chains through side chain redistribution, which corroborate with the extensive examples of high performing channel materials utilizing triethylene glycol as the oligoether side chain of choice. However, some examples of both seven-unit ethylene glycol and hybrid alkyl–glycol spacer side chain containing polymers have been demonstrated, with very impressive OECT performance parameters suggesting that more work into identifying the ideal glycol side chain length and composition, which differs for each polymer backbone, should be a focus for future research. A different approach would be to investigate the use of alternative hydrophilic side chains, as was the case for $p(NDI-T2-L2)$, which utilized bioinspired lysine chains as opposed to the common glycol units.[182] While this specific example did not yield the highest OECT performance, the bioelectronic application potential of this material far outweighs the meagre $[\mu C^*]$ value. On a par with the side chain toolbox expansion, polymer backbones should also be optimized to further improve electron transport properties

while maintaining or deepening the LUMO energy level. Early results from **PgNaN** suggest the fused polylactam-based acceptor−acceptor polymer motif as a promising n-type backbone with impressive electron mobilities and is worthy of additional research.[160] Meanwhile, the search for potential ways of enhancing air and water stability of n-type conductors by means of introducing new chromophores and sterically shielded structures with deep LUMO levels is expected to continue. Further investigation of the structure−property relationships with a discrete focus on morphological studies and the influence of the polymer molecular weight on the OECT performance is also anticipated. In this light, conceiving the design motifs for synthesizing the robust under deformation materials presumes the expansion of the wearable bioelectronic devices, based on OECTs.

In terms of the applications, the vastness of the field of bioelectronics renders OMIECs as true multipurpose materials, and even though the OECT has emerged as the most prevalent device, future and emergent materials are necessary to allow the overall field to continue to blossom. The development of the effective toolbox of healthcare, drug screening, and reliable health monitoring at the interface of electronics and biology is an ultimate goal of bioelectronics. OECTs can ensure stability of long-term biomedical devices owing to their decreased power consumption. The following step toward OECT translation into real-world applications would include accessing information on continuous changes in the film physicochemical composition upon the interaction with bodily fluids.[32] Furthermore, the possibility to fine-tune ion selectivity opens the path for the development of different biosensors. For instance, OECT-based biosensors can utilize materials with bespoke biological properties, such as mixed conductors modified with enzymes. Moreover, bioelectronics implies not simply utilization of new materials but the use of devices, meaning that the device architecture with all the constituting parts should also be considered.[216] As such, development of semisolid biocompatible electrolytes remains of prime importance. Overall, the improved material design, synthetic optimizations, and developing list of applications has propelled OMIECs to the forefront of the bioelectronics community. While undeniable progress has been made, in particular over the past decade, the plethora of documented materials now available and resultant synthetic design rules and structure−property relationships outlined throughout this review will surely allow the field to flourish at an accelerated rate.

AUTHOR INFORMATION

Corresponding Author

Christine K. Luscombe − *Materials Science and Engineering Department, University of Washington, Seattle, Washington 98195, United States; Department of Chemistry and Molecular Engineering & Sciences Institute, University of Washington, Seattle, Washington 98195, United States;* Present Address: C.K.L.: pi-Conjugated Polymers Unit, Okinawa Institute of Science & Technology Graduate University, Onna-son, Okinawa 904-0495, Japan.; orcid.org/0000-0001-7456-1343; Email: christine.luscombe@oist.jp

Authors

Nadzeya A. Kukhta − *Materials Science and Engineering Department, University of Washington, Seattle, Washington 98195, United States*

Adam Marks − *Department of Chemistry, University of Oxford, Oxford OX1 3TA, United Kingdom;* Present Address: A.M.: Department of Materials Science and Engineering, Stanford University, Stanford, California 94305, United States; orcid.org/0000-0001-9819-4349

Complete contact information is available at: https://pubs.acs.org/10.1021/acs.chemrev.1c00266

Author Contributions

[∇]N.A.K. and A.M. contributed equally.

Notes

The authors declare no competing financial interest.

Biographies

Nadzeya A. Kukhta is currently a postdoctoral researcher at the University of Washington in Seattle, USA, in the group of Prof. Christine K. Luscombe. She received her Ph.D. in Materials Engineering at Kaunas University of Technology, Lithuania, under the supervision of Prof. Juozas Vidas Grazulevicius. Nadzeya's Ph.D. research focused on the investigation of structure−property relationships of purely organic semiconductors for the OLED, OFET, and OPV applications. Upon the reception of her Doctorate degree, Nadzeya continued pursuing an academic career as a postdoctoral researcher at Durham University, UK, in the group of Prof. Martin R. Bryce. Throughout her three-year position at Durham, Nadzeya has been designing, synthesizing, and investigating photophysical properties of the emissive compounds exhibiting thermally activated delayed fluorescence (TADF) and room temperature phosphorescence (RTP) phenomena. Nadzeya's current research interests include stretchable electronics, mixed conductors, bioelectronics, and liquid crystals.

Adam Marks received his M.Sc. degree in Chemistry from Imperial College London in 2016. He then joined the group of Prof. Iain McCulloch, completing his Ph.D. in 2020, working on the development of OMIEC materials for bioelectronic applications. Since then, he followed the McCulloch group to the University of Oxford, where he was a postdoctoral research associate, focusing on the development of electron transport OMIEC materials. He is now a postdoctoral researcher with Prof. Alberto Salleo and Prof. William Chueh at Stanford University. His current research interests are focused on the synthetic development of novel materials for bioelectronic applications and thermoelectric devices. In addition Adam is also involved in the synthesis and evaluation of materials for polymeric electrocatalysis.

Christine K. Luscombe received her M.Sci. degree in Natural Sciences (Chemistry) from the University of Cambridge in 2000. She then completed her Ph.D. with Profs. Andrew Holmes and Wilhelm Huck in the Melveille Laboratory for Polymer Synthesis at the University of Cambridge. After completing her postdoctoral work with Prof. Jean M. J. Fréchet at UC Berkeley, she joined the Materials Science and Engineering Department at the University of Washington, Seattle, in 2006 and was the Robert J. Campbell Development Professor of Materials Science and Engineering and Professor of Chemistry at the University of Washington, Seattle. Since September 2021, she is a Professor at the Okinawa Institute of Science & Technology Graduate University in Japan. Her current research focuses on the synthesis of semiconducting polymers for organic electronics and has published >100 papers in this area of research. She serves as an Associate Editor for Macromolecules and is the President of the IUPAC Polymer Division.

REFERENCES

(1) Tarabella, G.; Mahvash Mohammadi, F.; Coppedè, N.; Barbero, F.; Iannotta, S.; Santato, C.; Cicoira, F. New Opportunities for Organic Electronics and Bioelectronics: Ions in Action. *Chem. Sci.* **2013**, *4*, 1395−1409.

(2) Simon, D. T.; Gabrielsson, E. O.; Tybrandt, K.; Berggren, M. Organic Bioelectronics: Bridging the Signaling Gap between Biology and Technology. *Chem. Rev.* **2016**, *116*, 13009−13041.

(3) Cherian, D.; Armgarth, A.; Beni, V.; Linderhed, U.; Tybrandt, K.; Nilsson, D.; Simon, D. T.; Berggren, M. Large-Area Printed Organic Electronic Ion Pumps. *Flex. Print.* **2019**, *4*, 022001.

(4) Xiao, K.; Wan, C.; Jiang, L.; Chen, X.; Antonietti, M. Bioinspired Ionic Sensory Systems: The Successor of Electronics. *Adv. Mater.* **2020**, *32*, 2000218.

(5) Pan, X.; Wang, Q.; Guo, R.; Cao, S.; Wu, H.; Ouyang, X.; Huang, F.; Gao, H.; Huang, L.; Zhang, F.; Chen, L.; Ni, Y.; Liu, K. An Adaptive Ionic Skin with Multiple Stimulus Responses and Moist-Electric Generation Ability. *J. Mater. Chem. A* **2020**, *8*, 17498−17506.

(6) Martin Varguez, P. E.; Brunel, F.; Raimundo, J.-M. Recent Electrochemical/Electrical Microfabricated Sensor Devices for Ionic and Polyionic Analytes. *ACS Omega* **2020**, *5*, 4733−4742.

(7) Yao, G.; Yin, C.; Wang, Q.; Zhang, T.; Chen, S.; Lu, C.; Zhao, K.; Xu, W.; Pan, T.; Gao, M.; Lin, Y. Flexible Bioelectronics for Physiological Signals Sensing and Disease Treatment. *J. Materiomics* **2020**, *6*, 397−413.

(8) Rashid, R. B.; Ji, X.; Rivnay, J. Organic Electrochemical Transistors in Bioelectronic Circuits. *Biosens. Bioelectron.* **2021**, *190*, 113461.

(9) Baek, P.; Voorhaar, L.; Barker, D.; Travas-Sejdic, J. Molecular Approach to Conjugated Polymers with Biomimetic Properties. *Acc. Chem. Res.* **2018**, *51*, 1581−1589.

(10) Dijk, G.; Rutz, A. L.; Malliaras, G. G. Stability of PEDOT:PSS-Coated Gold Electrodes in Cell Culture Conditions. *Adv. Mater. Technol.* **2020**, *5*, 1900662.

(11) Spira, M. E.; Hai, A. Multi-Electrode Array Technologies for Neuroscience and Cardiology. *Nat. Nanotechnol.* **2013**, *8*, 83−94.

(12) Berto, M.; Diacci, C.; Theuer, L.; Di Lauro, M.; Simon, D. T.; Berggren, M.; Biscarini, F.; Beni, V.; Bortolotti, C. A. Label Free Urea Biosensor Based on Organic Electrochemical Transistors. *Flex. Print.* **2018**, *3*, 024001.

(13) Manoli, K.; Magliulo, M.; Mulla, M. Y.; Singh, M.; Sabbatini, L.; Palazzo, G.; Torsi, L. Printable Bioelectronics To Investigate Functional Biological Interfaces. *Angew. Chem., Int. Ed.* **2015**, *54*, 12562−12576.

(14) Pappa, A.-M.; Parlak, O.; Scheiblin, G.; Mailley, P.; Salleo, A.; Owens, R. M. Organic Electronics for Point-of-Care Metabolite Monitoring. *Trends Biotechnol.* **2018**, *36*, 45−59.

(15) Van De Burgt, Y.; Lubberman, E.; Fuller, E. J.; Keene, S. T.; Faria, G. C.; Agarwal, S.; Marinella, M. J.; Alec Talin, A.; Salleo, A. A Non-Volatile Organic Electrochemical Device as a Low-Voltage

Artificial Synapse for Neuromorphic Computing. *Nat. Mater.* **2017**, *16*, 414−418.

(16) Koutsouras, D. A.; Malliaras, G. G.; Gkoupidenis, P. Emulating Homeoplasticity Phenomena with Organic Electrochemical Devices. *MRS Commun.* **2018**, *8*, 493−497.

(17) Tuchman, Y.; Mangoma, T. N.; Gkoupidenis, P.; Van De Burgt, Y.; John, R. A.; Mathews, N.; Shaheen, S. E.; Daly, R.; Malliaras, G. G.; Salleo, A. Organic Neuromorphic Devices: Past, Present, and Future Challenges. *MRS Bull.* **2020**, *45*, 619−630.

(18) Pappa, A.-M.; Curto, V. F.; Braendlein, M.; Strakosas, X.; Donahue, M. J.; Fiocchi, M.; Malliaras, G. G.; Owens, R. M. Organic Transistor Arrays Integrated with Finger-Powered Microfluidics for Multianalyte Saliva Testing. *Adv. Healthcare Mater.* **2016**, *5*, 2295−2302.

(19) Tang, H.; Yan, F.; Lin, P.; Xu, J.; Chan, H. L. W. Highly Sensitive Glucose Biosensors Based on Organic Electrochemical Transistors Using Platinum Gate Electrodes Modified with Enzyme and Nanomaterials. *Adv. Funct. Mater.* **2011**, *21*, 2264−2272.

(20) Moser, M.; Ponder, J. F.; Wadsworth, A.; Giovannitti, A.; McCulloch, I. Materials in Organic Electrochemical Transistors for Bioelectronic Applications: Past, Present, and Future. *Adv. Funct. Mater.* **2019**, *29*, 1807033.

(21) Khodagholy, D.; Doublet, T.; Quilichini, P.; Gurfinkel, M.; Leleux, P.; Ghestem, A.; Ismailova, E.; Hervé, T.; Sanaur, S.; Bernard, C.; Malliaras, G. G. In Vivo Recordings of Brain Activity Using Organic Transistors. *Nat. Commun.* **2013**, *4*, 1573.

(22) Ashtari, K.; Nazari, H.; Ko, H.; Tebon, P.; Akhshik, M.; Akbari, M.; Alhosseini, S. N.; Mozafari, M.; Mehravi, B.; Soleimani, M.; Ardehali, R.; Ebrahimi Warkiani, M.; Ahadian, S.; Khademhosseini, A. Electrically Conductive Nanomaterials for Cardiac Tissue Engineering. *Adv. Drug Delivery Rev.* **2019**, *144*, 162−179.

(23) Huang, W.; Chen, Y.; Chen, L.; Zhong, J.; Johri, A. M.; Zhou, J. Multimodality Imaging-Guided Local Injection of Eccentric Magnetic Microcapsules with Electromagnetically Controlled Drug Release. *Cancer Reports* **2019**, *2*, No. e1154.

(24) Jo, S. H.; Chang, T.; Ebong, I.; Bhadviya, B. B.; Mazumder, P.; Lu, W. Nanoscale Memristor Device as Synapse in Neuromorphic Systems. *Nano Lett.* **2010**, *10*, 1297−1301.

(25) Liu, D.; Rahman, M. M.; Ge, C.; Kim, J.; Lee, J. J. Highly Stable and Conductive PEDOT:PSS/Graphene Nanocomposites for Biosensor Applications in Aqueous Medium. *New J. Chem.* **2017**, *41*, 15458−15465.

(26) Feron, K.; Lim, R.; Sherwood, C.; Keynes, A.; Brichta, A.; Dastoor, P. Organic Bioelectronics: Materials and Biocompatibility. *Int. J. Mol. Sci.* **2018**, *19*, 2382.

(27) Harris, A. R.; Wallace, G. G. Organic Electrodes and Communications with Excitable Cells. *Adv. Funct. Mater.* **2018**, *28*, 1700587.

(28) Löffler, S.; Libberton, B.; Richter-Dahlfors, A. Organic Bioelectronic Tools for Biomedical Applications. *Electronics* **2015**, *4*, 879−908.

(29) Green, R. A.; Lovell, N. H.; Wallace, G. G.; Poole-Warren, L. A. Conducting Polymers for Neural Interfaces: Challenges in Developing an Effective Long-Term Implant. *Biomaterials* **2008**, *29*, 3393−3399.

(30) Aggas, J. R.; Lutkenhaus, J.; Guiseppi-Elie, A. Chemiresistive and Chemicapacitive Devices Formed via Morphology Control of Electroconductive Bio-Nanocomposites. *Adv. Electron. Mater.* **2018**, *4*, 1700495.

(31) Donahue, M. J.; Sanchez-Sanchez, A.; Inal, S.; Qu, J.; Owens, R. M.; Mecerreyes, D.; Malliaras, G. G.; Martin, D. C. Tailoring PEDOT Properties for Applications in Bioelectronics. *Mater. Sci. Eng., R* **2020**, *140*, 100546.

(32) Zeglio, E.; Inganäs, O. Active Materials for Organic Electrochemical Transistors. *Adv. Mater.* **2018**, *30*, 1800941.

(33) Dong, B. X.; Nowak, C.; Onorato, J. W.; Strzalka, J.; Escobedo, F. A.; Luscombe, C. K.; Nealey, P. F.; Patel, S. N. Influence of Side-Chain Chemistry on Structure and Ionic Conduction Characteristics of Polythiophene Derivatives: A Computational and Experimental Study. *Chem. Mater.* **2019**, *31*, 1418−1429.

(34) Pappa, A. M.; Ohayon, D.; Giovannitti, A.; Maria, I. P.; Savva, A.; Uguz, I.; Rivnay, J.; McCulloch, I.; Owens, R. M.; Inal, S. Direct Metabolite Detection with an N-Type Accumulation Mode Organic Electrochemical Transistor. *Sci. Adv.* **2018**, *4*, No. eaat0911.

(35) Savva, A.; Hallani, R.; Cendra, C.; Surgailis, J.; Hidalgo, T. C.; Wustoni, S.; Sheelamanthula, R.; Chen, X.; Kirkus, M.; Giovannitti, A.; Salleo, A.; McCulloch, I.; Inal, S. Balancing Ionic and Electronic Conduction for High-Performance Organic Electrochemical Transistors. *Adv. Funct. Mater.* **2020**, *30*, 1907657.

(36) Bischak, C. G.; Flagg, L. Q.; Yan, K.; Rehman, T.; Davies, D. W.; Quezada, R. J.; Onorato, J. W.; Luscombe, C. K.; Diao, Y.; Li, C. Z.; Ginger, D. S. A Reversible Structural Phase Transition by Electrochemically-Driven Ion Injection into a Conjugated Polymer. *J. Am. Chem. Soc.* **2020**, *142*, 7434−7442.

(37) Rivnay, J.; Inal, S.; Collins, B. A.; Sessolo, M.; Stavrinidou, E.; Strakosas, X.; Tassone, C.; Delongchamp, D. M.; Malliaras, G. G. Structural Control of Mixed Ionic and Electronic Transport in Conducting Polymers. *Nat. Commun.* **2016**, *7*, 11287.

(38) Flagg, L. Q.; Bischak, C. G.; Quezada, R. J.; Onorato, J. W.; Luscombe, C. K.; Ginger, D. S. P-Type Electrochemical Doping Can Occur by Cation Expulsion in a High-Performing Polymer for Organic Electrochemical Transistors. *ACS Mater. Lett.* **2020**, *2*, 254−260.

(39) Kittlesen, G. P.; White, H. S.; Wrighton, M. S. Chemical Derivatization of Microelectrode Arrays by Oxidation of Pyrrole and N-Methylpyrrole: Fabrication of Molecule-Based Electronic Devices. *J. Am. Chem. Soc.* **1984**, *106*, 7389−7396.

(40) Lamport, Z. A.; Haneef, H. F.; Anand, S.; Waldrip, M.; Jurchescu, O. D. Tutorial: Organic Field-Effect Transistors: Materials, Structure and Operation. *J. Appl. Phys.* **2018**, *124*, 071101.

(41) Koezuka, H.; Tsumura, A.; Ando, T. Field-Effect Transistor with Polythiophene Thin Film. *Synth. Met.* **1987**, *18*, 699−704.

(42) Sun, H.; Gerasimov, J.; Berggren, M.; Fabiano, S. N-Type Organic Electrochemical Transistors: Materials and Challenges. *J. Mater. Chem. C* **2018**, *6*, 11778−11784.

(43) Kim, S. H.; Hong, K.; Xie, W.; Lee, K. H.; Zhang, S.; Lodge, T. P.; Frisbie, C. D. Electrolyte-Gated Transistors for Organic and Printed Electronics. *Adv. Mater.* **2013**, *25*, 1822−1846.

(44) Zhao, D.; Fabiano, S.; Berggren, M.; Crispin, X. Ionic Thermoelectric Gating Organic Transistors. *Nat. Commun.* **2017**, *8*, 14214.

(45) Khodagholy, D.; Rivnay, J.; Sessolo, M.; Gurfinkel, M.; Leleux, P.; Jimison, L. H.; Stavrinidou, E.; Herve, T.; Sanaur, S.; Owens, R. M.; Malliaras, G. G. High Transconductance Organic Electrochemical Transistors. *Nat. Commun.* **2013**, *4*, 2133.

(46) Parr, Z. S.; Halaksa, R.; Finn, P. A.; Rashid, R. B.; Kovalenko, A.; Weiter, M.; Rivnay, J.; Krajčovič, J.; Nielsen, C. B. Glycolated Thiophene-Tetrafluorophenylene Copolymers for Bioelectronic Applications: Synthesis by Direct Heteroarylation Polymerisation. *ChemPlusChem* **2019**, *84*, 1384−1390.

(47) Onorato, J. W.; Luscombe, C. K. Morphological Effects on Polymeric Mixed Ionic/Electronic Conductors. *Mol. Sys. Des. Eng.* **2019**, *4*, 310−324.

(48) White, H. S.; Kittlesen, G. P.; Wrighton, M. S. Chemical Derivatization of an Array of Three Gold Microelectrodes with Polypyrrole: Fabrication of a Molecule-Based Transistor. *J. Am. Chem. Soc.* **1984**, *106*, 5375−5377.

(49) Thackeray, J. W.; White, H. S.; Wrighton, M. S. Poly(3-Methylthiophene)-Coated Electrodes: Optical and Electrical Properties as a Function of Redox Potential and Amplification of Electrical and Chemical Signals Using Poly(3-Methylthiophene)-Based Microelectrochemical Transistors. *J. Phys. Chem.* **1985**, *89*, 5133−5140.

(50) Paul, E. W.; Ricco, A. J.; Wrighton, M. S. Resistance of Polyaniline Films as a Function of Electrochemical Potential and the Fabrication of Polyaniline-Based Microelectronic Devices. *J. Phys. Chem.* **1985**, *89*, 1441−1447.

(51) Rani, V.; Santhanam, K. S. V. Polycarbazole-Based Electrochemical Transistor. *J. Solid State Electrochem.* **1998**, *2*, 99−101.

(52) Inal, S.; Rivnay, J.; Leleux, P.; Ferro, M.; Ramuz, M.; Brendel, J. C.; Schmidt, M. M.; Thelakkat, M.; Malliaras, G. G. A High Transconductance Accumulation Mode Electrochemical Transistor. *Adv. Mater.* **2014**, *26*, 7450−7455.

(53) Inal, S.; Malliaras, G. G.; Rivnay, J. Benchmarking Organic Mixed Conductors for Transistors. *Nat. Commun.* **2017**, *8*, 1767.

(54) Wang, Y.; Zeglio, E.; Liao, H.; Xu, J.; Liu, F.; Li, Z.; Maria, I. P.; Mawad, D.; Herland, A.; McCulloch, I.; Yue, W. Hybrid Alkyl-Ethylene Glycol Side Chains Enhance Substrate Adhesion and Operational Stability in Accumulation Mode Organic Electrochemical Transistors. *Chem. Mater.* **2019**, *31*, 9797−9806.

(55) Rivnay, J.; Inal, S.; Salleo, A.; Owens, R. M.; Berggren, M.; Malliaras, G. G. Organic Electrochemical Transistors. *Nat. Rev. Mater.* **2018**, *3*, 17086.

(56) Bernards, D. A.; MacAya, D. J.; Nikolou, M.; Defranco, J. A.; Takamatsu, S.; Malliaras, G. G. Enzymatic Sensing with Organic Electrochemical Transistors. *J. Mater. Chem.* **2008**, *18*, 116−120.

(57) Xu, M.; Obodo, D.; Yadavalli, V. K. The Design, Fabrication, and Applications of Flexible Biosensing Devices. *Biosens. Bioelectron.* **2019**, *124−125*, 96−114.

(58) Williamson, A.; Ferro, M.; Leleux, P.; Ismailova, E.; Kaszas, A.; Doublet, T.; Quilichini, P.; Rivnay, J.; Rózsa, B.; Katona, G.; Bernard, C.; Malliaras, G. G. Localized Neuron Stimulation with Organic Electrochemical Transistors on Delaminating Depth Probes. *Adv. Mater.* **2015**, *27*, 4405−4410.

(59) Lee, W.; Kim, D.; Rivnay, J.; Matsuhisa, N.; Lonjaret, T.; Yokota, T.; Yawo, H.; Sekino, M.; Malliaras, G. G.; Someya, T. Integration of Organic Electrochemical and Field-Effect Transistors for Ultraflexible, High Temporal Resolution Electrophysiology Arrays. *Adv. Mater.* **2016**, *28*, 9722−9728.

(60) Campana, A.; Cramer, T.; Simon, D. T.; Berggren, M.; Biscarini, F. Electrocardiographic Recording with Conformable Organic Electrochemical Transistor Fabricated on Resorbable Bioscaffold. *Adv. Mater.* **2014**, *26*, 3874−3878.

(61) Leleux, P.; Rivnay, J.; Lonjaret, T.; Badier, J.-M.; Bénar, C.; Hervé, T.; Chauvel, P.; Malliaras, G. G. Organic Electrochemical Transistors for Clinical Applications. *Adv. Healthcare Mater.* **2015**, *4*, 142−147.

(62) Fariat, G. C.; Duongt, D. T.; Salleo, A.; Polyzoidis, C. A.; Logothetidis, S.; Rivnay, J.; Owens, R.; Malliaras, G. G. Organic Electrochemical Transistors as Impedance Biosensors. *MRS Commun.* **2014**, *4*, 189−194.

(63) Gu, X.; Yao, C.; Liu, Y.; Hsing, I.-M. 16-Channel Organic Electrochemical Transistor Array for In Vitro Conduction Mapping of Cardiac Action Potential. *Adv. Healthcare Mater.* **2016**, *5*, 2345−2351.

(64) Ramuz, M.; Hama, A.; Rivnay, J.; Leleux, P.; Owens, R. M. Monitoring of Cell Layer Coverage and Differentiation with the Organic Electrochemical Transistor. *J. Mater. Chem. B* **2015**, *3*, 5971−5977.

(65) Zhang, Y.; Inal, S.; Hsia, C.; Ferro, M.; Ferro, M.; Daniel, S.; Owens, R. M. Supported Lipid Bilayer Assembly on PEDOT:PSS Films and Transistors. *Adv. Funct. Mater.* **2016**, *26*, 7304−7313.

(66) Sessolo, M.; Rivnay, J.; Bandiello, E.; Malliaras, G. G.; Bolink, H. J. Ion-Selective Organic Electrochemical Transistors. *Adv. Mater.* **2014**, *26*, 4803−4807.

(67) Guo, K.; Wustoni, S.; Koklu, A.; Díaz-Galicia, E.; Moser, M.; Hama, A.; Alqahtani, A. A.; Ahmad, A. N.; Alhamlan, F. S.; Shuaib, M.; Pain, A.; McCulloch, I.; Arold, S. T.; Grünberg, R.; Inal, S. Rapid Single-Molecule Detection of COVID-19 and MERS Antigens via Nanobody-Functionalized Organic Electrochemical Transistors. *Nat. biomed. eng.* **2021**, *5*, 666−677.

(68) Jakešová, M.; Sjöström, T. A.; Đerek, V.; Poxson, D.; Berggren, M.; Głowacki, E. D.; Simon, D. T. Wireless Organic Electronic Ion Pumps Driven by Photovoltaics. *npj Flex. Electron.* **2019**, *3*, 14.

(69) Arbring Sjöström, T.; Berggren, M.; Gabrielsson, E. O.; Janson, P.; Poxson, D. J.; Seitanidou, M.; Simon, D. T. A Decade of Iontronic Delivery Devices. *Adv. Mater. Technol.* **2018**, *3*, 1700360.

(70) Bihar, E.; Deng, Y.; Miyake, T.; Saadaoui, M.; Malliaras, G. G.; Rolandi, M. A Disposable Paper Breathalyzer with an Alcohol Sensing Organic Electrochemical Transistor. *Sci. Rep.* **2016**, *6*, 27582.

(71) Gualandi, I.; Tonelli, D.; Mariani, F.; Scavetta, E.; Marzocchi, M.; Fraboni, B. Selective Detection of Dopamine with an All PEDOT:PSS Organic Electrochemical Transistor. *Sci. Rep.* **2016**, *6*, 35419.

(72) Tybrandt, K.; Kollipara, S. B.; Berggren, M. Organic Electrochemical Transistors for Signal Amplification in Fast Scan Cyclic Voltammetry. *Sens. Actuators, B* **2014**, *195*, 651−656.

(73) Lin, P.; Luo, X.; Hsing, I. M.; Yan, F. Organic Electrochemical Transistors Integrated in Flexible Microfluidic Systems and Used for Label-Free DNA Sensing. *Adv. Mater.* **2011**, *23*, 4035−4040.

(74) Jonsson, A.; Inal, S.; Uguz, L.; Williamson, A. J.; Kergoat, L.; Rivnay, J.; Khodagholy, D.; Berggren, M.; Bernard, C.; Malliaras, G. G.; Simon, D. T. Bioelectronic Neural Pixel: Chemical Stimulation and Electrical Sensing at the Same Site. *Proc. Natl. Acad. Sci. U. S. A.* **2016**, *113*, 9440−9445.

(75) Wang, Y.; Wang, Z.; Su, Z.; Cai, S. Stretchable and Transparent Ionic Diode and Logic Gates. *Extreme Mech. Lett.* **2019**, *28*, 81−86.

(76) Han, S. H.; Kwon, S. R.; Baek, S.; Chung, T. D. Ionic Circuits Powered by Reverse Electrodialysis for an Ultimate Iontronic System. *Sci. Rep.* **2017**, *7*, 14068.

(77) Gerasimov, J. Y.; Gabrielsson, R.; Forchheimer, R.; Stavrinidou, E.; Simon, D. T.; Berggren, M.; Fabiano, S. An Evolvable Organic Electrochemical Transistor for Neuromorphic Applications. *Adv. Sci.* **2019**, *6*, 1801339.

(78) Han, J.-H.; Kim, K. B.; Bae, J. H.; Kim, B. J.; Kang, C. M.; Kim, H. C.; Chung, T. D. Ion Flow Crossing Over a Polyelectrolyte Diode on a Microfluidic Chip. *Small* **2011**, *7*, 2629−2639.

(79) Svensson, P. O.; Nilsson, D.; Forchheimer, R.; Berggren, M. A Sensor Circuit Using Reference-Based Conductance Switching in Organic Electrochemical Transistors. *Appl. Phys. Lett.* **2008**, *93*, 203301.

(80) Braendlein, M.; Pappa, A.-M.; Ferro, M.; Lopresti, A.; Acquaviva, C.; Mamessier, E.; Malliaras, G. G.; Owens, R. M. Lactate Detection in Tumor Cell Cultures Using Organic Transistor Circuits. *Adv. Mater.* **2017**, *29*, 1605744.

(81) Braendlein, M.; Lonjaret, T.; Leleux, P.; Badier, J.-M.; Malliaras, G. G. Voltage Amplifier Based on Organic Electrochemical Transistor. *Adv. Sci.* **2017**, *4*, 1600247.

(82) Gkoupidenis, P.; Schaefer, N.; Garlan, B.; Malliaras, G. G. Neuromorphic Functions in PEDOT:PSS Organic Electrochemical Transistors. *Adv. Mater.* **2015**, *27*, 7176−7180.

(83) Xu, W.; Min, S. Y.; Hwang, H.; Lee, T. W. Organic Core-Sheath Nanowire Artificial Synapses with Femtojoule Energy Consumption. *Sci. Adv.* **2016**, *2*, No. e1501326.

(84) Gkoupidenis, P.; Koutsouras, D. A.; Malliaras, G. G. Neuromorphic Device Architectures with Global Connectivity through Electrolyte Gating. *Nat. Commun.* **2017**, *8*, 15448.

(85) Gumyusenge, A.; Melianas, A.; Keene, S. T.; Salleo, A. Materials Strategies for Organic Neuromorphic Devices. *Annu. Rev. Mater. Res.* **2021**, *51*, 47−71.

(86) Berggren, M.; Crispin, X.; Fabiano, S.; Jonsson, M. P.; Simon, D. T.; Stavrinidou, E.; Tybrandt, K.; Zozoulenko, I. Ion Electron-Coupled Functionality in Materials and Devices Based on Conjugated Polymers. *Adv. Mater.* **2019**, *31*, 1805813.

(87) Kim, J. H.; Kim, S.; Kim, G.; Yoon, M. Designing Polymeric Mixed Conductors and Their Application to Electrochemical-Transistor-Based Biosensors. *Macromol. Biosci.* **2020**, *20*, 2000211.

(88) Paulsen, B. D.; Tybrandt, K.; Stavrinidou, E.; Rivnay, J. Organic Mixed Ionic-Electronic Conductors. *Nat. Mater.* **2020**, *19*, 13−26.

(89) Ajayaghosh, A. Donor-Acceptor Type Low Band Gap Polymers: Polysquaraines and Related Systems. *Chem. Soc. Rev.* **2003**, *32*, 181−191.

(90) Scholes, D. T.; Yee, P. Y.; Lindemuth, J. R.; Kang, H.; Onorato, J.; Ghosh, R.; Luscombe, C. K.; Spano, F. C.; Tolbert, S. H.; Schwartz, B. J. The Effects of Crystallinity on Charge Transport and the

Structure of Sequentially Processed F4TCNQ-Doped Conjugated Polymer Films. *Adv. Funct. Mater.* **2017**, *27*, 1702654.

(91) Holliday, S.; Donaghey, J. E.; McCulloch, I. Advances in Charge Carrier Mobilities of Semiconducting Polymers Used in Organic Transistors. *Chem. Mater.* **2014**, *26* (1), 647−663.

(92) Tatum, W. K.; Luscombe, C. K. π-Conjugated Polymer Nanowires: Advances and Perspectives toward Effective Commercial Implementation. *Polym. J.* **2018**, *50*, 659−669.

(93) Chang, J. F.; Sirringhaus, H.; Giles, M.; Heeney, M.; McCulloch, I. Relative Importance of Polaron Activation and Disorder on Charge Transport in High-Mobility Conjugated Polymer Field-Effect Transistors. *Phys. Rev. B: Condens. Matter Mater. Phys.* **2007**, *76*, 205204.

(94) Noriega, R.; Rivnay, J.; Vandewal, K.; Koch, F. P. V.; Stingelin, N.; Smith, P.; Toney, M. F.; Salleo, A. A General Relationship between Disorder, Aggregation and Charge Transport in Conjugated Polymers. *Nat. Mater.* **2013**, *12*, 1038−1044.

(95) Agrawal, R. C.; Pandey, G. P. Solid Polymer Electrolytes: Materials Designing and All-Solid-State Battery Applications: An Overview. *J. Phys. D: Appl. Phys.* **2008**, *41*, 223001.

(96) Shah, D. B.; Olson, K. R.; Karny, A.; Mecham, S. J.; DeSimone, J. M.; Balsara, N. P. Effect of Anion Size on Conductivity and Transference Number of Perfluoroether Electrolytes with Lithium Salts. *J. Electrochem. Soc.* **2017**, *164*, A3511−A3517.

(97) Kumar, P. P.; Yashonath, S. Ionic Conduction in the Solid State. *Proc. - Indian Acad. Sci., Chem. Sci.* **2006**, *118*, 135−154.

(98) Aziz, S. B.; Woo, T. J.; Kadir, M. F. Z.; Ahmed, H. M. A Conceptual Review on Polymer Electrolytes and Ion Transport Models. *J. Sci.: Adv. Mater. Devices* **2018**, *3*, 1−17.

(99) Cheng, S.; Smith, D. M.; Li, C. Y. How Does Nanoscale Crystalline Structure Affect Ion Transport in Solid Polymer Electrolytes? *Macromolecules* **2014**, *47*, 3978−3986.

(100) Xue, Z.; He, D.; Xie, X. Poly(Ethylene Oxide)-Based Electrolytes for Lithium-Ion Batteries. *J. Mater. Chem. A* **2015**, *3*, 19218−19253.

(101) Stavrinidou, E.; Leleux, P.; Rajaona, H.; Khodagholy, D.; Rivnay, J.; Lindau, M.; Sanaur, S.; Malliaras, G. G. Direct Measurement of Ion Mobility in a Conducting Polymer. *Adv. Mater.* **2013**, *25*, 4488−4493.

(102) Amdursky, N.; Głowacki, E. D.; Meredith, P. Macroscale Biomolecular Electronics and Ionics. *Adv. Mater.* **2019**, *31*, 1802221.

(103) Flagg, L. Q.; Giridharagopal, R.; Guo, J.; Ginger, D. S. Anion-Dependent Doping and Charge Transport in Organic Electrochemical Transistors. *Chem. Mater.* **2018**, *30*, 5380−5389.

(104) Cendra, C.; Giovannitti, A.; Savva, A.; Venkatraman, V.; McCulloch, I.; Salleo, A.; Inal, S.; Rivnay, J. Role of the Anion on the Transport and Structure of Organic Mixed Conductors. *Adv. Funct. Mater.* **2019**, *29*, 1807034.

(105) Kunugi, Y.; Harima, Y.; Yamashita, K.; Ohta, N.; Ito, S. Charge Transport in a Regioregular Poly(3-Octylthiophene) Film. *J. Mater. Chem.* **2000**, *10*, 2673−2677.

(106) Wang, S.; Ha, M.; Manno, M.; Daniel Frisbie, C.; Leighton, C. Hopping Transport and the Hall Effect near the Insulator-Metal Transition in Electrochemically Gated Poly(3-Hexylthiophene) Transistors. *Nat. Commun.* **2012**, *3*, 1210.

(107) Paulsen, B. D.; Frisbie, C. D. Dependence of Conductivity on Charge Density and Electrochemical Potential in Polymer Semiconductors Gated with Ionic Liquids. *J. Phys. Chem. C* **2012**, *116*, 3132−3141.

(108) Lim, J.; Li, Y.; Alsem, D. H.; So, H.; Lee, S. C.; Bai, P.; Cogswell, D. A.; Liu, X.; Jin, N.; Yu, Y. S.; Salmon, N. J.; Shapiro, D. A.; Bazant, M. Z.; Tyliszczak, T.; Chueh, W. C. Origin and Hysteresis of Lithium Compositional Spatiodynamics within Battery Primary Particles. *Science* **2016**, *353*, 566−571.

(109) Berggren, M.; Malliaras, G. G. How Conducting Polymer Electrodes Operate. *Science* **2019**, *364*, 233−234.

(110) Kaim, W.; Fiedler, J. Spectroelectrochemistry: The Best of Two Worlds. *Chem. Soc. Rev.* **2009**, *38*, 3373−3382.

(111) Giovannitti, A.; Rashid, R. B.; Thiburce, Q.; Paulsen, B. D.; Cendra, C.; Thorley, K.; Moia, D.; Mefford, J. T.; Hanifi, D.; Weiyuan, D.; Moser, M.; Salleo, A.; Nelson, J.; McCulloch, I.; Rivnay, J. Energetic Control of Redox-Active Polymers toward Safe Organic Bioelectronic Materials. *Adv. Mater.* **2020**, *32*, 1908047.

(112) Giovannitti, A.; Thorley, K. J.; Nielsen, C. B.; Li, J.; Donahue, M. J.; Malliaras, G. G.; Rivnay, J.; McCulloch, I. Redox-Stability of Alkoxy-BDT Copolymers and Their Use for Organic Bioelectronic Devices. *Adv. Funct. Mater.* **2018**, *28*, 1706325.

(113) Garcia-Belmonte, G.; Bisquert, J.; Popkirov, G. S. Determination of the Electronic Conductivity of Polybithiophene Films at Different Doping Levels Using in Situ Electrochemical Impedance Measurements. *Appl. Phys. Lett.* **2003**, *83*, 2178−2180.

(114) Ren, X.; Pickup, P. G. Ion Transport in Polypyrrole and a Polypyrrole/Polyanion Composite. *J. Phys. Chem.* **1993**, *97*, 5356−5362.

(115) Guo, K.; Wustoni, S.; Koklu, A.; Díaz-Galicia, E.; Moser, M.; Hama, A.; Alqahtani, A.; Ahmad, A.; Alhamlan, F.; Shuaib, M.; Pain, A.; McCulloch, I.; Arold, S.; Grünberg, R.; Inal, S. Rapid single-molecule detection of COVID-19 and MERS antigens via nanobody-functionalized organic electrochemical transistors. *Nt. Biomed. Eng.* **2021**, *5*, 666−667.

(116) Paterson, A. F.; Savva, A.; Wustoni, S.; Tsetseris, L.; Paulsen, B. D.; Faber, H.; Emwas, A. H.; Chen, X.; Nikiforidis, G.; Hidalgo, T. C.; Moser, M.; Maria, I. P.; Rivnay, J.; McCulloch, I.; Anthopoulos, T. D.; Inal, S. Water Stable Molecular N-Doping Produces Organic Electrochemical Transistors with High Transconductance and Record Stability. *Nat. Commun.* **2020**, *11*, 3004.

(117) Savva, A.; Wustoni, S.; Inal, S. Ionic-to-Electronic Coupling Efficiency in PEDOT:PSS Films Operated in Aqueous Electrolytes. *J. Mater. Chem. C* **2018**, *6*, 12023−12030.

(118) Franco-Gonzalez, J. F.; Zozoulenko, I. v. Molecular Dynamics Study of Morphology of Doped PEDOT: From Solution to Dry Phase. *J. Phys. Chem. B* **2017**, *121*, 4299−4307.

(119) Paulsen, B. D.; Wu, R.; Takacs, C. J.; Steinrück, H.; Strzalka, J.; Zhang, Q.; Toney, M. F.; Rivnay, J. Time-Resolved Structural Kinetics of an Organic Mixed Ionic-Electronic Conductor. *Adv. Mater.* **2020**, *32*, 2003404.

(120) Thomas, E. M.; Brady, M. A.; Nakayama, H.; Popere, B. C.; Segalman, R. A.; Chabinyc, M. L. X-Ray Scattering Reveals Ion-Induced Microstructural Changes During Electrochemical Gating of Poly(3-Hexylthiophene). *Adv. Funct. Mater.* **2018**, *28*, 1803687.

(121) Savva, A.; Cendra, C.; Giugni, A.; Torre, B.; Surgailis, J.; Ohayon, D.; Giovannitti, A.; McCulloch, I.; di Fabrizio, E.; Salleo, A.; Rivnay, J.; Inal, S. Influence of Water on the Performance of Organic Electrochemical Transistors. *Chem. Mater.* **2019**, *31*, 927−937.

(122) Giridharagopal, R.; Flagg, L. Q.; Harrison, J. S.; Ziffer, M. E.; Onorato, J.; Luscombe, C. K.; Ginger, D. S. Electrochemical Strain Microscopy Probes Morphology-Induced Variations in Ion Uptake and Performance in Organic Electrochemical Transistors. *Nat. Mater.* **2017**, *16*, 737−742.

(123) Friedlein, J. T.; Rivnay, J.; Dunlap, D. H.; McCulloch, I.; Shaheen, S. E.; McLeod, R. R.; Malliaras, G. G. Influence of Disorder on Transfer Characteristics of Organic Electrochemical Transistors. *Appl. Phys. Lett.* **2017**, *111*, 023301.

(124) Chung, J.; Khot, A.; Savoie, B. M.; Boudouris, B. W. 100th Anniversary of Macromolecular Science Viewpoint: Recent Advances and Opportunities for Mixed Ion and Charge Conducting Polymers. *ACS Macro Lett.* **2020**, *9*, 646−655.

(125) Liu, Y.; Duzhko, V. V.; Page, Z. A.; Emrick, T.; Russell, T. P. Conjugated Polymer Zwitterions: Efficient Interlayer Materials in Organic Electronics. *Acc. Chem. Res.* **2016**, *49*, 2478−2488.

(126) Elschner, A.; Kirchmeyer, S.; Lovenich, W.; Merker, U.; Reuter, K. *PEDOT: Principles and Applications of an Intrinsically Conductive Polymer*; CRC Press: Boca Raton, FL, 2010.

(127) Gu, Z.; Kanto, T.; Tsuchiya, K.; Ogino, K. Synthesis of Poly(3-Hexylthiophene)-b-Poly(Ethylene Oxide) for Application to Photovoltaic Device. *J. Photopolym. Sci. Technol.* **2010**, *23*, 405−406.

(128) Shirakawa, H. The Discovery of Polyacetylene Film: The Dawning of an Era of Conducting Polymers. *Angew. Chem., Int. Ed.* **2001**, *40*, 2574−2580.

(129) Bubnova, O.; Crispin, X. Towards Polymer-Based Organic Thermoelectric Generators. *Energy Environ. Sci.* **2012**, *5*, 9345−9362.

(130) Cheng, Y.-J.; Yang, S.-H.; Hsu, C.-S. Synthesis of Conjugated Polymers for Organic Solar Cell Applications. *Chem. Rev.* **2009**, *109*, 5868−5923.

(131) Salaneck, W. R.; Friend, R. H.; Brédas, J. L. Electronic Structure of Conjugated Polymers: Consequences of Electron-Lattice Coupling. *Phys. Rep.* **1999**, *319*, 231−251.

(132) Chandrasekhar, P. *Conducting Polymers, Fundamentals and Applications*; Springer, 1999.

(133) Sirringhaus, H.; Brown, P. J.; Friend, R. H.; Nielsen, M. M.; Bechgaard, K.; Langeveld-Voss, B. M. W.; Spiering, A. J. H.; Janssen, R. A. J.; Meijer, E. W.; Herwig, P.; de Leeuw, D. M. Two-Dimensional Charge Transport in Self-Organized, High-Mobility Conjugated Polymers. *Nature* **1999**, *401*, 685−688.

(134) McCulloch, I.; Heeney, M.; Bailey, C.; Genevicius, K.; MacDonald, I.; Shkunov, M.; Sparrowe, D.; Tierney, S.; Wagner, R.; Zhang, W.; Chabinyc, M. L.; Kline, R. J.; McGehee, M. D.; Toney, M. F. Liquid-Crystalline Semiconducting Polymers with High Charge-Carrier Mobility. *Nat. Mater.* **2006**, *5*, 328−333.

(135) Coropceanu, V.; Cornil, J.; da Silva Filho, D. A.; Olivier, Y.; Silbey, R.; Brédas, J.-L. Charge Transport in Organic Semiconductors. *Chem. Rev.* **2007**, *107*, 926−952.

(136) Wang, C.; Dong, H.; Hu, W.; Liu, Y.; Zhu, D. Semiconducting π-Conjugated Systems in Field-Effect Transistors: A Material Odyssey of Organic Electronics. *Chem. Rev.* **2012**, *112*, 2208−2267.

(137) Sommer, M. Conjugated Polymers Based on Naphthalene Diimide for Organic Electronics. *J. Mater. Chem. C* **2014**, *2*, 3088−3098.

(138) Nielsen, C. B.; Turbiez, M.; McCulloch, I. Recent Advances in the Development of Semiconducting DPP-Containing Polymers for Transistor Applications. *Adv. Mater.* **2013**, *25*, 1859−1880.

(139) Stalder, R.; Mei, J.; Graham, K. R.; Estrada, L. A.; Reynolds, J. R. Isoindigo, a Versatile Electron-Deficient Unit For High-Performance Organic Electronics. *Chem. Mater.* **2014**, *26*, 664−678.

(140) Snyder, G. J.; Toberer, E. S. Complex Thermoelectric Materials. *Nat. Mater.* **2008**, *7*, 105−114.

(141) Kang, K.; Watanabe, S.; Broch, K.; Sepe, A.; Brown, A.; Nasrallah, I.; Nikolka, M.; Fei, Z.; Heeney, M.; Matsumoto, D.; Marumoto, K.; Tanaka, H.; Kuroda, S. I.; Sirringhaus, H. 2D Coherent Charge Transport in Highly Ordered Conducting Polymers Doped by Solid State Diffusion. *Nat. Mater.* **2016**, *15*, 896−902.

(142) Kroon, R.; Kiefer, D.; Stegerer, D.; Yu, L.; Sommer, M.; Müller, C. Polar Side Chains Enhance Processability, Electrical Conductivity, and Thermal Stability of a Molecularly p-Doped Polythiophene. *Adv. Mater.* **2017**, *29*, 1700930.

(143) Yamamoto, J.; Furukawa, Y. Electronic and Vibrational Spectra of Positive Polarons and Bipolarons in Regioregular Poly(3-Hexylthiophene) Doped with Ferric Chloride. *J. Phys. Chem. B* **2015**, *119*, 4788−4794.

(144) Giovannitti, A.; Nielsen, C. B.; Sbircea, D.-T.; Inal, S.; Donahue, M.; Niazi, M. R.; Hanifi, D. A.; Amassian, A.; Malliaras, G. G.; Rivnay, J.; McCulloch, I. N-Type Organic Electrochemical Transistors with Stability in Water. *Nat. Commun.* **2016**, *7*, 13066.

(145) Khodagholy, D.; Rivnay, J.; Sessolo, M.; Gurfinkel, M.; Leleux, P.; Jimison, L. H.; Stavrinidou, E.; Herve, T.; Sanaur, S.; Owens, R. M.; Malliaras, G. G. High Transconductance Organic Electrochemical Transistors. *Nat. Commun.* **2013**, *4*, 2133.

(146) Facchetti, A. π-Conjugated Polymers for Organic Electronics and Photovoltaic Cell Applications. *Chem. Mater.* **2011**, *23*, 733−758.

(147) Brixi, S.; Melville, O. A.; Mirka, B.; He, Y.; Hendsbee, A. D.; Meng, H.; Li, Y.; Lessard, B. H. Air and Temperature Sensitivity of N-Type Polymer Materials to Meet and Exceed the Standard of N2200. *Sci. Rep.* **2020**, *10*, 4014.

(148) Jones, B. A.; Facchetti, A.; Wasielewski, M. R.; Marks, T. J. Tuning Orbital Energetics in Arylene Diimide Semiconductors.

Materials Design for Ambient Stability of n-Type Charge Transport. *J. Am. Chem. Soc.* **2007**, *129*, 15259−15278.

(149) de Leeuw, D. M.; Simenon, M. M. J.; Brown, A. R.; Einerhand, R. E. F. Stability of N-Type Doped Conducting Polymers and Consequences for Polymeric Microelectronic Devices. *Synth. Met.* **1997**, *87*, 53−59.

(150) Quinn, J. T. E.; Zhu, J.; Li, X.; Wang, J.; Li, Y. Recent Progress in the Development of N-Type Organic Semiconductors for Organic Field Effect Transistors. *J. Mater. Chem. C* **2017**, *5*, 8654−8681.

(151) Zhan, X.; Facchetti, A.; Barlow, S.; Marks, T. J.; Ratner, M. A.; Wasielewski, M. R.; Marder, S. R. Rylene and Related Diimides for Organic Electronics. *Adv. Mater.* **2011**, *23*, 268−284.

(152) Griggs, S.; Marks, A.; Bristow, H.; McCulloch, I. N-Type Organic Semiconducting Polymers: Stability Limitations, Design Considerations and Applications. *J. Mater. Chem. C* **2021**, *9*, 8099−8128.

(153) Briseno, A. L.; Kim, F. S.; Babel, A.; Xia, Y.; Jenekhe, S. A. N-Channel Polymer Thin Film Transistors with Long-Term Air-Stability and Durability and Their Use in Complementary Inverters. *J. Mater. Chem.* **2011**, *21*, 16461.

(154) Babel, A.; Jenekhe, S. A. High Electron Mobility in Ladder Polymer Field-Effect Transistors. *J. Am. Chem. Soc.* **2003**, *125*, 13656−13657.

(155) Kim, R.; Amegadze, P. S. K.; Kang, I.; Yun, H.-J.; Noh, Y.-Y.; Kwon, S.-K.; Kim, Y.-H. High-Mobility Air-Stable Naphthalene Diimide-Based Copolymer Containing Extended π-Conjugation for n-Channel Organic Field Effect Transistors. *Adv. Funct. Mater.* **2013**, *23*, 5719−5727.

(156) Kang, B.; Kim, R.; Lee, S. B.; Kwon, S.-K.; Kim, Y.-H.; Cho, K. Side-Chain-Induced Rigid Backbone Organization of Polymer Semiconductors through Semifluoroalkyl Side Chains. *J. Am. Chem. Soc.* **2016**, *138*, 3679−3686.

(157) Chua, L.; Zaumseil, J.; Chang, J.; Ou, E. C.; Ho, P.; Sirringhaus, H.; Friend, R. H. General Observation of N-Type Field-Effect Behaviour in Organic Semiconductors. *Nature* **2005**, *434*, 194−199.

(158) Giovannitti, A.; Maria, I. P.; Hanifi, D.; Donahue, M. J.; Bryant, D.; Barth, K. J.; Makdah, B. E.; Savva, A.; Moia, D.; Zetek, M. M. M.; Barnes, P. R. F. F.; Reid, O. G.; Inal, S.; Rumbles, G.; Malliaras, G. G.; Nelson, J.; Rivnay, J.; Mcculloch, I. The Role of the Side Chain on the Performance of N-Type Conjugated Polymers in Aqueous Electrolytes. *Chem. Mater.* **2018**, *30*, 2945−2953.

(159) Nielsen, C. B.; Giovannitti, A.; Sbircea, D.-T. T.; Bandiello, E.; Niazi, M. R.; Hanifi, D. A.; Sessolo, M.; Amassian, A.; Malliaras, G. G.; Rivnay, J.; McCulloch, I. Molecular Design of Semiconducting Polymers for High-Performance Organic Electrochemical Transistors. *J. Am. Chem. Soc.* **2016**, *138*, 10252−10259.

(160) Chen, X.; Marks, A.; Paulsen, B. D.; Wu, R.; Rashid, R. B.; Chen, H.; Alsufyani, M.; Rivnay, J.; McCulloch, I. N -Type Rigid Semiconducting Polymers Bearing Oligo(Ethylene Glycol) Side Chains for High-Performance Organic Electrochemical Transistors. *Angew. Chem., Int. Ed.* **2021**, *60*, 9368−9373.

(161) Roncali, J. Synthetic Principles for Bandgap Control in Linear π-Conjugated Systems. *Chem. Rev.* **1997**, *97*, 173−205.

(162) Roncali, J. Molecular Engineering of the Band Gap of π-Conjugated Systems: Facing Technological Applications. *Macromol. Rapid Commun.* **2007**, *28*, 1761−1775.

(163) Kleinhenz, N.; Yang, L.; Zhou, H.; Price, S. C.; You, W. Low-Band-Gap Polymers That Utilize Quinoid Resonance Structure Stabilization by Thienothiophene: Fine-Tuning of HOMO Level. *Macromolecules* **2011**, *44*, 872−877.

(164) Mei, J.; Bao, Z. Side Chain Engineering in Solution-Processable Conjugated Polymers. *Chem. Mater.* **2014**, *26*, 604−615.

(165) Chandran, D.; Lee, K.-S. Diketopyrrolopyrrole: A Versatile Building Block for Organic Photovoltaic Materials. *Macromol. Res.* **2013**, *21*, 272−283.

(166) Chen, Z.; Zheng, Y.; Yan, H.; Facchetti, A. Naphthalenedicarboximide- vs Perylenedicarboximide-Based Copolymers. Synthesis

and Semiconducting Properties in Bottom-Gate N-Channel Organic Transistors. *J. Am. Chem. Soc.* **2009**, *131*, 8−9.

(167) Lei, T.; Wang, J.-Y.; Pei, J. Roles of Flexible Chains in Organic Semiconducting Materials. *Chem. Mater.* **2014**, *26*, 594−603.

(168) Moia, D.; Giovannitti, A.; Szumska, A. A.; Maria, I. P.; Rezasoltani, E.; Sachs, M.; Schnurr, M.; Barnes, P. R. F.; McCulloch, I.; Nelson, J. Design and Evaluation of Conjugated Polymers with Polar Side Chains as Electrode Materials for Electrochemical Energy Storage in Aqueous Electrolytes. *Energy Environ. Sci.* **2019**, *12*, 1349−1357.

(169) Szweda, R.; Chendo, C.; Charles, L.; Baxter, P. N. W.; Lutz, J. F. Synthesis of Oligoarylacetylenes with Defined Conjugated Sequences Using Tailor-Made Soluble Polymer Supports. *Chem. Commun.* **2017**, *53*, 8312−8315.

(170) Giovannitti, A.; Sbircea, D. T.; Inal, S.; Nielsen, C. B.; Bandiello, E.; Hanifi, D. A.; Sessolo, M.; Malliaras, G. G.; McCulloch, I.; Rivnay, J. Controlling the Mode of Operation of Organic Transistors through Side-Chain Engineering. *Proc. Natl. Acad. Sci. U. S. A.* **2016**, *113*, 12017−12022.

(171) Giovannitti, A.; Nielsen, C. B.; Rivnay, J.; Kirkus, M.; Harkin, D. J.; White, A. J. P.; Sirringhaus, H.; Malliaras, G. G.; McCulloch, I. Sodium and Potassium Ion Selective Conjugated Polymers for Optical Ion Detection in Solution and Solid State. *Adv. Funct. Mater.* **2016**, *26*, 514−523.

(172) Wadsworth, A.; Moser, M.; Marks, A.; Little, M. S. M. S.; Gasparini, N.; Brabec, C. J. C. J.; Baran, D.; Mcculloch, I. Critical Review of the Molecular Design Progress in Non-Fullerene Electron Acceptors towards Commercially Viable Organic Solar Cells. *Chem. Soc. Rev.* **2019**, *48*, 1596.

(173) Chen, X.; Zhang, Z.; Ding, Z.; Liu, J.; Wang, L. Diketopyrrolopyrrole-Based Conjugated Polymers Bearing Branched Oligo(Ethylene Glycol) Side Chains for Photovoltaic Devices. *Angew. Chem., Int. Ed.* **2016**, *55*, 10376−10380.

(174) Kiefer, D.; Giovannitti, A.; Sun, H.; Biskup, T.; Hofmann, A.; Koopmans, M.; Cendra, C.; Weber, S.; Anton Koster, L. J.; Olsson, E.; Rivnay, J.; Fabiano, S.; McCulloch, I.; Müller, C. Enhanced N-Doping Efficiency of a Naphthalenediimide-Based Copolymer through Polar Side Chains for Organic Thermoelectrics. *ACS Energy Lett.* **2018**, *3*, 278−285.

(175) Lu, Y.; Yu, Z.-D.; Liu, Y.; Ding, Y.-F.; Yang, C.-Y.; Yao, Z.-F.; Wang, Z.-Y.; You, H.-Y.; Cheng, X.-F.; Tang, B.; Wang, J.-Y.; Pei, J. The Critical Role of Dopant Cations in Electrical Conductivity and Thermoelectric Performance of N-Doped Polymers. *J. Am. Chem. Soc.* **2020**, *142*, 15340−15348.

(176) Meng, B.; Song, H.; Chen, X.; Xie, Z.; Liu, J.; Wang, L. Replacing Alkyl with Oligo(Ethylene Glycol) as Side Chains of Conjugated Polymers for Close π-π Stacking. *Macromolecules* **2015**, *48*, 4357−4363.

(177) Schmode, P.; Savva, A.; Kahl, R.; Ohayon, D.; Meichsner, F.; Dolynchuk, O.; Thurn-Albrecht, T.; Inal, S.; Thelakkat, M. The Key Role of Side Chain Linkage in Structure Formation and Mixed Conduction of Ethylene Glycol Substituted Polythiophenes. *ACS Appl. Mater. Interfaces* **2020**, *12*, 13029−13039.

(178) Maria, I. P.; Paulsen, B. D.; Savva, A.; Ohayon, D.; Wu, R.; Hallani, R.; Basu, A.; Du, W.; Anthopoulos, T. D.; Inal, S.; Rivnay, J.; McCulloch, I.; Giovannitti, A. The Effect of Alkyl Spacers on the Mixed Ionic-Electronic Conduction Properties of N-Type Polymers. *Adv. Funct. Mater.* **2021**, *31*, 2008718.

(179) Nicolini, T.; Surgailis, J.; Savva, A.; Scaccabarozzi, A. D.; Nakar, R.; Thuau, D.; Wantz, G.; Richter, L. J.; Dautel, O.; Hadziioannou, G.; Stingelin, N. A Low-Swelling Polymeric Mixed Conductor Operating in Aqueous Electrolytes. *Adv. Mater.* **2021**, *33*, 2005723.

(180) Schmode, P.; Ohayon, D.; Reichstein, P. M.; Savva, A.; Inal, S.; Thelakkat, M. High-Performance Organic Electrochemical Transistors Based on Conjugated Polyelectrolyte Copolymers. *Chem. Mater.* **2019**, *31*, 5286−5295.

(181) Khau, B. v.; Savagian, L. R.; de Keersmaecker, M.; Gonzalez, M. A.; Reichmanis, E. Carboxylic Acid Functionalization Yields

Solvent-Resistant Organic Electrochemical Transistors. *ACS Mater. Lett.* **2019**, *1*, 599−605.

(182) Kawan, M.; Hidalgo, T. C.; Du, W.; Pappa, A. M.; Owens, R. M.; McCulloch, I.; Inal, S. Monitoring Supported Lipid Bilayers with N-Type Organic Electrochemical Transistors. *Mater. Horiz.* **2020**, *7*, 2348−2358.

(183) Moser, M.; Hidalgo, T. C.; Surgailis, J.; Gladisch, J.; Ghosh, S.; Sheelamanthula, R.; Thiburce, Q.; Giovannitti, A.; Salleo, A.; Gasparini, N.; Wadsworth, A.; Zozoulenko, I.; Berggren, M.; Stavrinidou, E.; Inal, S.; McCulloch, I. Side Chain Redistribution as a Strategy to Boost Organic Electrochemical Transistor Performance and Stability. *Adv. Mater.* **2020**, *32*, 2002748.

(184) MacDiarmid, A. G. Polyaniline and Polypyrrole: Where Are We Headed? *Synth. Met.* **1997**, *84*, 27−34.

(185) Kumar, D.; Sharma, R. C. Advances in Conductive Polymers. *Eur. Polym. J.* **1998**, *34*, 1053−1060.

(186) Baker, C. O.; Huang, X.; Nelson, W.; Kaner, R. B. Polyaniline Nanofibers: Broadening Applications for Conducting Polymers. *Chem. Soc. Rev.* **2017**, *46*, 1510−1525.

(187) Williams, G.; McMurray, H. N. Factors Affecting Acid-Base Stability of the Interface Between Polyaniline Emeraldine Salt and Oxide Covered Metal. *Electrochem. Solid-State Lett.* **2005**, *8*, B42.

(188) Piro, B.; Mattana, G.; Zrig, S.; Anquetin, G.; Battaglini, N.; Capitao, D.; Maurin, A.; Reisberg, S. Fabrication and Use of Organic Electrochemical Transistors for Sensing of Metabolites in Aqueous Media. *Appl. Sci.* **2018**, *8*, 928.

(189) Tourillon, G.; Garnier, F. Stability of Conducting Poly-thiophene and Derivatives. *J. Electrochem. Soc.* **1983**, *130*, 2042−2044.

(190) Heywang, G.; Jonas, F. Poly(Alkylenedioxythiophene)s—New, Very Stable Conducting Polymers. *Adv. Mater.* **1992**, *4*, 116−118.

(191) de Keersmaecker, M.; Lang, A. W.; Österholm, A. M.; Reynolds, J. R. All Polymer Solution Processed Electrochromic Devices: A Future without Indium Tin Oxide? *ACS Appl. Mater. Interfaces* **2018**, *10*, 31568−31579.

(192) Inal, S.; Rivnay, J.; Hofmann, A. I.; Uguz, I.; Mumtaz, M.; Katsigiannopoulos, D.; Brochon, C.; Cloutet, E.; Hadziioannou, G.; Malliaras, G. G. Organic Electrochemical Transistors Based on PEDOT with Different Anionic Polyelectrolyte Dopants. *J. Polym. Sci., Part B: Polym. Phys.* **2016**, *54*, 147−151.

(193) Shi, H.; Liu, C.; Jiang, Q.; Xu, J. Effective Approaches to Improve the Electrical Conductivity of PEDOT:PSS: A Review. *Adv. Electron. Mater.* **2015**, *1*, 1500017.

(194) Huang, J.; Miller, P. F.; de Mello, J. C.; de Mello, A. J.; Bradley, D. D. C. Influence of Thermal Treatment on the Conductivity and Morphology of PEDOT/PSS Films. *Synth. Met.* **2003**, *139*, 569−572.

(195) Cameron, J.; Skabara, P. J. The Damaging Effects of the Acidity in PEDOT:PSS on Semiconductor Device Performance and Solutions Based on Non-Acidic Alternatives. *Mater. Horiz.* **2020**, *7*, 1759−1772.

(196) Alemu Mengistie, D.; Wang, P.-C.; Chu, C.-W. Effect of Molecular Weight of Additives on the Conductivity of PEDOT:PSS and Efficiency for ITO-Free Organic Solar Cells. *J. Mater. Chem. A* **2013**, *1*, 9907.

(197) Ouyang, J.; Xu, Q.; Chu, C.-W.; Yang, Y.; Li, G.; Shinar, J. On the Mechanism of Conductivity Enhancement in Poly(3,4-Ethylenedioxythiophene):Poly(Styrene Sulfonate) Film through Solvent Treatment. *Polymer* **2004**, *45*, 8443−8450.

(198) Benor, A.; Takizawa, S. ya; Pérez-Bolívar, C.; Anzenbacher, P. Efficiency Improvement of Fluorescent OLEDs by Tuning the Working Function of PEDOT:PSS Using UV-Ozone Exposure. *Org. Electron.* **2010**, *11*, 938−945.

(199) Lin, Y. J.; Yang, F. M.; Huang, C. Y.; Chou, W. Y.; Chang, J.; Lien, Y. C. Increasing the Work Function of Poly(3,4-Ethyl-enedioxythiophene) Doped with Poly(4-Styrenesulfonate) by Ultra-violet Irradiation. *Appl. Phys. Lett.* **2007**, *91*, 092127.

(200) Rivnay, J.; Leleux, P.; Ferro, M.; Sessolo, M.; Williamson, A.; Koutsouras, D. A.; Khodagholy, D.; Ramuz, M.; Strakosas, X.; Owens,

R. M.; Benar, C.; Badier, J. M.; Bernard, C.; Malliaras, G. G. High-Performance Transistors for Bioelectronics through Tuning of Channel Thickness. *Sci. Adv.* **2015**, *1*, No. e1400251.

(201) Johansson, T.; Mammo, W.; Svensson, M.; Andersson, M. R.; Inganäs, O. Electrochemical Bandgaps of Substituted Polythiophenes. *J. Mater. Chem.* **2003**, *13*, 1316−1323.

(202) Leclerc, M.; Daoust, G. Structural Effects in Alkyl and Alkoxy-Substituted Polythiophenes. *Synth. Met.* **1991**, *41*, 529−532.

(203) Lo, C. K.; Gautam, B. R.; Selter, P.; Zheng, Z.; Oosterhout, S. D.; Constantinou, I.; Knitsch, R.; Wolfe, R. M. W.; Yi, X.; Brédas, J. L.; So, F.; Toney, M. F.; Coropceanu, V.; Hansen, M. R.; Gundogdu, K.; Reynolds, J. R. Every Atom Counts: Elucidating the Fundamental Impact of Structural Change in Conjugated Polymers for Organic Photovoltaics. *Chem. Mater.* **2018**, *30*, 2995−3009.

(204) Estrada, L. A.; Deininger, J. J.; Kamenov, G. D.; Reynolds, J. R. Direct (Hetero)Arylation Polymerization: An Effective Route to 3,4-Propylenedioxythiophene-Based Polymers with Low Residual Metal Content. *ACS Macro Lett.* **2013**, *2*, 869−873.

(205) Liu, Q.; Bottle, S. E.; Sonar, P. Developments of Diketopyrrolopyrrole-Dye-Based Organic Semiconductors for a Wide Range of Applications in Electronics. *Adv. Mater.* **2020**, *32*, 1903882.

(206) Moser, M.; Savva, A.; Thorley, K.; Paulsen, B. D.; Hidalgo, T. C.; Ohayon, D.; Chen, H.; Giovannitti, A.; Marks, A.; Gasparini, N.; Wadsworth, A.; Rivnay, J.; Inal, S.; McCulloch, I. Polaron Delocalization in Donor-Acceptor Polymers and Its Impact on Organic Electrochemical Transistor Performance. *Angew. Chem.* **2021**, *133*, 7856−7864.

(207) Krauss, G.; Meichsner, F.; Hochgesang, A.; Mohanraj, J.; Salehi, S.; Schmode, P.; Thelakkat, M. Polydiketopyrrolopyrroles Carrying Ethylene Glycol Substituents as Efficient Mixed Ion-Electron Conductors for Biocompatible Organic Electrochemical Transistors. *Adv. Funct. Mater.* **2021**, *31*, 2010048.

(208) Wu, X.; Liu, Q.; Surendran, A.; Bottle, S. E.; Sonar, P.; Leong, W. L. Enhancing the Electrochemical Doping Efficiency in Diketopyrrolopyrrole-Based Polymer for Organic Electrochemical Transistors. *Adv. Electron. Mater.* **2021**, *7*, 2000701.

(209) Lee, H. K. H.; Li, Z.; Constantinou, I.; So, F.; Tsang, S. W.; So, S. K. Batch-to-Batch Variation of Polymeric Photovoltaic Materials: Its Origin and Impacts on Charge Carrier Transport and Device Performances. *Adv. Eng. Mater.* **2014**, *4*, 1400768.

(210) Ohayon, D.; Savva, A.; Du, W.; Paulsen, B. D.; Uguz, I.; Ashraf, R. S.; Rivnay, J.; McCulloch, I.; Inal, S. Influence of Side Chains on the N-Type Organic Electrochemical Transistor Perform-ance. *ACS Appl. Mater. Interfaces* **2021**, *13*, 4253−4266.

(211) Sun, H.; Vagin, M.; Wang, S.; Crispin, X.; Forchheimer, R.; Berggren, M.; Fabiano, S. Complementary Logic Circuits Based on High-Performance n-Type Organic Electrochemical Transistors. *Adv. Mater.* **2018**, *30*, 1704916.

(212) Ashley, C. E.; Carnes, E. C.; Phillips, G. K.; Padilla, D.; Durfee, P. N.; Brown, P. A.; Hanna, T. N.; Liu, J.; Phillips, B.; Carter, M. B.; Carroll, N. J.; Jiang, X.; Dunphy, D. R.; Willman, C. L.; Petsev, D. N.; Evans, D. G.; Parikh, A. N.; Chackerian, B.; Wharton, W.; Peabody, D. S.; Brinker, C. J. The Targeted Delivery of Multi-component Cargos to Cancer Cells by Nanoporous Particle-Supported Lipid Bilayers. *Nat. Mater.* **2011**, *10*, 389−397.

(213) Lee, J.; Kalin, A. J.; Yuan, T.; Al-Hashimi, M.; Fang, L. Fully Conjugated Ladder Polymers. *Chem. Sci.* **2017**, *8*, 2503−2521.

(214) Surgailis, J.; Savva, A.; Druet, V.; Paulsen, B. D.; Wu, R.; Hamidi-Sakr, A.; Ohayon, D.; Nikiforidis, G.; Chen, X.; McCulloch, I.; Rivnay, J.; Inal, S. Mixed Conduction in an N-Type Organic Semiconductor in the Absence of Hydrophilic Side-Chains. *Adv. Funct. Mater.* **2021**, *31*, 2010165.

(215) Rivnay, J.; Owens, R. M.; Malliaras, G. G. The Rise of Organic Bioelectronics. *Chem. Mater.* **2014**, *26*, 679−685.

(216) Inal, S.; Rivnay, J.; Suiu, A. O.; Malliaras, G. G.; McCulloch, I. Conjugated Polymers in Bioelectronics. *Acc. Chem. Res.* **2018**, *51*, 1368−1376.